University of Alberta

Fabrication of Metal Matrix Composites by Friction Stir Processing

by

Hossein Izadi

A thesis submitted to the Faculty of Graduate Studies and Research
in partial fulfillment of the requirements for the degree of

Doctor of Philosophy
in
Materials Engineering

Department of Chemical and Materials Engineering

Spring 2014
Edmonton, Alberta

Abstract

This thesis focuses on fabrication of aluminum matrix composites using friction stir processing. Al 5059 alloy was selected as the matrix alloy, and the effect of processing parameters on microstructure and mechanical properties of this alloy was studied in detail.

Friction stir processing was conducted using three different tools with different rotation speeds. Microstructural characterization was carried out by optical microscopy, SEM and TEM. It was shown that fine grains form in the stir zone as a result of dynamic recrystallization and these fine grains do not grow during the cooling cycle because of the effect of magnesium on reducing grain boundary mobility. TEM analysis also showed that the microstructure contained $Al_6(Mn,Fe)$ particles with two different morphologies. It was confirmed that refinement of these particles can more effectively pin the grain boundaries and suppress grain growth.

Grain size measurement was performed on the samples to investigate the effect of process parameters on recrystallization and grain growth in the stir zone. Mechanical properties were also obtained by microhardness and tensile tests. A tool with 3 flats in combination with a rotation speed of 454 RPM provides slightly higher grain refinement and subsequent mechanical properties. It is shown that friction stir processing reduces the fraction of elongated precipitates that form on the grain boundaries of the base material, and this resulted in approximately a 10% improvement in elongation to failure in friction stir processed Al 5059

samples. Particle fragmentation also appeared to increase the rate of work hardening, which also likely contributed to enhanced ductility.

A multi-pass multi-tool FSP technique using different processing parameters was proposed for fabrication of Al 5059/Al_2O_3 and Al 5059/CNT composites. A uniform distribution of reinforcing particles was achieved in both cases with a uniform hardness profile through the stir zone. The microhardness of the composites was significantly higher than the original aluminum alloy. However, it was noted that the thermo-mechanical cycles during processing of the Al/CNT composites have destroyed the tubular structure of the CNTs.

Acknowledgment

I would like to offer my sincerest gratitude to my supervisor Dr. Adrian Gerlich for giving me the opportunity to work on this project. Without his invaluable support, inspiring guidance and countless hours of involvement, I could have never finished my PhD career. I am for ever indebted to him for the moments when he patiently taught me how to think and behave like a professional researcher. I am very proud and honored to have the intelligent guidance and help of one of the best. Thank you Adrian, now and always!

I am also grateful to my co-supervisor Dr. Patricio Mendez for all his kind support and for managing the CCWJ in such a friendly yet professional way. I believe his amazing vision and hard work will bring a fantastic future for the CCWJ.

I want to express my appreciation to my final oral examining committee members: Dr. Judy Schneider, Dr. Robert Luth and Dr. John Nychka for the invaluable discussions and the time they devoted to reviewing this thesis.

I would like to acknowledge Natural Sciences and Engineering Research Council of Canada and Defence R&D Canada for financial assistant with this project.

I would like to extend warm thanks and appreciation to all the past and current members of the CCWJ for their cooperation, friendship and all the good memories. My special thanks go to: Kevin Scott, Stuart Guest, Sahar Salimi, Thilan Liyanage, Steven Borle, Matthew Dewar, Ata Kamyabi, Gentry Wood, Jordan Tsui, Nairn Barnes and Dancy Bogdanovic.

I am most grateful to my parents and brothers for their endless help, support, and encouragement, not only during the course of this work but throughout my life. My parents have always lovingly supported me in achieving my goals; words are inadequate to acknowledge their help. I am especially thankful to my oldest brother Iman and his family for all their support from the very first day we entered Canada. I would also like to extend my appreciation to my in-laws for their love and support. Finally, my deepest gratitude goes to my beloved wife for her patience and moral support throughout this work. This dissertation could not be done without her dedication and sacrifice.

Table of contents

List of Tables

List of Figures

Chapter 1: Introduction

1.1 Overview

1.1.1 Friction Stir Processing

Friction stir processing (FSP) is a solid state material processing technique based on the principles of friction stir welding (FSW) developed by The Welding Institute in 1991 [1]. In FSW a rotating tool with a specially designed pin and shoulder moves along the weld seam; the high rotating speed of the tool along with the frictional forces between the work piece and the shoulder promote joining by frictional heating, softening and severe plastic deformation. The process is shown schematically in Figure 1-1. Severe plastic deformation and stirring action imposed by the tool during the process has created many interesting applications for friction stir processing [2], examples are microstructural modification and homogenization of cast alloys and powder metallurgy fabricated parts [3-9] and production and homogenization of metal matrix composites [10-18].

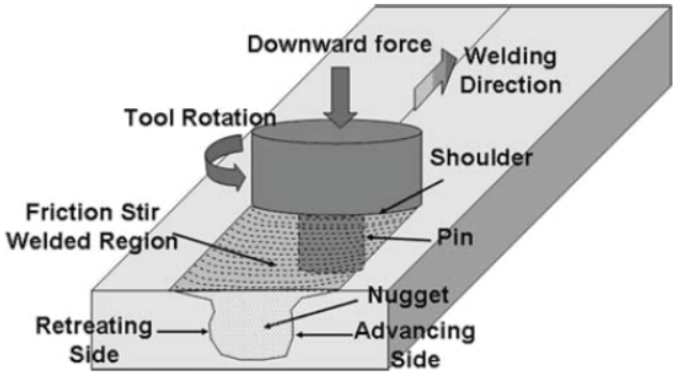

Figure 1-1: Principles of friction stir welding [17].

Although FSP is a novel processing method, it has found remarkable applications in different industries due to its significant advantages in comparison

to other metalworking techniques. These advantages include: 1) few processing steps with relatively simple equipment, 2) good control of material properties by optimizing the process parameters (such as tool geometry, rotation speed, traverse speed, downward force, cooling rate), 3) controlled selective modification of microstructure, and 4) good environmental friendliness and energy efficiency.

Friction stir processing (FSP) is a severe plastic deformation process that involves high strain rate deformation and no bulk melting; therefore it can be utilized for microstructural modification of parts fabricated via different methods such as powder metallurgy and casting. For example, Oh-Ishi and McNelly have shown that FSP of as-cast NiAl bronze results in refinement and homogenization of the microstructure as well as closure of porosities [8]. Santella *et al*. friction stir processed sand-cast ingots of A356 and A319 aluminum alloys with a simple cylindrical tool at 1000 RPM and 1.7 mm/s. They have indicated that after 5 or 6 FSP passes the shape and distribution of the intermetallic phases became uniform, and the porosity and dendritic microstructures were eliminated, see Figure 1-2. This leads to a significant increase in hardness, tensile strength, elongation and fatigue life of the samples. For example the microhardness of the A319 sample was increased from an average of 709 MPa in the as-cast condition to an average of 802 MPa after FSP [19]. Other researchers have also applied FSP to different aluminum, magnesium and titanium cast alloys in order to achieve a homogenized microstructure with refined grains and improved mechanical properties [3-5, 9, 20-25].

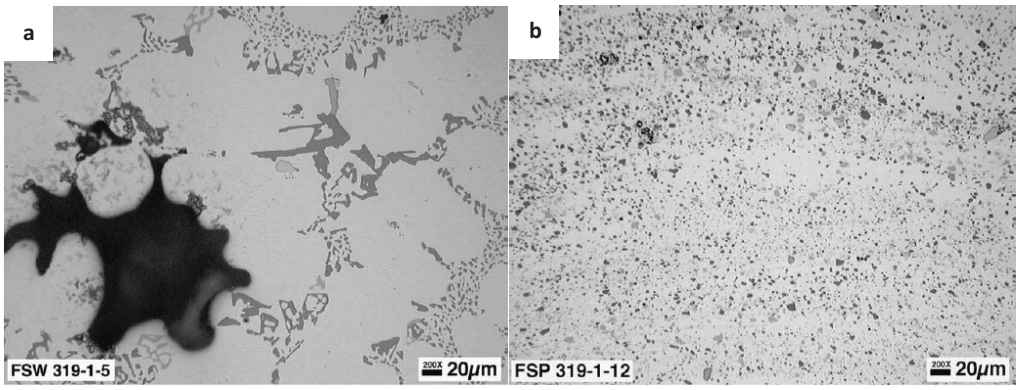

Figure 1-2: Microstructure of sand-cast A319 a) before FSP and b) after FSP [19].

Friction stir processing has also been utilized as a secondary process for homogenization of composites produced by other techniques. For example, Morisada *et al*. have thermally sprayed a layer of WC-CrC-Ni on a SKD61 steel substrate and then modified the composite overlay by FSP. Their results show that FSP eliminates the defects in the WC-CrC-Ni layer and refines the Ni binder and the Cr_3C_2 particles. The microhardness of the layer increased from 1200 HV, in the as-sprayed state, to 2000 HV after one FSP pass [14]. Zahmatkesh and Enayati produced a layer of Al/10% Al_2O_3 on Al 2024 substrate by using air plasma spray and then applied FSP to improve the distribution of alumina particles [26]. They achieved a surface composite layer of 600 μm thickness with this method. In a recent study, Hodder *et al*. applied FSP to a surface composite layer of Al/Al_2O_3 which was produced by cold gas dynamic spraying at low pressure. The redistribution of particles imposed by FSP significantly improved the mechanical properties [13].

During FSP the rotation of the tool mixes the material in the stir zone and this feature has been used for composite fabrication by many researchers [18]. Production of defect free bulk and surface composites with a good distribution of

the reinforcing material has been reported for different MMCs such as aluminum matrix composites (Al/SiC [27-36], Al/Al_2O_3 [37-39], Al/NiTi[40], Al/CNT[41-45], Al/Fullerene[46], Al/Ni[47], Al/TiO_2[48], Al/TiC and B_4C [49]), magnesium matrix composites (AZ31/nano ZrO_2 and nano SiO_2[50], AZ61/ SiO_2[16], AZ31/SiC[51], AZ31/CNT[15], AZ31/C_{60} [52], AZ31/Al_2O_3 [53], AZ63/SiC [54], AZ91/SiC and MoS_2 [55, 56], AZ91/Al_2O_3 [57], AZ91/SiO_2 [58], AZ91/carbon fiber [59]), copper matrix composites (Cu/SiC [60, 61], Cu/CNT [62]) and steel matrix composites (L316/SiC [63], mild steel/nano TiC [64]). Generally the process involves the incorporation of the reinforcement into the matrix and then applying FSP to mix the two. Some amount of secondary particles is inserted in a groove or holes on the surface of the base plate along the path of the tool travel. When the stirring tool passes through this material it effectively mixes the reinforcement with the matrix. However the main issue of this method is how to prevent loss of the inserted particles during the process. The most widely used solution is to perform one FSP pass on the groove with a cylindrical tool having no pin after inserting the particles and before starting the actual FSP with the ordinary tool [33, 35, 37, 53]. Lim *et al*. and Mahmoud *et al*. [41, 65] have covered the groove with a thin plate and then applied FSP on this plate along the groove, so there would be no material loss, however making a bond between the original plate and the "cover plate" remains an issue and needs special tool design and careful control of other process parameters. Some other researchers [66-69] have used a more complicated procedure; they have first prepared a powder preform using conventional powder metallurgy and then inserted it into the

groove. This method seems to be applicable for in situ composites [67-69], or in composites where the reinforcement is not a ceramic particle or nanosized material [66], since compacting such materials involves special equipment and high pressures.

One should also note that uncontrolled loss of reinforcement also introduces another problem in which one may not have control over the amount of the reinforcement. This makes it impossible to achieve a target percentage of the secondary material during the fabrication procedure.

Another major issue of friction stir welding/processing of composite materials is tool wear [64, 65, 70, 71], which happens as a result of contact between the hard particles and the tool in conjunction with the high stresses induced during FSP. Prado *et al*. have indicated extensive tool wear when friction stir welding Al 6061/ 20 vol% Al_2O_3 with tool made up of carbon steel [71], see Figure 1-3. Considerable tool wear is also reported for a tool made up of hard WC-Co alloy during FSW of Al-Si reinforced with 30 vol% of SiC [70].

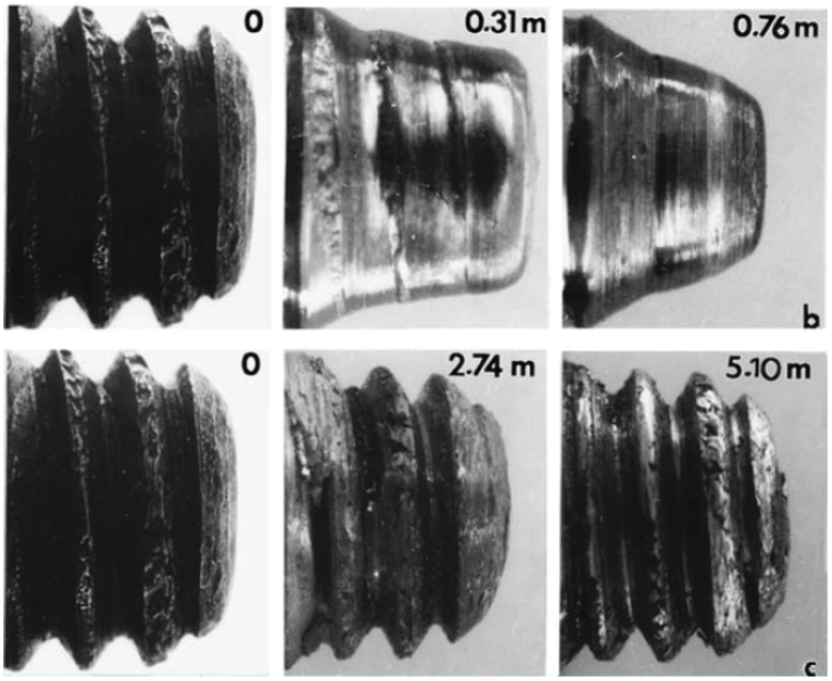

Figure 1-3: Tool wear during FSW of Al 6061 reinforced with b) 20 and c) 0, vol% of Al_2O_3. Linear distances traveled by the tool are indicated, all welds were performed at 1000 rpm [71].

1.1.2 Heat generation during Friction Stir Welding/Friction Stir Processing and temperature profile

During FSW/FSP heat is generated by three mechanisms: friction, plastic deformation and viscous dissipation and as the temperature increases to near the melting point of the work piece material amount of heat generated due to friction and plastic deformation decreases and viscous dissipation would be the dominant mechanism [72].

The friction between the rotating tool and the work piece is the source of frictional heating and is directly proportional to rotation speed and radius of the tool [73]. The rate of heat generated at the contact interface between two sliding surfaces (here tool and work piece surface), P_f, is given by:

$$P_f = \eta F_N V_x \quad (1.1)$$

Where η is the coefficient of kinetic friction defined by the ratio of frictional force to normal force, F_N is the normal force and Vx is the sliding velocity of the surfaces [72]. Factors affecting frictional heating during FSW/FSP are: tool geometry, material properties of the work piece, tool rotation and travel speeds, tool tilt angle (the angle between the spindle of the machine and the normal of the work piece surface) and plunging force [72].

When a material is subjected to mechanical work, as in FSW/FSP, a minor fraction of the energy induced by plastic deformation will be stored in the form of increased defect density (such as dislocations and grain boundaries) and increased surface area of sheared (cut) precipitates within the mechanically affected zone, however the vast majority of energy (around 95%) will heat the work piece [74, 75]. Under adiabatic conditions the amount of heat generated by mechanical deformation, E_D, can be expressed as:

$$E_D = \beta \int \sigma d\varepsilon \quad (1.2)$$

where σ is the von Mises flow stress during deformation, ε is the von Mises equivalent strain, and β is the fraction of mechanical work converted to heat. In the case of equation (1.2) E_D changes with strain, strain rate and temperature during deformation so as the temperature approaches the solidus temperature of the alloy, material softening reduces the amount of produced energy [72].

However these all in turn depend on work piece material's properties and welding parameters.

After some frictional heating and severe plastic deformation, the material around the tool experiences sticking to the tool rather than sliding. Under such conditions viscous dissipation driven by high shear stresses at the tool/work piece interface, will act as another important heat source [76]. In other words, viscous dissipation shows the amount of mechanical work converted irreversibly into heat by viscous effects within a fluid [77]. The rate of energy generated due to viscous dissipation, P_v, can be expressed by the following equation which is simplified from [72]:

$$P_v=\mu\left\{2\left[\left(\frac{\partial u}{\partial x}\right)^2+\left(\frac{\partial v}{\partial y}\right)^2+\left(\frac{\partial w}{\partial z}\right)^2\right]+\left(\frac{\partial v}{\partial x}+\frac{\partial u}{\partial y}\right)^2+\left(\frac{\partial w}{\partial x}+\frac{\partial u}{\partial z}\right)^2+\left(\frac{\partial w}{\partial y}+\frac{\partial u}{\partial z}\right)^2-\frac{2}{3}\left(\frac{\partial u}{\partial x}+\frac{\partial v}{\partial y}+\frac{\partial w}{\partial z}\right)^2\right\} \quad (1.3)$$

where u, v, w, are the velocities in directions x, y, z, respectively, and μ is the kinematic viscosity of the fluid given by:

$$\mu=\frac{\tau}{\sqrt{3\dot{\varepsilon}}} \quad (1.4)$$

where τ is shear stress and $\dot{\varepsilon}$ is the strain rate [72].

Temperature profile dictated by these three heating mechanisms affects microstructure and mechanical properties of the FSW/FSP material, so it is of significant interest to understand the temperature change during FSW/FSP. Many studies have been done regarding this for different materials, for example Figure

1-4 shows temperature profile of friction stir welded Ti-6Al-4V alloy [74]. As shown in Figure 1-4, areas around the tool and near the surface experience the maximum temperature.

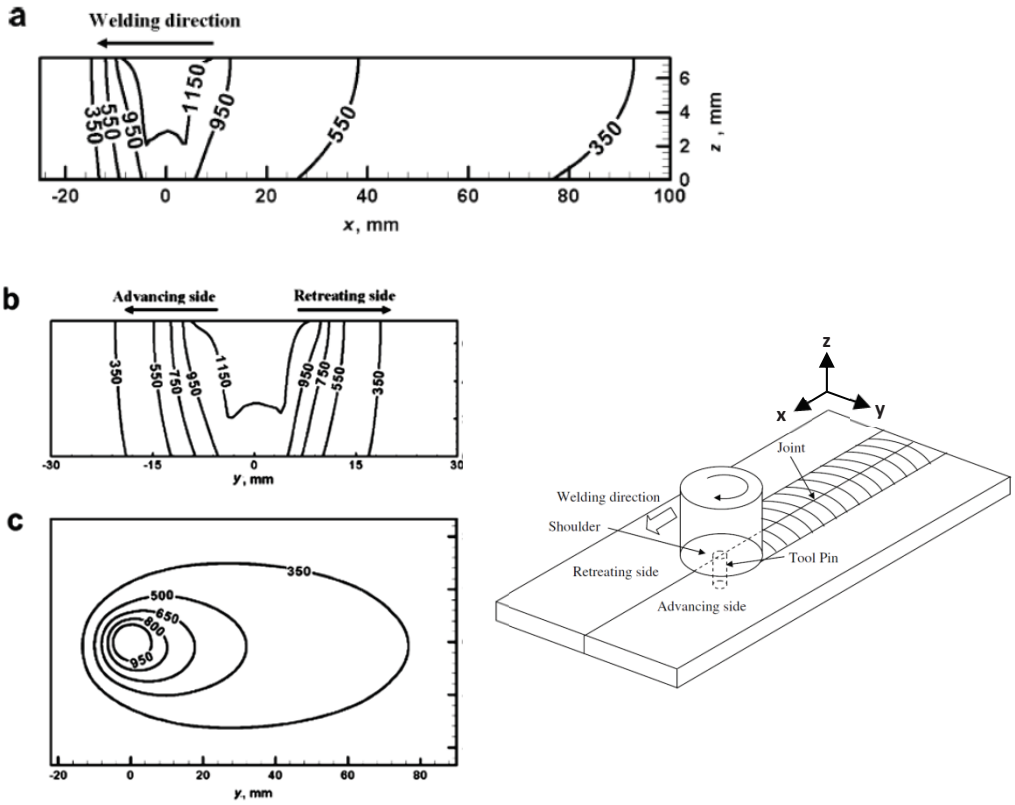

Figure 1-4: Temperature profile for a Ti-6Al-4V alloy friction stir weld, a) xz plane, b) yz plane, and c) z plane i.e. top surface. Rotation speed was 275 rpm and travel speed was 1.6 mm/s[74].

1.1.3 Material Flow and Mixing during Friction Stir Welding/Friction Stir Processing

Formation of a defect free weld directly depends on the material flow during FSW. On the other hand in FSP, material flow determines the development of microstructural features and in the special case of composite fabrication by FSP material flow in the stir zone governs the particle distribution. Thus, studying the material flow has been approached by many different methods in recent years,

using various techniques such as tracking of tracer particles post-welding by microscopy [78, 79], microstructural analysis of dissimilar alloy joints [80, 81], in-situ observation using x-ray transmission systems [82], simulation by numerical modeling [83-86], and using analog materials like coloured plasticine [87]. This aspect is not completely understood yet and remains the subject of many papers [88, 89]. Generally speaking, three types of flow transport the deformed material during FSW/FSP [74]: 1) tool rotation and the friction between the tool and the work piece material, heat and stir the softened material near the tool, 2) a downward material flow in the region close to the tool created when using a threaded pin which in turn causes an upward motion at the outer periphery of the mixing region of the stir zone; and 3) material flow along the welding direction as a result of travelling movement of the rotating tool. It is shown that majority of the material flow, caused by these three types, happens through the retreating side [74].

When considering FSP for fabrication of composites this mixing must be considered in order to control the distribution of material. First, stirring around the pin of the tool creates a rotating and mixing zone, the thickness of which depends on materials properties, welding parameters and rate of heat transfer to the tool [74]. Second, as mentioned before, use of a threaded pin induces mixing which helps particle distribution in both vertical and longitudinal directions during composite fabrication by FSP. Generally, the amount of mixing increases when applying higher rotation speeds or lower travel speeds [90]. Su *et al*. [91] have shown that by using a threaded tool, intermixing happens during friction stir

welding of dissimilar Al alloys, when the material from the locations beneath the shoulder and at the end of the pin is transferred to the top of the thread on the pin and is moved downward by the pin thread. This process happens during each single rotation of the tool and forms intermingled lamella which is then discharged from the bottom of the thread and moves outwards and upwards following a helical vertical rotational flow path, Figure 1-5.

Gerlich *et al*. [92] have indicated that the width of this intermixed region increases with the dwell time in friction stir spot welding which implies larger intermixed regions may be achieved in friction stir seam welding by decreasing the travel speed.

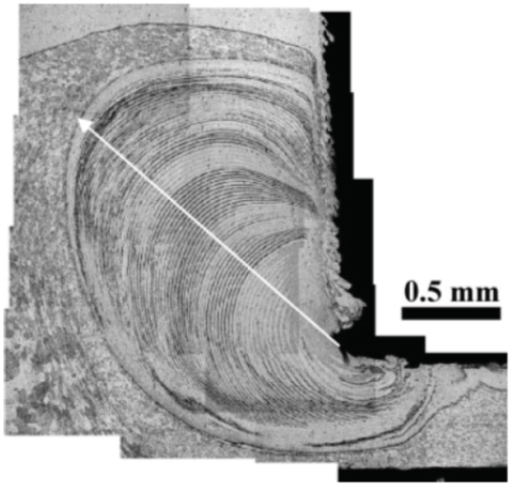

Figure 1-5: Intermixed region formed during Al 5754/Al 6111 friction stir spot welding, showing intermingled lamellae [92].

1.1.4 Microstructure

Typical cross section of a FSW joint has three different zones: 1) heat affected zone (HAZ), 2) nugget or stir zone and 3) thermomechanically affected zone (TMAZ) which is the region between HAZ and nugget, Figure 1-6. The stir

zone is the central region of the weld where dynamic recrystallization occurs as a result of high temperature and severe plastic deformation, leading to the formation of fine equiaxed grains, Figure 1-6-d. In FSW/FSP, tool geometry, composition and temperature of the work piece material, vertical pressure, cooling rate and process parameters significantly influence grain size in the nugget zone [74]. Table 1-1 shows grain size values for some FSW/FSP aluminum alloys. Microstructures of the material in this region usually contain a banded structure consisting of the so called “onion rings”, Figure 1-6. The spacing between these bands equals the distance the tool moves forward during each single rotation [93, 94]. Such microstructure is attributed to variations in: 1) grain size [95], 2) particles or precipitates distribution [93, 95], 3) crystallographic texture [96], 4) dislocation density [90], and 5) chemistry due to intermixing of dissimilar alloys [97]. Krishnan [94] has shown that these variations are caused when the frictional heating heats the material and the forward movement of the tool extrudes the material around to the retreating side which leads to the formation of the bands during tool rotation.

In the TMAZ, grains are heated and plastically deformed but not completely recrystallized; therefore they are not as fine and equiaxed as stir zone grains. Finally, HAZ is only affected by temperature and not by mechanical work so the main change in HAZ microstructure is the coarsening of the grains or precipitates [72].

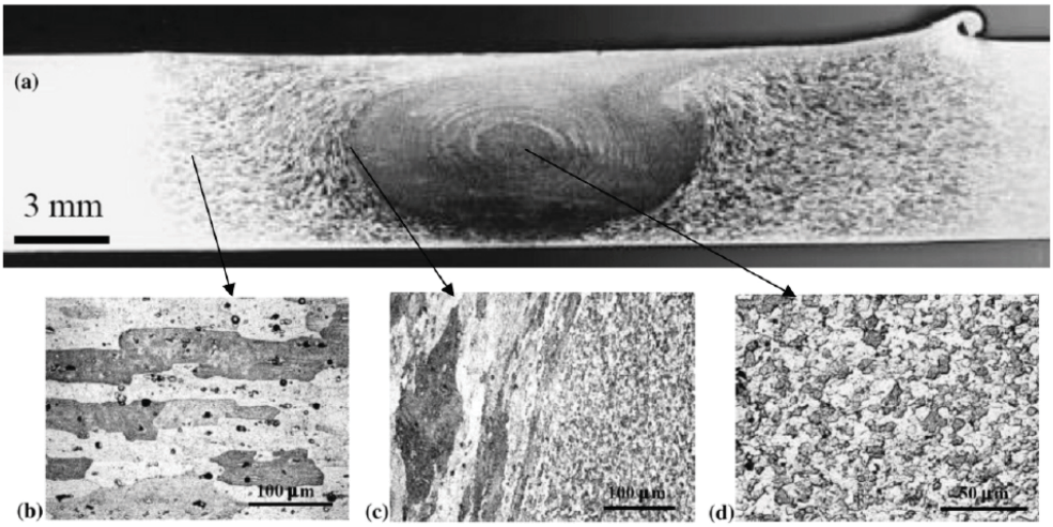

Figure 1-6: Optical micrographs of microstructure of an Al 2014 friction stir weld showing different regions: a) weld overview, b) heat affected zone, c) TMAZ/stir zone boundary, and d) stir zone [72].

Table 1-1: Summary of grain size in nugget zone of FSW/FSP aluminum alloys [2].

Material	Plate thickness (mm)	Tool geometry	Rotation rate (rpm)	Traverse speed (mm/min)	Grain size (μm)
7075Al-T6	6.35	–	–	127	2–4
6061Al-T6	6.3	Cylindrical	300–1000	90–150	10
Al–Li–Cu	7.6	–	–	–	9
7075Al-T651	6.35	Threaded, cylindrical	350, 400	102, 152	3.8, 7.5
6063Al-T4, T5	4.0	–	360	800–2450	5.9–17.8
6013Al-T4, T6	4.0	–	1400	400–450	10–15
1100Al	6.0	Cylindrical	400	60	4
5054Al	6.0	–	–	–	6
1080Al-O	4.0	–	–	–	20
5083Al-O	6.0	–	–	–	4
2017Al-T6	3	Threaded, cylindrical	1250	60	9–10
2095Al	1.6	–	1000	126–252	1.6
Al–Cu–Mg–Ag–T6	4.0	–	850	75	5
2024Al-T351	6.0	–	–	80	2–3
7010Al-T7651	6.35	–	180, 450	95	1.7, 6
7050Al-T651	6.35	–	350	15	1–4
Al–4Mg–1Zr	10	Threaded, cylindrical	350	102	1.5
2024Al	6.35	Threaded, cylindrical	200–300	25.4	2.0–3.9
7475Al	6.35	–	–	–	2.2
5083Al	6.35	Threaded, cylindrical	400	25.4	6.0
2519Al-T87	25.4	–	275	101.6	2–12

In the case of aluminum alloys, it is also important to study the behaviour of precipitates in the microstructure during any process. Survivability of strengthening precipitates highly depends on temperature changes. However they may survive the process but lose their effectiveness or even deteriorate mechanical properties if they become coarsened. It has been shown that maximum temperature of the stir zone during FSW/FSP may reach as high as 0.9 T_m for several aluminum alloys [72] which is high enough to dissolve precipitates or cause coarsening at the outer region of the stir zone. The dissolution rate of a plate-like particle with half thickness of *B* may be approximated by the following equation [72]:

$$\frac{dB}{dt} = -\frac{C_i - C_m}{C_p - C_i}\sqrt{\frac{D}{\pi t}} \quad (1.5)$$

where, t is time, C_i is the concentration at the dissolving interface, C_m is the concentration of solute in the matrix, C_p is the concentration of the particle, and D is the diffusion rate of the element controlling dissolution of the particle. It is also suggested that beside the effect of temperature, severe plastic deformation induced during FSW/FSP may enhance precipitate evolution by accelerated diffusion rates and shortened diffusion distances [2]. However other than dissolution, coarsening of the strengthening precipitates will also affect the mechanical properties of the work piece. During coarsening particles below a critical radius will dissolve increasing the solute content of the matrix which in

turn allows other precipitates to grow. This critical radius, r_c, is given by the Gibbs-Thompson relation [72]:

$$r_c = \frac{2\gamma V_m}{RT}\left(ln\left(\frac{C_m}{C_e}\right)\right)^{-1} \quad (1.6)$$

where γ is the particle-matrix interfacial energy, V_m is the molar volume of the precipitates, R is the universal gas constant, T is temperature, and C_e is the equilibrium solute content at the particle-matrix interface. It should be considered that aging behavior and precipitate evolution in aluminum matrix composites are different than in aluminum alloys, and it is stated that reinforced materials age more rapidly [98]. Effects of secondary ceramic particles on age hardening of aluminum alloys include: 1) enhanced nucleation of semi coherent precipitates on dislocations generated due to the mismatch in coefficient of thermal expansion of matrix and reinforcement, 2) higher diffusivity of the matrix due to the increase in dislocation density and number of grain boundaries, 3) decrease in the number of vacancies (as a result of increase in the number of vacancy sinks) which reduces diffusivity of the matrix and limits formation of GP zones, and 4) internal residual stress fields which affect precipitation of high coherency strain precipitates [98].

According to well defined experimental and theoretical models, the strength of the matrix alloy increases linearly with the size of fine shearable precipitates up to the peak aged condition [99]. Beyond this point, particles are no more shearable and the mechanism of interaction between particles and dislocations changes from shearing to the formation of so-called Orowan loops

[100] through which the alloy strength decreases by increasing the precipitates size. Therefore precipitation coarsening during FSW/FSP of heat treated peak aged alloys can lead to a remarkable decrease in mechanical properties in the matrix. For example Marzoli *et al*. have reported dissolution of precipitates during FSW of AA6061/Al_2O_3 composite which lead to a hardness drop in the stir zone [101]. In the literature precipitate dissolution, coarsening and reprecipitation have been reported in different regions during FSW/FSP of a variety of aluminum alloys [17, 74, 90]. Fragmentation assisted dissolution of particles has been observed as well [102]. Regarding the dissolution and coarsening of the strengthening precipitates, one of the advantages of adding ceramic reinforcements to aluminum matrixes is that they are thermally stable and can maintain their strengthening contribution at elevated temperatures.

1.1.5 Mechanical Properties of Metal Matrix Composite

Metal matrix composites indicate significantly improved mechanical properties over monolithic materials. Among MMCs reinforced with different kinds of reinforcements particulate reinforced MMCs are more attractive due to their simple fabrication methods, isotropic properties and cost effectiveness [103]. Generally incorporation of reinforcing particles to a metal matrix improves strain hardening, Young's modulus, hardness, yield strength and ultimate tensile strength but reduces the ductility. Table 1-2 shows mechanical properties of different aluminum matrix composites.

Table 1-2: Mechanical properties of aluminum matrix composites [104].

Matrix	Reinforcement, content (vol.%)	Yield strength R_e (MPa)	Tensile strength R_m (MPa)	Elongation (%)
Al	–	64	90	21
Al	SiC, 20	117	200	10
2014-T6	–	429	476	7.5
2014-T6	SiC, 10	457	508	1.8
2014-T6	Al_2O_3, 20	495	515	1.2
6061-T6	–	275	290	18
6061-T6	SiC, 15	290	340	5.5
6061-T6	SiC, 20	345	410	4.9
6061-T6	SiC, 30	380	435	1.8
6061-T6	Al_2O_3, 20	307	349	5.3
7091-T6	–	520	590	10.2
7091-T6	SiC, 20	500	560	1.8

It has been shown that two types of strengthening mechanism may occur in particle reinforced metal matrix composites: direct and indirect. Direct strengthening happens as a result of load transfer from the matrix to the reinforcing particles and indirect strengthening happens due to the effects of the particles on the microstructure and deformation behaviour of the matrix [105]. Increase in yield strength and work hardening directly partly relates to load transfer strengthening processes [98] whereas increased density of dislocations and hindering of dislocation movements caused by particles is mainly responsible for the enhanced hardness and also yield and ultimate tensile strengths as an indirect mechanism [81]. The coefficient of thermal expansion (CTE) mismatch between the metal matrix and ceramic particles induces stresses at the matrix/particle interface during thermal cycles, which can lead to localized plastic deformation or microplasticity and increased number of dislocations [98, 105]. On the other hand, under tensile or compressive forces, mismatch in elastic modulus between the matrix and the particles also plays an important role in creating

microplasticity and increasing dislocation density [105]. Such microplasticity is known to be an important cause for yield strength improvement [98].

Decohesion at matrix/reinforcement interface and particle fracture often initiate premature failure during deformation of composites. Interface decohesion has been shown to happen more in very soft matrixes such as pure aluminum or at elevated temperatures, but at temperatures around room temperature composite failure usually occurs as a result of particle fracture [106]. Under loading when the matrix starts to deform plastically followed by work hardening, the load carried out by the particles will gradually increase. After a while this increase in load will lead to particle fracture. When a single particle fails, the load relaxed by its fracture will introduce plastic deformation to the matrix until the matrix reaches its maximum strain hardening capacity. Then the relaxed load will be transferred to the neighbouring particles where it causes more reinforcements to fail. Finally the composite will fail following a ductile fracture mechanism by void nucleation and coalescence happening in the matrix. It should be noted that fractured particles are good source of void nucleation and growth as well [106, 107]**.** Considering particles dimensions, large particles are more likely to contain a critical sized flaw so they are more prone to fracture; probably this is why composites with finer particles often show better ductility [105-107]. But by utilizing fine particles the total interfacial area increases so interfacial decohesion is more probable to happen. Therefore high stresses are needed to fracture the particles or cause interfacial decohesion, and also it is harder for the damage to

accumulate so the composite will exhibit better ductility [107]. Figure 1-7 shows the effect of particle size on ductility of some aluminum matrix composites.

Particle distribution also significantly affects ductility of a composite. Figure 1-8 shows the ductility of A356/SiC composite as a function of extrusion ratio, considering that higher extrusion ratios produce a composite with better particle distribution. Non-uniform distribution of reinforcements accelerates damage accumulation and hence decreases ductility [98]. It will be discussed later that experimental results show FSP is really successful in producing a composite with very uniform dispersion of the reinforcement.

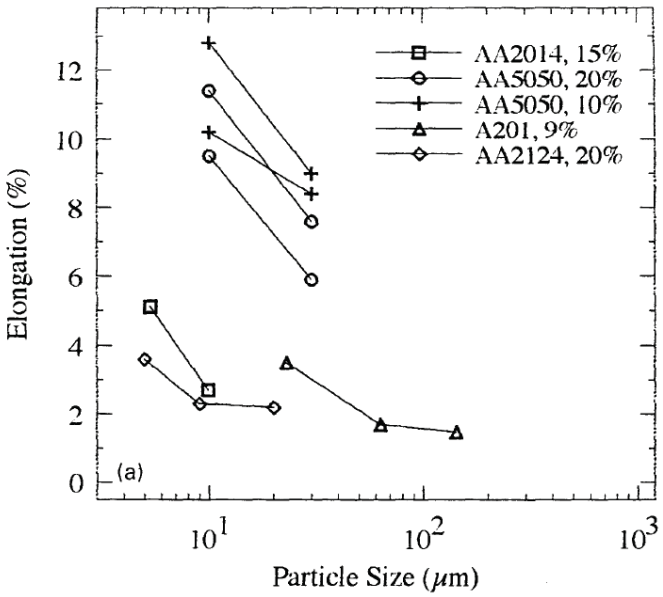

Figure 1-7: Effect of SiC particle size on ductility of different aluminum matrixes [98].

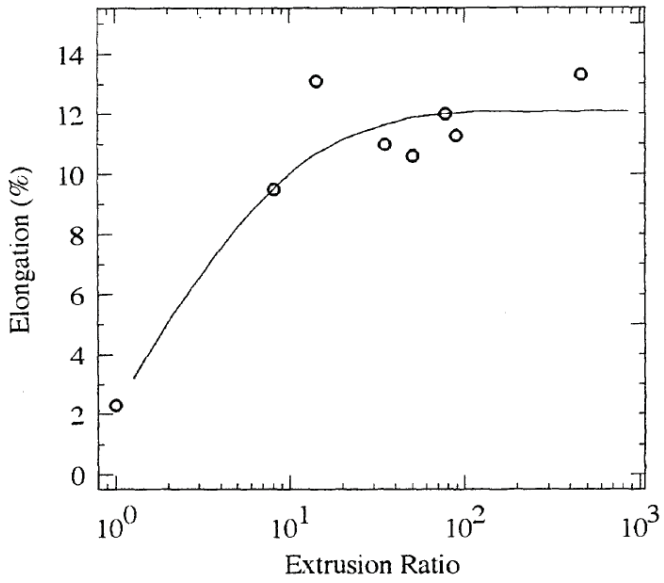

Figure 1-8: Effect of extrusion ratio (particle distribution) on ductility of A356 aluminum alloy reinforced with 15%vol SiC particles [98].

1.2 Effect of Friction Stir Processing Parameters on Metal Matrix Composites Properties

1.2.1 Microstructure

The microstructure of FSW/FSP composites generally shows the same three regions as ordinary FSW/FSP joints, but HAZ is usually very small and limited. This occurs because the existence of ceramic particles increases the thermal stability of the metal matrix. Of course it depends on the properties and volume percentage of the reinforcement [108]. Marzoli *et al*. have attributed the lower heat input sensitivity of MMCs to the limited flow of the plasticized material caused by the secondary particles which may postpone the recrystallization too [101]. FSP distributes reinforcing particles only to the extent of the stir zone which is slightly larger than the tool. Mahmoud *et al*. have shown

that nugget size increases with rotation speed and tool size as a result of more heat generation and plastic deformation. They have also reported that although the tool profile affects the particles distribution but it has no significant effect on the size of the stir zone [65].

As discussed before, dynamic recrystallization during FSW/FSP generates fine and equiaxed grains in the stir zone. However the final grain size strongly depends on process parameters. Finer grains may be achieved by decreasing rotation speed, which confines grain growth, or by increasing the degree of deformation which promotes recrystallization [2]. Secondary particles also play an important role on the size of the recrystallized grains in friction stir processed MMCs. According to the literature they can improve grain refinement by: 1) grain boundary pinning [37, 51, 55, 65, 109] 2) increasing the induced strain and dislocation density [27, 51, 55, 98, 107, 109, 110], and 3) acting as nucleation sites [37, 55, 110-112]. Grain boundary pinning and particle assisted nucleation highly depend on particle properties, for example large particles may not restrict grain boundary migration or enhance grain nucleation. But all secondary particles increase induced strain by creating stress concentration centers and confining dislocation movement. These factors effectively improve grain refinement, for example Morisada *et al*. have measured the grain size of friction stir processed AZ31 magnesium alloy and reported the grain size of 6 μm and 12.9 μm for AZ31 with and without SiC particles respectively [51]. Shafiei *et al*. have produced Al/Al_2O_3 nanocomposite by FSP with the matrix having some grains less than 300

nm in size [37] which is much finer than friction stir welded/processed unreinforced aluminum which typically achieves grain sizes >1 μm.

As mentioned before the microstructure of the stir zone contains a banded structure in conventional monolithic friction stir welded parts, several papers [12, 46, 110, 113] have also reported formation of such structure in different friction stir welded/processed composites. However these bands are not necessarily formed by segregation of reinforcing particles to the bands. For example, Feng *et al*. have explained that reinforcing particles are not segregated along the bands of onion rings suggesting that the shear stress had not been large enough to drive the reinforcing particles to segregate [110].

1.2.2 Particle size and distribution

Shear stresses caused by tool rotation during FSW/FSP may change shape and size of the particles. Particle fracture and refinement have been reported extensively [12, 27, 65, 67, 114-116]. Mahmoud *et al*. have investigated the effects of tool shape on fabrication of Al/SiC composite via FSP and observed more particle fracture when using square or triangle probe in comparison to circular pin [65]. It is also shown that higher rotation speeds and lower travel speeds promote particle fragmentation [115] which is probably due to the resulting increase in shear stresses. Pirondi *et al*. have studied the shape factor of Al_2O_3 particles in aluminum matrix before and after friction stir welding and indicated that erosion caused on the surface of the particles by tool rotation increases particles roundness [114]. Tewari *et al*. have used advanced

characterization techniques and proved particle rotation and reorientation after FSP on extruded Al/SiC composite [30]. Fracture has also been reported for fiber or tube (i.e. high aspect ratio) reinforcements [42, 48] following almost the same behaviour mentioned above for particles.

FSP is known to be very successful in producing composites with good uniform distribution of the secondary particles [17, 18, 110]. It is known that process parameters may affect particle distribution in different ways; by applying low axial force or low target depth particles will not distribute at all and with high axial force or high target depth all the particles will be pushed away from the pin surface so a moderate depth gives best distribution [27, 38]. It is shown that a square probe tool is more effective in uniformly distributing SiC particles in an aluminum matrix when compared to circular or triangle probe tools [65], similar results have been also reported for Al/TiB_2 composites produced by FSP [117]. Azizieh *et al*. have stated best Al_2O_3 distribution in AZ31 matrix can be achieved by using a tool having a circular threaded pin without flutes [53]. Increasing travel speed may lead to lower heat input which could result in incomplete martial flow needed for particle distribution [15], and so repeated FSP passes may be needed to improve distribution by introducing more stirring and mixing [38, 50, 116]. Tool rotation determines the stirring and mixing of the stir zone material [2] therefore an increase in tool rotation speed causes more stirring and mixing which generally results in better particle distribution [15, 53]. On the other hand low rotation speeds results in limited heat generation and as the material flow is affected by the heat input, complete mixing needed for uniform particle distribution will not

occur. However Mahmoud *et al*. have reported best particle distribution by decreasing the rotation speed to as low as possible to achieve a defect-free nugget, though no detailed explanation was provided [65, 116]. In a recent work Lim *et al*. have indicated some agglomerations of the carbon nanotubes in aluminum matrix [41] which might be due to the nano size or high aspect ratio of the reinforcement or inadequate process parameters.

1.2.3 Hardness

For non-heat treatable aluminum alloys, where there is no precipitation hardening usually the stir zone shows the maximum hardness because of: 1) grain refinement caused by severe plastic deformation introduced during FSW/FSP [65, 69, 108, 118] and 2) decreased size and increased number of particles as a result of particle fragmentation happened during FSW/FSP [65, 108, 118]. If these alloys are processed in the work hardened condition there might be a hardness decrease in the HAZ as a result of recovery of work hardening [116]. Figure 1-9 schematically shows the hardness response in friction stir welded/processed non heat treatable aluminum alloys. For heat treatable aluminum alloys which are not in the peak aged condition, the maximum hardness will also appear in the nugget [12, 37] following the same reasons and also probably due to formation of strengthening precipitates in the stir zone. But as discussed before in Section 1.1.4 for heat treatable aluminum alloys that are in peak aged condition, temperature variations during FSW/FSP may lead to particle coarsening, dissolution and reprecipitation.

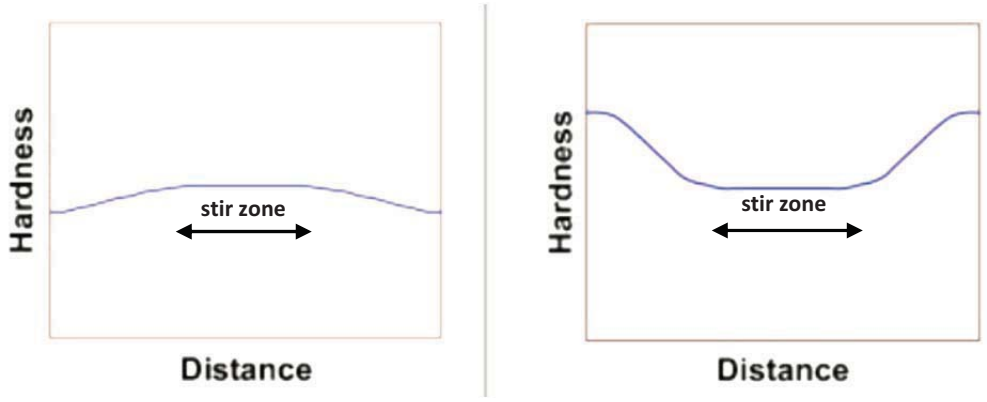

a) b)

Figure 1-9: Schematic plots showing hardness profile in friction stir welded/processed non heat treatable aluminum alloys, a) in the annealed condition and b) in the work hardened condition. Modified from [90].

It is suggested that the general decrease is attributed to the effect of thermal cycles on the precipitates in a way that they are coarsened in HAZ and dissolved in the nugget [38, 41, 90]. Results for magnesium based composites processed by FSP also show significant improvement in hardness which in addition to the strengthening effect of the particles is related to the grain refinement that occurs during FSP [16, 50, 52, 55].

1.2.4 Toughness

As shown in Figure 1-10, Amirizad *et al*. have reported enhanced elongation to failure in the stir zone of friction stir welded A356/SiC cast composites. They have attributed this improvement to microstructure modification, uniform distribution of SiC particles and elimination of the micro porosity created during casting [108].

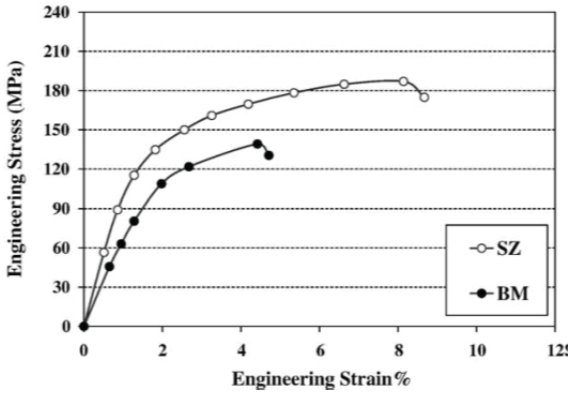

Figure 1-10: Tensile properties of friction stir welded A36/15%volSiC [108].

Berbon *et al*. have friction stir processed an aluminum matrix composite produced by powder metallurgy and extrusion. The ductility of the composite was remarkably improved after FSP which is mainly due to microstructure modification and effective improvement in particle distribution. Figure 1-11 shows microstructure of their samples in the as-extruded condition and after FSP. It can be concluded from this Figure that FSP is really effective in eliminating porosities and enhancing the particle distribution which lead to increased ductility of the composite [11].

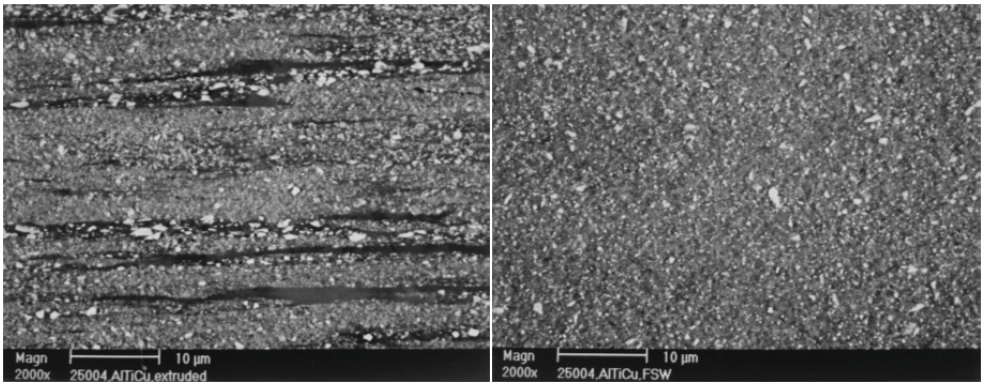

Figure 1-11: Al/Al_3Ti composite microstructure, left as-extruded and right friction stir processed [11].

As explained in Section 1.5, the ductility of a composite depends on size, shape and distribution of the particles as well as the microstructure and mechanical properties of the matrix. Comparing FSP with other fabrication methods for MMCs, this method has the potential to produce composites with better toughness by: 1) decreasing particles size through breaking them [12, 67, 114, 116], 2) increasing the roundness of the particles which reduces stress intensity available at sharp edges [114], 3) increasing homogeneity of particle distribution [11, 55], 4) modifying microstructure of the matrix [11, 108], and 5) reducing the grain size of the matrix [11, 114, 119].

1.3 Microstructure and mechanical properties of Al 5XXX series alloys

1.3.1 Microstructural behavior and strengthening mechanisms in Al 5XXX series alloys

Al 5XXX series are a group of not heat treatable wrought aluminum alloys with applications in ship building, military, aerospace and auto industries [120]. The main alloying element is Mg which provides strength by solid solution strengthening and work hardening and also improves corrosion resistance [121]. Other alloying elements such as Cr, Fe, Mn, Zr, Cu and Si may also be added to these alloys for different properties and applications. For example Cr is usually added to enhance corrosion resistance [122] and Zr is added (as in Al 5059) to

promote grain refinement by forming fine grain boundary pinning dispersoids [123]. Addition of iron, manganese, zinc, silicon and copper to Al-Mg alloys leads to formation of precipitates that can contribute to strength [122]. The most widely reported precipitate in Al 5XXX series alloys are the $Al_6(Mn,Fe)$ type particles [6, 124, 125], but depending on the alloy composition other precipitates may also exist in the microstructure [121, 126, 127].

Microstructure of friction stir welded/processed Al 5XXX series alloys usually consists of fine equiaxed grains, which are formed as a result of dynamic recrystallization, along with a considerable amount of precipitates [102, 128, 129]. The size of the recrystallized grains and volume fraction of the precipitates depends on chemical composition of the alloy and processing conditions. Considering the effect of Mg on grain boundary mobility and dislocation density, alloys with higher Mg content (more than 3 wt%) have finer recrystallized grains. Submicron sized grains are achieved in friction stir welds of Al 5083 using a rotation speed of 560 rpm and a travel speed of 25 mm/min [130].

Generally any microstructural feature that interferes with dislocation motion causes strengthening and can be considered as a strengthening mechanism, examples are: crystal lattice defects, grain boundaries, solute atoms, precipitates and other dislocations [100]. In Al-Mg alloys, the effectiveness of each of these parameters depends on the chemical composition and deformation and heat treatment history of the alloy and this is why these alloys may or may not follow the Hall-Petch behavior, for example see [102, 131, 132]. In this regard a good model for strengthening in Al-Mg alloys should consider all the above mentioned

mechanisms as suggested by Huskins and Ramesh for Al 5083 [133]. Generally in metallic materials yield stress or hardness is mathematically related to grain size by Hall-Petch relation [134, 135]:

$$H = H_0 + k_H d^{-\frac{1}{2}} \quad (1.7)$$

where H is hardness, d is grain diameter and H_0 and k_H are Hall-Petch constants.

Magnesium being the major alloying element in Al 5059, mostly goes into solid solution and results in strengthening through solute/dislocation interaction and other alloying elements such as manganese, silicon and iron form precipitates that strengthen the alloy via precipitate/dislocation interaction [133, 136, 137]. Dislocation/dislocation interaction may contribute to strength as well. Al-Mg alloys exhibit particularly high dislocation densities after plastic deformation [138] which is related to the effect of Mg on hindering dislocation annihilation [139]. As in these alloys Mg atoms are substitutional, they tend to diffuse to the dislocation core and form clusters to reduce the lattice energy. Such clusters of Mg atoms delay the dislocation's movement [133]. It is showed that in ultrafine grained Al-Mg alloys additional mechanisms related to stacking faults and nanotwins, and nonequilibrium grain boundaries also contribute to strength [138].

However among the above mentioned strengthening mechanisms, the overall strength of an alloy is highly influenced by grain size or volume fraction of the precipitates. In an alloy with a random distribution of particles with radius r volume fraction f, the average distance between particles L can be measured by [125]:

$$L = \left(\frac{2\pi}{3f}\right)^{0.5} r \quad (1.8)$$

Depending on the properties of the precipitates for each specific alloy if *L* is larger than the grain size then dislocation/grain boundary interaction is more probable than dislocation/precipitate interaction and therefore grain refinement can cause strengthening following the Hall-Petch relationship; but if *L* is smaller than the grain size, strengthening by the precipitates is the dominant strengthening mechanism. In Al-Mg alloys with minor additions of other alloying elements the volume fraction of precipitates is low, and therefore a Hall-Petch relation can be found between the grain size and strength (or hardness) as shown for example for friction stir welds of Al 5052 [128]. In the case of Al-Mg alloys with higher amount of other alloying elements, such as Mn, Fe, Si and Cr, strengthening is significantly affected by precipitates, as shown for example for Al 5083 [125].

1.3.2 Grain Growth in Al 5XXX series alloys

It is generally believed that fine recrystallized grains form during friction stir welding and then as the weld cools down to room temperature grain growth may occur, for example see [132]. Grain sizes in the range of 1 – 10 μm are extensively reported for different aluminum alloys friction stir welded/processed with different process parameters [2], but it was shown that submicron sized grains are also achievable by rapid cooling of the plates right after the process which stops the grain growth. For example Yazdipour *et al*. [130] have utilized a mixture of methanol and dry ice to rapidly cool the material behind the tool

during friction stir welding of Al 5083. They have shown this results in the formation of grains in the range of 80 nm to 0.9 μm using a rotation speed of 560 rpm and a travel speed of 25 mm/min. Gerlich *et al*. [129] have compared the average size of stir zone grains in air-cooled and rapidly-cooled (in a mixture of methanol and liquid nitrogen) friction stir spot welds of Al 6061 and Al 5754 to study the grain growth behavior during the cooling cycle of the welds. No evidence of grain growth has been observed in Al 5754 which they have attributed to the solute drag effect of Mg on reducing the grain boundary mobility. On the other hand, in the stir zone of Al 6061 welds normal grain growth was observed which was represented using an Arrhenius growth equation:

$$d_f^2 - d_0^2 = A_0 \cdot exp\left(\frac{-Q}{R_g T}\right) \cdot t \qquad (1.9)$$

where d_f and d_0 are the final and initial grain diameters, A_0 is a constant, Q is the activation energy, T is the absolute temperature and R_g is the universal gas constant. Equation (1.9) has also been used for grain size evolution during FSW of Al 5083, where no evidence of abnormal grain growth was observed [140]. Robson *et al*. [141] have developed a model for stir zone grain evolution based on geometrical dynamic recrystallization followed by grain growth. They have used the particle controlled grain growth equation for the relation between grain size and annealing time:

$$\frac{dR}{dt} = A\left(\frac{1}{R} - \frac{1}{R_m}\right) \qquad (1.10)$$

where R is the grain radius, t is time and A is the reduced grain boundary mobility, R_m is the limiting grain size. Their model predicts the formation of submicron sized grains as a result of the initial recrystallization and subsequent rapid grain growth in the region behind the pin. Then the growth rate decreases as the material cools down. The resulting final grain size will be smaller than R_m. They have successfully applied their model to predict grain sizes in Al 2524 friction stir welds [141].

In many applications friction stir welded/processed parts are heat treated for annealing or aging, therefore it is of significant interest to study the evolution of stir zone microstructure under thermal cycles. Many attempts have been done to model grain growth in friction stir welded/processed parts during heat treatment and to predict the stir zone grain size. Chen *et al*. [142] have studied the mechanism of grain coarsening in friction stir welded Al 5083 post weld heat treated at 738 K for 5 minutes and showed that abnormal grain growth is the mechanism of the formation of coarse grains (larger than 100 μm) within the welds having as-welded grain diameters smaller than 3 μm. However they have not suggested any model for the case of normal grain growth. Their results agree well with Humphrey's model [143] which predicts grain growth behavior (whether it is normal or abnormal) based on starting grain size and a particle pinning parameter. Other researchers have also used this model to predict microstructural stability in heat treated friction stir welds [144-146]. Depending on the annealing temperature, as-welded grain size and particles properties abnormal grain growth has been also reported in post weld heat treated

microstructure of friction stir welded Al 1100 [147], Al-4.5%Cu-1.5%Mg [148], Al 2095 [149], Al 2024 [150], Al 2014 [151], Al 2195 [152], Al 2004 [153], Al-6.8%Si [144], Al 5083 [154], Al 6082 [155], Al 7010 [146], Al 7075 [156]. Further information on abnormal grain growth in friction stir welded/processed aluminum alloys may be found in [157].

Furukawa *et al*. have fabricated submicron sized grains in Al-3% Mg alloy by Equal Channel Angular Pressing (ECAP) and torsion straining [158]. After annealing their samples at different temperatures in the range of 323 to 803 K for 1 hour, they have reported two distinct values for activation energy of grain growth which are related to the boundary structure. At very small grain sizes where the boundaries are mostly in non-equilibrium condition, movement of extrinsic dislocations on boundaries leads to a low activation energy of ~25 KJ/mole but at larger grain sizes where the boundaries have an equilibrium configuration, grain boundary diffusion leads to a high activation energy of ~85 KJ/mole [158, 159]. This difference in grain growth activation energy between nano-sized and micron-sized grains has been also observed for Al 5083 [160]. Furthermore it is indicated in another study on Al-3% Mg alloy that the ECAP processed samples with an average grain size of ~0.2 μm showed no grain growth up to 473 K and after annealing for 32 hours only recovery occurred [159, 161]. This grain size stability up to 473 K has been attributed to the presence of impurities (mostly Fe and Si) in this alloy which leads to precipitation of very fine dispersoids on grain boundaries [162].

1.4 Research Objective and Thesis Structure

The objective of this thesis study is to first investigate the microstructure and mechanical properties of Al 5059 before and after friction stir processing and then produce Al 5059 matrix composites reinforced with different particles using friction stir processing.

Despite the good mechanical properties and corrosion resistance of Al 5059, the details regarding the physical metallurgy and mechanical properties of this alloy are very limited in the literature; no information is available about the microstructural features such as precipitates or the dominant strengthening mechanism in this alloy. In addition, friction stir welding/processing can be a good joining/processing method for this alloy in different applications, therefore it is important to determine the effect of processing parameters on properties of Al 5059. In Chapter 2 microstructure and mechanical properties of Al 5059 are investigated when friction stir processed using different rotation and travel speeds and tool geometries and finally the parameters that give the best mechanical properties are determined. According to the importance of grain size in terms of the mechanical properties, grain growth behaviour of friction stir processed Al 5059 during subsequent heat treatment is studied in Chapter 3 and a model is suggested that relates grain size to annealing time. Chapter 4 proposes the developed multi pass/multi tool method for MMCs fabrication by FSP. Different reinforcing materials have been tested and effect of processing parameters on mechanical properties of the produced composites is investigated.

1.5 References

[1] Thomas WM, Nicholas ED, Needham JD, Murch MG, Templesmith P, Daws CJ. 1991.

[2] Mishra RS, Ma ZY. Friction stir welding and processing. Materials Science and Engineering R: Reports 2005;50.

[3] Arora HS, Singh H, Dhindaw BK. Some observations on microstructural changes in a Mg-based AE42 alloy subjected to friction stir processing. Metallurgical and Materials Transactions B: Process Metallurgy and Materials Processing Science 2012;43:92-108.

[4] Cavaliere P, De Marco PP. Friction stir processing of AM60B magnesium alloy sheets. Materials Science and Engineering A 2007;462:393-7.

[5] Feng AH, Ma ZY. Enhanced mechanical properties of Mg-Al-Zn cast alloy via friction stir processing. Scripta Materialia 2007;56:397-400.

[6] Fuller CB, Mahoney MW. The effect of friction stir processing on 5083-H321/5356 Al arc welds: Microstructural and mechanical analysis. Metallurgical and Materials Transactions A: Physical Metallurgy and Materials Science 2006;37:3605-15.

[7] Fuller MD, Swaminathan S, Zhilyaev AP, McNelley TR. Microstructural transformations and mechanical properties of cast NiAl bronze: Effects of fusion welding and friction stir processing. Materials Science and Engineering A 2007;463:128-37.

[8] Oh-Ishi K, McNelley TR. Microstructural modification of as-cast NiAl bronze by friction stir processing. Metallurgical and Materials Transactions A: Physical Metallurgy and Materials Science 2004;35 A:2951-61.

[9] Tsujikawa M, Chung SW, Tanaka M, Takigawa Y, Oki S, Higashi K. High-strengthening of Mg - 5.5 mass % Y-4.3 mass % Zn cast alloy by friction stir processing. Materials Transactions 2005;46:3081-4.

[10] Bauri R, Yadav D, Suhas G. Effect of friction stir processing (FSP) on microstructure and properties of Al-TiC in situ composite. Materials Science and Engineering A 2011;528:4732-9.

[11] Berbon PB, Bingel WH, Mishra RS, Bampton CC, Mahoney MW. Friction stir processing: A tool to homogenize nanocomposite aluminum alloys. Scripta Materialia 2001;44:61-6.

[12] Cavaliere P. Mechanical properties of Friction Stir Processed 2618/Al2O3 metal matrix composite. Composites Part A: Applied Science and Manufacturing 2005;36:1657-65.

[13] Hodder KJ, Izadi H, McDonald AG, Gerlich AP. Fabrication of aluminum–alumina metal matrix composites via cold gas dynamic spraying at low pressure followed by friction stir processing. Materials Science and Engineering: A 2012;556:114-21.

[14] Morisada Y, Fujii H, Mizuno T, Abe G, Nagaoka T, Fukusumi M. Modification of thermally sprayed cemented carbide layer by friction stir processing. Surface and Coatings Technology 2010;204:2459-64.

[15] Morisada Y, Fujii H, Nagaoka T, Fukusumi M. MWCNTs/AZ31 surface composites fabricated by friction stir processing. Materials Science and Engineering A 2006;419:344-8.

[16] Lee CJ, Huang JC, Hsieh PJ. Mg based nano-composites fabricated by friction stir processing. Scripta Materialia 2006;54:1415-20.

[17] Ma ZY. Friction stir processing technology: A review. Metallurgical and Materials Transactions A: Physical Metallurgy and Materials Science 2008;39 A:642-58.

[18] Gan YX, Solomon D, Reinbolt M. Friction Stir Processing of Particle Reinforced Composite Materials. Materials 2010;3:329-50.

[19] Santella ML, Engstrom T, Storjohann D, Pan TY. Effects of friction stir processing on mechanical properties of the cast aluminum alloys A319 and A356. Scripta Materialia 2005;53:201-6.

[20] Nakata K, Kim YG, Fujii H, Tsumura T, Komazaki T. Improvement of mechanical properties of aluminum die casting alloy by multi-pass friction stir processing. Materials Science and Engineering A 2006;437:274-80.

[21] Pilchak AL, Norfleet DM, Juhas MC, Williams JC. Friction stir processing of investment-cast Ti-6Al-4V: Microstructure and properties. Metallurgical and Materials Transactions A: Physical Metallurgy and Materials Science 2008;39:1519-24.

[22] Ma ZY, Sharma SR, Mishra RS. Microstructural modification of As-cast Al-Si-Mg alloy by friction stir processing. Metallurgical and Materials Transactions A: Physical Metallurgy and Materials Science 2006;37:3323-36.

[23] Ni DR, Xue P, Ma ZY. Effect of multiple-pass friction stir processing overlapping on microstructure and mechanical properties of as-cast NiAl bronze. Metallurgical and Materials Transactions A: Physical Metallurgy and Materials Science 2011;42:2125-35.

[24] Sun N, Apelian D. Friction stir processing of aluminum cast alloys for high performance applications. JOM 2011;63:44-50.

[25] Xiao BL, Yang Q, Yang J, Wang WG, Xie GM, Ma ZY. Enhanced mechanical properties of Mg-Gd-Y-Zr casting via friction stir processing. Journal of Alloys and Compounds 2011;509:2879-84.

[26] Zahmatkesh B, Enayati MH. A novel approach for development of surface nanocomposite by friction stir processing. Materials Science and Engineering A 2010;527:6734-40.

[27] Mishra RS, Ma ZY, Charit I. Friction stir processing: A novel technique for fabrication of surface composite. Materials Science and Engineering A 2003;341:307-10.

[28] Liu P, Shi Q, Bian X, Xu S, Ren G. Microstructure of a novel Al-based amorphous reinforced aluminum metal matrix composite. Hanjie Xuebao/Transactions of the China Welding Institution 2009;30:13-6.

[29] Mahmoud ERI, Takahashi M, Shibayanagi T, Ikeuchi K. Wear characteristics of surface-hybrid-MMCs layer fabricated on aluminum plate by friction stir processing. Wear 2010;268:1111-21.

[30] Tewari A, Spowart JE, Gokhale AM, Mishra RS, Miracle DB. Characterization of the effects of friction stir processing on microstructural

changes in DRA composites. Materials Science and Engineering A 2006;428:80-90.

[31] Wang W, Shi Qy, Liu P, Li Hk, Li T. A novel way to produce bulk SiCp reinforced aluminum metal matrix composites by friction stir processing. Journal of Materials Processing Technology 2009;209:2099-103.

[32] Alidokht SA, Abdollah-zadeh A, Soleymani S, Assadi H. Microstructure and tribological performance of an aluminium alloy based hybrid composite produced by friction stir processing. Mater Design 2011;32:2727-33.

[33] Devaraju A, Kumar A, Kotiveerachari B. Influence of rotational speed and reinforcements on wear and mechanical properties of aluminum hybrid composites via friction stir processing. Materials and Design 2013;45:576-85.

[34] Salehi M, Saadatmand M, Aghazadeh Mohandesi J. Optimization of process parameters for producing AA6061/SiC nanocomposites by friction stir processing. Transactions of Nonferrous Metals Society of China (English Edition) 2012;22:1055-63.

[35] Soleymani S, Abdollah-zadeh A, Alidokht SA. Microstructural and tribological properties of Al5083 based surface hybrid composite produced by friction stir processing. Wear 2012;278-279:41-7.

[36] Sharifitabar M, Sarani A, Khorshahian S, Shafiee Afarani M. Fabrication of 5052Al/Al2O3 nanoceramic particle reinforced composite via friction stir processing route. Materials and Design 2011;32:4164-72.

[37] Shafiei-Zarghani A, Kashani-Bozorg SF, Zarei-Hanzaki A. Microstructures and mechanical properties of Al/Al2O3 surface nano-composite layer produced by friction stir processing. Materials Science and Engineering A 2009;500:84-91.

[38] Yang M, Xu C, Wu C, Lin KC, Chao YJ, An L. Fabrication of AA6061/Al2O3 nano ceramic particle reinforced composite coating by using friction stir processing. Journal of Materials Science 2010;45:4431-8.

[39] Mazaheri Y, Karimzadeh F, Enayati MH. A novel technique for development of A356/Al2O3 surface nanocomposite by friction stir processing. Journal of Materials Processing Technology 2011;211:1614-9.

[40] Dixit M, Newkirk JW, Mishra RS. Properties of friction stir-processed Al 1100-NiTi composite. Scripta Materialia 2007;56:541-4.

[41] Lim DK, Shibayanagi T, Gerlich AP. Synthesis of multi-walled CNT reinforced aluminium alloy composite via friction stir processing. Materials Science and Engineering A 2009;507:194-9.

[42] Johannes LB, Yowell LL, Sosa E, Arepalli S, Mishra RS. Survivability of single-walled carbon nanotubes during friction stir processing. Nanotechnology 2006;17:3081-4.

[43] Izadi H, Gerlich AP. Distribution and stability of carbon nanotubes during multi-pass friction stir processing of carbon nanotube/aluminum composites. Carbon 2012;50:4744-9.

[44] Liu Q, Ke L, Liu F, Huang C, Xing L. Microstructure and mechanical property of multi-walled carbon nanotubes reinforced aluminum matrix composites fabricated by friction stir processing. Materials and Design 2013;45:343-8.

[45] Xu W, Ke L, Li X, Zhang Z, Zhao X. Study of carbon nanotubes on wear performance of aluminum matrix composites by friction stir processing. Corvallis, OR2011. p. 307-11.

[46] Morisada Y, Fujii H, Nagaoka T, Nogi K, Fukusumi M. Fullerene/A5083 composites fabricated by material flow during friction stir processing. Composites Part A: Applied Science and Manufacturing 2007;38:2097-101.

[47] Yadav D, Bauri R. Nickel particle embedded aluminium matrix composite with high ductility. Materials Letters 2010;64:664-7.

[48] Zhang L, Chandrasekar R, Howe JY, West MK, Hedin NE, Arbegast WJ, *et al*. A Metal Matrix Composite Prepared from Electrospun TiO2 Nanofibers and an Al 1100 Alloy via Friction Stir Processing. Applied Materials and Interfaces 2009;1:987-91.

[49] Rejil CM, Dinaharan I, Vijay SJ, Murugan N. Microstructure and sliding wear behavior of AA6360/(TiC+B 4C) hybrid surface composite layer synthesized by friction stir processing on aluminum substrate. Materials Science and Engineering A 2012;552:336-44.

[50] Chang CI, Wang YN, Pei HR, Lee CJ, Du XH, Huang JC. Microstructure and Mechanical Properties of Nano-ZrO2 and Nano-SiO2 Particulate Reinforced AZ31-Mg Based Composites Fabricated by Friction Stir Processing. Key Engineering Materials 2007;351:114-9.

[51] Morisada Y, Fujii H, Nagaoka T, Fukusumi M. Effect of friction stir processing with SiC particles on microstructure and hardness of AZ31. Materials Science and Engineering A 2006;433:50-4.

[52] Morisada Y, Fujii H, Nagaoka T, Fukusumi M. Nanocrystallized magnesium alloy - uniform dispersion of C₆₀ molecules. Scripta Materialia 2006;55:1067-70.

[53] Azizieh M, Kokabi AH, Abachi P. Effect of rotational speed and probe profile on microstructure and hardness of AZ31/Al 2O 3 nanocomposites fabricated by friction stir processing. Materials and Design 2011;32:2034-41.

[54] Sun K, Shi QY, Sun YJ, Chen GQ. Microstructure and mechanical property of nano-SiCp reinforced high strength Mg bulk composites produced by friction stir processing. Materials Science and Engineering A 2012;547:32-7.

[55] Asadi P, Faraji G, Besharati MK. Producing of AZ91/SiC composite by friction stir processing (FSP). International Journal of Advanced Manufacturing Technology 2010:1-14.

[56] Asadi P, Givi MKB, Abrinia K, Taherishargh M, Salekrostam R. Effects of SiC particle size and process parameters on the microstructure and hardness of AZ91/SiC composite layer fabricated by FSP. J of Materi Eng and Perform 2011;20:1554-62.

[57] Faraji G, Asadi P. Characterization of AZ91/alumina nanocomposite produced by FSP. Materials Science and Engineering A 2011;528:2431-40.

[58] Mostafapour A, Khayyamin D, Keshmiri R. The Effect of Process Parameters on Microstructural Characteristics of AZ91/SiO2 Composite Fabricated by FSP. Materials Science and Engineering: A 2012.

[59] Mertens A, Simar A, Delannay F. C fibres - Mg matrix composites produced by squeeze casting and friction stir processing: Microstructure & mechanical behaviour. Quebec City, QC2012. p. 1221-6.

[60] Barmouz M, Besharati Givi MK, Seyfi J. On the role of processing parameters in producing Cu/SiC metal matrix composites via friction stir processing: Investigating microstructure, microhardness, wear and tensile behavior. Materials Characterization 2011;62:108-17.

[61] Asadi P, Besharati Givi MK, Barmouz M. Effect of SiC volume fraction on the microstructural and mechanical properties of Cu/SiC composite layer fabricated by FSP. Paris2011. p. 500-5.

[62] Chen W, Huang C, Ke L. A novel way to fabricate carbon nanotubes reinforced copper matrix composites by Friction Stir Processing. Shenyang, Liaoning2012. p. 524-9.

[63] Salekrostam R, Givi MKB, Asadi P, Bahemmat P. Influence of friction stir processing parameters on the fabrication of SiC/316L surface composite Deffects and Diffusion Forum 2010;297-301:221-6.

[64] Ghasemi-Kahrizsangi A, Kashani-Bozorg SF. Microstructure and mechanical properties of steel/TiC nano-composite surface layer produced by friction stir processing. Surface and Coatings Technology 2012;209:15-22.

[65] Mahmoud ERI, Takahashi M, Shibayanagi T, Ikeuchi K. Effect of friction stir processing tool probe on fabrication of SiC particle reinforced composite on aluminium surface. Science and Technology of Welding and Joining 2009;14:413-25.

[66] Ke L, Huang C, Xing L, Huang K. Al-Ni intermetallic composites produced in situ by friction stir processing. Journal of Alloys and Compounds.

[67] Hsu CJ, Chang CY, Kao PW, Ho NJ, Chang CP. Al-Al3Ti nanocomposites produced in situ by friction stir processing. Acta Materialia 2006;54:5241-9.

[68] Hsu CJ, Kao PW, Ho NJ. Intermetallic-reinforced aluminum matrix composites produced in situ by friction stir processing. Materials Letters 2007;61:1315-8.

[69] Hsu CJ, Kao PW, Ho NJ. Ultrafine-grained Al-Al2Cu composite produced in situ by friction stir processing. Scripta Materialia 2005;53:341-5.

[70] Liu HJ, Feng JC, Fujii H, Nogi K. Wear characteristics of a WC-Co tool in friction stir welding of AC4A+30 vol%SiCp composite. International Journal of Machine Tools and Manufacture 2005;45:1635-9.

[71] Prado RA, Murr LE, Shindo DJ, Soto KF. Tool wear in the friction-stir welding of aluminum alloy 6061 + 20% Al2O3: A preliminary study. Scripta Materialia 2001;45:75-80.

[72] Gerlich A. Local Melting and Tool Slippage during Friction Stir Spot Welding of Aluminum Alloys. Toronto: University of Toronto; 2007.

[73] Park K. DEVELOPMENT AND ANALYSIS OF ULTRASONIC ASSISTED FRICTION STIR WELDING PROCESS: University of Michigan; 2009.

[74] Nandan R, DebRoy T, Bhadeshia HKDH. Recent advances in friction-stir welding - Process, weldment structure and properties. Progress in Materials Science 2008;53:980-1023.

[75] Yalavarthy H. FRICTION STIR WELDING PROCESS AND MATERIAL MICROSTRUCTURE EVOLUTION MODELING IN 2000 AND 5000 SERIES OF ALUMINUM ALLOY: Clemson University; 2009.

[76] Darras BM. INTEGRATED THERMO-MECHANICAL INVESTIGATIONS OF FRICTION STIR PROCESSING OF LIGHT WEIGHT ALLOYS: University of Kentucky; 2008.

[77] Marghitu DB. Mechanical Engineer's Handbook: Academic Press; 2001.

[78] Seidel TU, Reynolds AP. Visualization of the material flow in AA2195 friction-stir welds using a marker insert technique. Metallurgical and Materials Transactions A: Physical Metallurgy and Materials Science 2001;32:2879-84.

[79] Fratini L, Buffa G, Palmeri D, Hua J, Shivpuri R. Material flow in FSW of AA7075-T6 butt joints: Numerical simulations and experimental verifications. Science and Technology of Welding and Joining 2006;11:412-21.

[80] Ouyang JH, Kovacevic R. Material flow and microstructure in the friction stir butt welds of the same and dissimilar aluminum alloys. J of Materi Eng and Perform 2002;11:51-63.

[81] Kainer KU. Metal Matrix Composites: Wiley-VCH; 2006.

[82] Morisada Y, Fujii H, Kawahito Y, Nakata K, Tanaka M. Three-dimensional visualization of material flow during friction stir welding by two pairs of X-ray transmission systems. Scripta Materialia 2011;65:1085-8.

[83] Colegrove PA, Shercliff HR. Experimental and numerical analysis of aluminium alloy 7075-T7351 friction stir welds. Science and Technology of Welding and Joining 2003;8:360-8.

[84] Bastier A, Maitournam MH, Dang Van K, Roger F. Steady state thermomechanical modelling of friction stir welding. Science and Technology of Welding and Joining 2006;11:278-88.

[85] Nandan R, Roy GG, Debroy T. Numerical simulation of three dimensional heat transfer and plastic flow during friction stir welding. Metallurgical and Materials Transactions A: Physical Metallurgy and Materials Science 2006;37:1247-59.

[86] Xu S, Deng X, Reynolds AP, Seidel TU. Finite element simulation of material flow in friction stir welding. Science and Technology of Welding and Joining 2001;6:191-3.

[87] Liechty BC, Webb BW. The use of plasticine as an analog to explore material flow in friction stir welding. Journal of Materials Processing Technology 2007;184:240-50.

[88] Yang Q, Mironov S, Sato YS, Okamoto K. Material flow during friction stir spot welding. Materials Science and Engineering A 2010;527:4389-98.

[89] Mukherjee S, Ghosh AK. Flow visualization and estimation of strain and strain-rate during friction stir process. Materials Science and Engineering A 2010;527:5130-5.

[90] Threadgilll PL, Leonard AJ, Shercliff HR, Withers PJ. Friction stir welding of aluminium alloys. International Materials Reviews 2009;54:49-93.

[91] SU P, Gerlich AP, North TH, BENDZSAK GJ. Intermixing in Dissimilar Friction Stir Spot Welds. METALLURGICAL AND MATERIALS TRANSACTIONS A 2007;38 A:584 - 95.

[92] Gerlich A, Su P, Yamamoto M, North TH. Material flow and intermixing during dissimilar friction stir welding. Science and Technology of Welding and Joining 2008;13:254-64.

[93] Sutton MA, Yang B, Reynolds AP, Taylor R. Microstructural studies of friction stir welds in 2024-T3 aluminum. Materials Science and Engineering A 2002;323:160-6.

[94] Krishnan KN. On the formation of onion rings in friction stir welds. Materials Science and Engineering A 2002;327:246-51.

[95] Mahoney MW, Rhodes CG, Flintoff JG, Spurling RA, Bingel WH. Properties of friction-stir-welded 7075 T651 aluminum. Metallurgical and Materials Transactions A: Physical Metallurgy and Materials Science 1998;29:1955-64.

[96] Schneider JA, Nunes Jr AC. Characterization of plastic flow and resulting microtextures in a friction stir weld. Metallurgical and Materials Transactions B: Process Metallurgy and Materials Processing Science 2004;35:777-83.

[97] Yin YH, Sun N, North TH, Hu SS. Microstructures and mechanical properties in dissimilar AZ91/AZ31 spot welds. Materials Characterization 2010;61:1018-28.

[98] Sinclair I, Gregson PJ. Structural performance of discontinuous metal matrix composites. Materials Science and Technology 1997;13:709-26.

[99] Esmaeili S, Lloyd DJ, Poole WJ. A yield strength model for the Al-Mg-Si-Cu alloy AA6111. Acta Materialia 2003;51:2243-57.

[100] Dietre GE. Mechanical Metallurgy: McGraw-Hill; 1988.

[101] Marzoli LM, Strombeck AV, Dos Santos JF, Gambaro C, Volpone LM. Friction stir welding of an AA6061/Al₂O₃/20p reinforced alloy. Composites Science and Technology 2006;66:363-71.

[102] Attallah MM, Davis CL, Strangwood M. Microstructure-microhardness relationships in friction stir welded AA5251. Journal of Materials Science 2007;42:7299-306.

[103] Chawla N, Shen Y-L. Mechanical Behavior of Particle Reinforced Metal Matrix Composites. ADVANCED ENGINEERING MATERIALS 2001;3:357-70.

[104] Kaczmara JW, Pietrzakb K, WøosinÂskic W. The production and application of metal matrix composite materials. Journal of Materials Processing Technology 2000;106:58-67.

[105] Dai LH, Ling Z, Bai YL. Size-dependent inelastic behavior of particle-reinforced metal-matrix composites. Composites Science and Technology 2001;61:1057-63.

[106] Llorca J, González C. Microstructural factors controlling the strength and ductility of particle-reinforced metal-matrix composites. Journal of the Mechanics and Physics of Solids 1998;46:1-28.

[107] Doel TJA, Bowen P. Tensile properties of particulate-reinforced metal matrix composites. Composites Part A: Applied Science and Manufacturing 1996;27:655-65.

[108] Amirizad M, Kokabi AH, Gharacheh MA, Sarrafi R, Shalchi B, Azizieh M. Evaluation of microstructure and mechanical properties in friction stir welded A356 + 15%SiC_p cast composite. Materials Letters 2006;60:565-8.

[109] Hu CM, Lai CM, Du XH, Ho NJ, Huang JC. Enhanced tensile plasticity in ultrafine-grained metallic composite fabricated by friction stir process. Scripta Materialia 2008;59:1163-6.

[110] Feng AH, Xiao BL, Ma ZY. Effect of microstructural evolution on mechanical properties of friction stir welded AA2009/SiCp composite. Composites Science and Technology 2008;68:2141-8.

[111] Ceschini L, Boromei I, Minak G, Morri A, Tarterini F. Effect of friction stir welding on microstructure, tensile and fatigue properties of the AA7005/10 vol.%Al₂O_{3p} composite. Composites Science and Technology 2007;67:605-15.

[112] Najafi M, Nasiri AM, Kokabi AH. Microstructure and hardness of friction stir processed AZ31 with SiC _P. International Journal of Modern Physics B 2008;22:2879-85.

[113] Lee CJ, Huang JC, Hsieh PL. Using friction stir processing to fabricate Mg based composites with nano fillers. Key Engineering Materials 2006;313:69-74.

[114] Pirondi A, Collini L. Analysis of crack propagation resistance of Al-Al₂O₃ particulate-reinforced composite friction stir welded butt joints. International Journal of Fatigue 2009;31:111-21.

[115] Jun Q, Zhili F, Hanbing X, Frederick DA, Jolly BC, David SA. Producing a composite surface using friction stir processing. Seattle, WA2008. p. 33-6.

[116] Mahmoud ERI, Ikeuchi K, Takahashi M. Fabrication of SiC particle reinforced composite on aluminium surface by friction stir processing. Science and Technology of Welding and Joining 2008;13:607-18.

[117] Vijay SJ, Murugan N. Influence of tool pin profile on the metallurgical and mechanical properties of friction stir welded Al–10wt.% TiB2 metal matrix composite. Mater Design 2010;31:3585-9.

[118] Lee IS, Kao PW, Ho NJ. Microstructure and mechanical properties of Al-Fe in situ nanocomposite produced by friction stir processing. Intermetallics 2008;16:1104-8.

[119] Chang CI, Wang YN, Pei HR, Lee CJ, Huang JC. On the hardening of friction stir processed Mg-AZ31 based composites with 5-20% nano-ZrO2 and nano-SiO2 particles. Materials Transactions 2006;47:2942-9.

[120] Ancona A, Daurelio G, De Filippis L, Ludovico A, Spera A. CO2 laser welding of aluminium shipbuilding industry alloys: AA 5083, AA 5383, AA 5059, and AA 6082. XIV International Symposium on Gas Flow, Chemical Lasers, and High-Power Lasers: International Society for Optics and Photonics; 2003. p. 577-87.

[121] Frankel GS, Xia Z. Localized corrosion and stress corrosion cracking resistance of friction stir welded aluminum alloy 5454. Corrosion 1999;55:139-50.

[122] Dieter GE. ASM Handbook, Volume 20 - Materials Selection and Design. ASM International. p. 385.

[123] Hasegawa H, Komura S, Utsunomiya A, Horita Z, Furukawa M, Nemoto M, *et al*. Thermal stability of ultrafine-grained aluminum in the presence of Mg and Zr additions. Materials Science and Engineering: A 1999;265:188-96.

[124] Martinez De La Puente S, Verlinden B, Delaey L. Hot workability of an Al-Mg alloy AA5182 with 1 wt% Cu. Journal of Materials Science 1994;29:6167-74.

[125] Sato YS, Park SHC, Kokawa H. Microstructural factors governing hardness in friction-stir welds of solid-solution-hardened Al alloys. Metallurgical and Materials Transactions A: Physical Metallurgy and Materials Science 2001;32:3033-42.

[126] Fonda RW, Pao PS, Jones HN, Feng CR, Connolly BJ, Davenport AJ. Microstructure, mechanical properties, and corrosion of friction stir welded Al 5456. Materials Science and Engineering A 2009;519:1-8.

[127] Wen W, Zhao Y, Morris JG. The effect of Mg precipitation on the mechanical properties of 5xxx aluminum alloys. Materials Science and Engineering A 2005;392:136-44.

[128] Sun Y, Fujii H, Takaki N, Okitsu Y. Novel spot friction stir welding of 6061 and 5052 Al alloys. Science and Technology of Welding & Joining 2011;16:605-12.

[129] Gerlich A, Yamamoto M, North TH. Strain rates and grain growth in Al 5754 and Al 6061 friction stir spot welds. Metallurgical and Materials Transactions A: Physical Metallurgy and Materials Science 2007;38:1291-302.

[130] Yazdipour A, Shafiei M A, Dehghani K. Modeling the microstructural evolution and effect of cooling rate on the nanograins formed during the friction stir processing of Al5083. Materials Science and Engineering A 2009;527:192-7.

[131] Sato YS, Urata M, Kokawa H, Ikeda K. Hall-Petch relationship in friction stir welds of equal channel angular-pressed aluminium alloys. Materials Science and Engineering A 2003;354:298-305.

[132] Sato Y, Urata M, Kokawa H. Parameters controlling microstructure and hardness during friction-stir welding of precipitation-hardenable aluminum alloy 6063. Metallurgical and Materials Transactions A 2002;33:625-35.

[133] Huskins E, Cao B, Ramesh K. Strengthening mechanisms in an Al–Mg alloy. Materials Science and Engineering: A 2010;527:1292-8.

[134] Hall E. The deformation and ageing of mild steel: III discussion of results. Proceedings of the Physical Society Section B 1951;64:747.

[135] Petch N. The cleavage strength of polycrystals. J Iron Steel Inst 1953;174:25-8.

[136] Zander J, Sandström R, Vitos L. Modelling mechanical properties for non-hardenable aluminium alloys. Computational materials science 2007;41:86-95.

[137] Ryen Ø, Holmedal B, Nijs O, Nes E, Sjölander E, Ekström H-E. Strengthening mechanisms in solid solution aluminum alloys. Metallurgical and Materials Transactions A 2006;37:1999-2006.

[138] Liu MP, Roven HJ, Murashkin MY, Valiev RZ, Kilmametov A, Zhang Z, *et al*. Structure and mechanical properties of nanostructured Al–Mg alloys processed by severe plastic deformation. Journal of Materials Science 2013:1-8.

[139] Gubicza J, Chinh N, Csanadi T, Langdon T, Ungar T. Microstructure and strength of severely deformed fcc metals. Materials Science and Engineering: A 2007;462:86-90.

[140] Grujicic M, Pandurangan B, Yen CF, Cheeseman BA. Modifications in the AA5083 Johnson-Cook Material Model for Use in Friction Stir Welding Computational Analyses. J of Materi Eng and Perform 2011:1-11.

[141] Robson JD, Campbell L. Model for grain evolution during friction stir welding of aluminium alloys. Science and Technology of Welding and Joining 2010;15:171-6.

[142] Chen K, Gan W, Okamoto K, Chung K, Wagoner RH. The mechanism of grain coarsening in friction-stir-welded AA5083 after heat treatment. Metallurgical and Materials Transactions A: Physical Metallurgy and Materials Science 2011;42:488-507.

[143] Humphreys FJ. A unified theory of recovery, recrystallization and grain growth, based on the stability and growth of cellular microstructures - II. The effect of second-phase particles. Acta Materialia 1997;45:5031-9.

[144] Jana S, Mishra RS, Baumann JA, Grant G. Effect of process parameters on abnormal grain growth during friction stir processing of a cast Al alloy. Materials Science and Engineering A 2010;528:189-99.

[145] Charit I, Mishra RS, Mahoney MW. Multi-sheet structures in 7475 aluminum by friction stir welding in concert with post-weld superplastic forming. Scripta Materialia 2002;47:631-6.

[146] Hassan KAA, Norman AF, Price DA, Prangnell PB. Stability of nugget zone grain structures in high strength Al-alloy friction stir welds during solution treatment. Acta Materialia 2003;51:1923-36.

[147] Sato YS, Watanabe H, Kokawa H. Grain growth phenomena in friction stir welded 1100 Al during post-weld heat treatment. Science and Technology of Welding and Joining 2007;12:318-23.

[148] Safarkhanian MA, Goodarzi M, Boutorabi SMA. Effect of abnormal grain growth on tensile strength of Al-Cu-Mg alloy friction stir welded joints. Journal of Materials Science 2009;44:5452-8.

[149] Attallah MM, Salem HG. Friction stir welding parameters: A tool for controlling abnormal grain growth during subsequent heat treatment. Materials Science and Engineering A 2005;391:51-9.

[150] Aydin H, Bayram A, Durgun I. The effect of post-weld heat treatment on the mechanical properties of 2024-T4 friction stir-welded joints. Materials and Design 2010;31:2568-77.

[151] Zhang Z, Xiao BL, Ma ZY. Influence of post weld heat treatment on microstructure and mechanical properties of friction stir-welded 2014Al-T6 alloy. Quebec City, QC2012. p. 299-304.

[152] Hales SJ, Tayon WA. Heat treatment of a friction-stir-welded and spin-formed Al-Li alloy. Como2011. p. 2496-501.

[153] Minton T, Au J. Stability of friction stir welds at superplastic forming temperatures. 2009. p. 117-25.

[154] Kim D, Badarinarayan H, Kim JH, Kim C, Okamoto K, Wagoner RH, *et al*. Numerical simulation of friction stir butt welding process for AA5083-H18 sheets. European Journal of Mechanics, A/Solids 2010;29:204-15.

[155] Cerri E. Thermal stability of fine grains as a function of process parameters in FSW butt joints. 2011. p. 249-54.

[156] Goloborodko A, Ito T, Yun X, Motohashi Y, Itoh G. Friction stir welding of a commercial 7075-T6 aluminum alloy: Grain refinement, thermal stability and tensile properties. Materials Transactions 2004;45:2503-8.

[157] Charit I, Mishra RS. Abnormal grain growth in friction stir processed alloys. Scripta Materialia 2008;58:367-71.

[158] Furukawa M, Horita Z, Nemoto M, Valiev RZ, Langdon TG. Microhardness measurements and the hall-petch relationship in an Al-Mg alloy with submicrometer grain size. Acta Materialia 1996;44:4619-29.

[159] Wang J, Iwahashi Y, Horita Z, Furukawa M, Nemoto M, Valiev RZ, *et al*. An investigation of microstructural stability in an Al-Mg alloy with submicrometer grain size. Acta Materialia 1996;44:2973-82.

[160] Tellkamp VL, Dallek S, Cheng D, Lavernia EJ. Grain growth behavior of a nanostructured 5083 Al-Mg alloy. Journal of Materials Research 2001;16:938-44.

[161] Wang J, Furukawa M, Horita Z, Nemoto M, Valiev RZ, Langdon TG. Enhanced grain growth in an Al-Mg alloy with ultrafine grain size. Materials Science and Engineering: A 1996;216:41-6.

[162] Morris DG, Muñoz-Morris MA. Microstructure of severely deformed Al-3Mg and its evolution during annealing. Acta Materialia 2002;50:4047-60.

Chapter 2: Effect of Friction Stir Processing Parameters on Microstructure and Mechanical Properties of Al 5059[1]

[1] A version of this chapter has been published: H. Izadi, A. Nolting, C. Munro, A. Gerlich, Effect of Friction Stir Processing Parameters on Microstructure and Mechanical Properties of AL 5059, Proceedings of the 9th International Conference on Trends in Welding Research, 2012 ASM International.

2.1 Overview

Since in this work, friction stir processing is used for fabrication of metal matrix composites; this chapter examines the effect of processing parameters solely on the microstructural and mechanical properties of the matrix alloy, which is Al 5059. Friction stir processing is a severe plastic deformation process that involves the same principals of FSW; however a monolithic plate is processed rather than joining two components. As the process involves high strain rate deformation and no bulk melting occurs, it may be utilized as a secondary processing tool for microstructural modification and mechanical properties improvement, as discussed in Chapter 1.

Continuous or discontinuous dynamic recrystallization generally occurs in the processed region due to high strain rates, temperatures and strains involved in friction stir welding and processing, resulting in a final microstructure which consists of very fine grains. Tool geometry, rotation and travel speeds dictate the material flow, deformation process, strain rate and amount of heat generated during FSP. In this regard the objective of this chapter is to determine the effect of tool geometry, rotation speed and travel speed on microstructures and mechanical properties in friction stir processed Al 5059.

2.2 Experimental Procedure

The as-received material was 6.3 mm thick Al 5059 alloy with a composition of Al-5.26Mg-0.79Mn-0.5Zn-0.09Fe-0.07Si-0.02Ti, in the rolled and H131 temper condition. The Al 5059 is a wrought aluminum alloy which derives

its strength from a combination of work hardening and solution strengthening rather than precipitation. This is considered to be an advantage of non-heat treatable alloys, as usually there is a remarkable drop in the hardness of heat treatable aluminum alloys due to precipitate dissolution and coarsening in the stir zone when FSW is applied. The hardness may be restored by post-weld heat treatment but it will cause undesired grain growth as well. The key feature in this approach is that the Al 5059 metal matrix will maintain its hardness after friction stir processing due to grain refinement, and further strengthening can be achieved by the incorporation of reinforcing particles.

The equipment used to investigate friction stir processing was an *Induma* milling machine modified for friction stir welding/processing, as shown in Figure 2-1. This machine is capable of tool rotation speeds from 40 to 1600 rpm and travel speeds of 10 to 800 mm/min. It is equipped with a *JR3* multi-axis force-torque load cell and a data acquisition system which allows to measure tool forces and torques in all directions. It also has a position display screen that shows the (x, y, z) position of the tool. In order to verify the accuracy and repeatability of the positioning system and the load cell, a series of tests were performed before the actual experiments and the obtained results confirmed the functionality of the set-up.

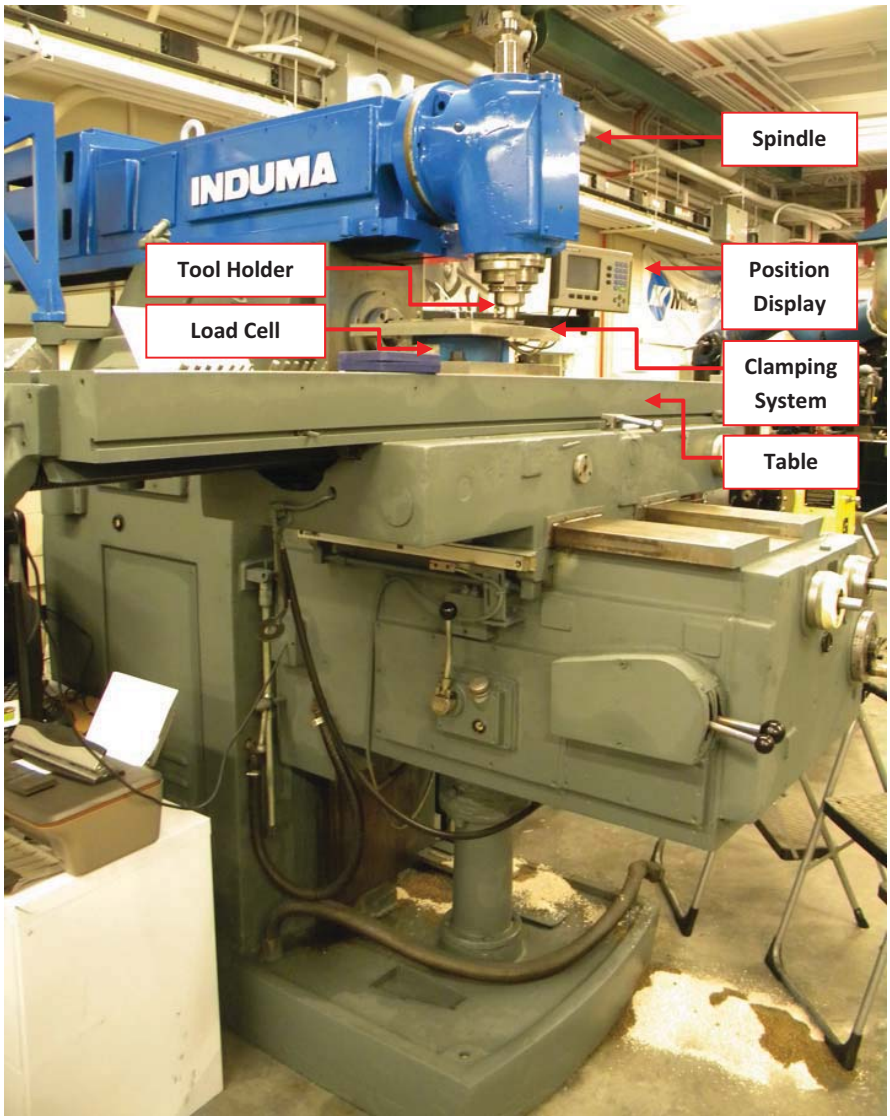

Figure 2-1: The milling machine used for friction stir processing.

Friction stir processing was performed at 454, 638, 894 and 1595 rpm rotation speeds and travel speeds of 33 and 88 mm/min using 3 different tool geometries, with the axial load maintained between 5 and 7 kN. Figure 2-2 shows the geometries of the 3 tools studied.

a)

b)

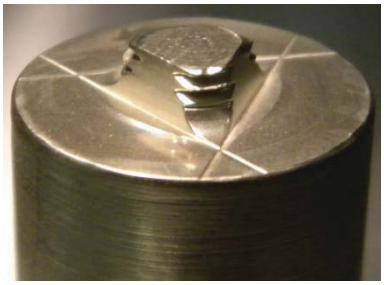

c)

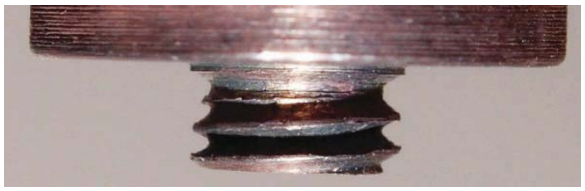

Figure 2-2: Tool geometries studied for friction stir processing of Al 5059, (a) grooved pin (concentric threads with no helix), (b) 3-flat threaded pin, and (c) conventional threaded pin.

After friction stir processing, samples were sectioned, polished and electroetched in Barker's reagent (5 mL HBF_4 (48%) in 200 mL water) for 50 seconds at 20 V DC and examined with polarized light using a Nikon Eclipse MA200 optical microscope. The same procedure was followed for SEM microscopy however samples were etched in Keller's reagent (1 ml 48% HF, 1.5 ml HCl and 10 ml nitric acid in 87.5 ml distilled water). Sample preparation for TEM involved using a twin jet electropolisher, in a solution of 30 vol% of HNO_3 and 70 vol% of methanol at a temperature of -35 ºC (238 K) and voltage of 12 V. A JEOL 2010 TEM operating at 200 kV was used. For grain size measurement the equivalent circle diameter was obtained by measuring the area of individual grains in the middle of the stir zone.

Tensile testing was conducted on an MTS series 370 servo-hydraulic load frame equipped with a 25 kN load cell. Strain was monitored with an MTS 634.31F.24 model extensometer with 10 mm knife edge separation. All tests were performed in displacement control, at a rate which produced an equivalent initial strain rate of approximately 0.015 /min. Yield strength was determined by the 0.2% offset yield method and elongation at fracture was measured as the extensometer elongation when failure occurred. The specimens had a thickness of 2.0 mm, a width of either 3.75 or 3.25 mm, and a reduced area 20 mm long, figure 2-3. These dimensions were chosen to ensure that mainly stir zone material was located in the gauge section, while still maximizing the cross sectional area of the gauge section.

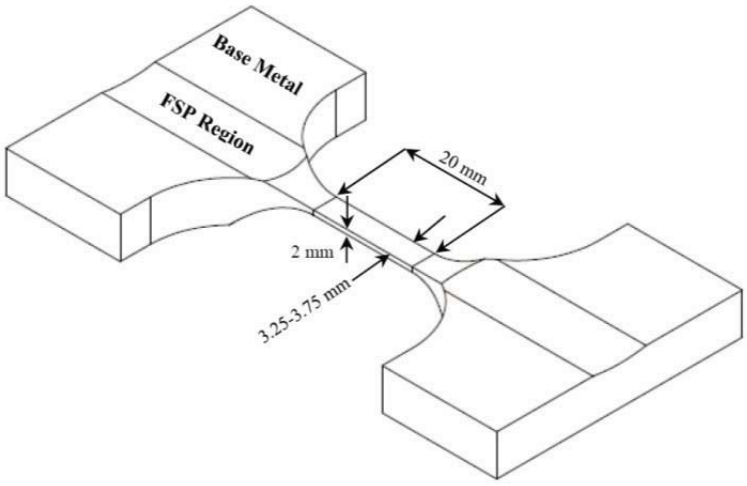

Figure 2-3 Schematic drawing showing the dimensions of the tensile specimens and their location relative to the friction stir processed region.

Microhardness tests were conducted utilizing a Tukon 2500 automatic hardness measurement system using a dwell time of 15 S and 200 g load.

2.3 Results and Discussion

2.3.1 Microstructure

Figure 2-4 shows the microstructure of the as received material. Elongated grains and pancake-shaped microstructure are formed as a result of rolling in the starting material.

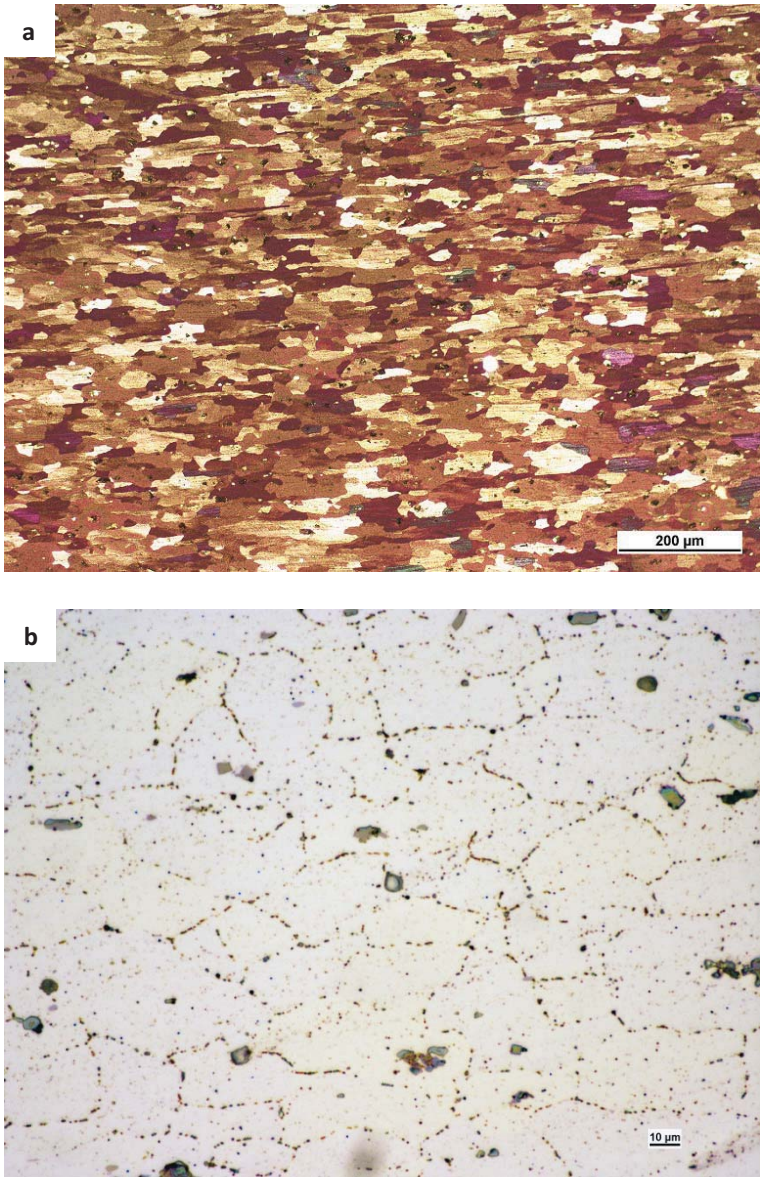

Figure 2-4: Microstructure of the base material: a) electroetched for 50 seconds in HBF_4, polarized light imaging and b) electroetched for 10 seconds in HBF_4, bright field imaging.

Figure 2-4-b indicates elongated precipitates along grain boundaries. Formation of precipitates on grain boundaries is common in aluminium alloys with high magnesium content [1-3] and can enhance micro voids formation and coalesce and lead to reduced ductility [4-6].

Depending on the chemical composition of the alloy different second phase particles may exist in the microstructure. $Al_6(Mn,Fe)$, Al_3Fe, Mg_2Si, $Al_7(Fe,Cr)$, Al_8Mg_5, $Al_{13}Cr_2$, $Al_{13}(Cr,Mn)_2$, $Al_{12}(Fe,Mn)_3Si$, $Al_3(Mn,Fe,Cu)$ and Al_3Zr precipitates are typically found in 5XXX series aluminum alloys [1-10]. Martinez *et al*. have shown that adding 1 wt% copper (Al 5059 contents 0.25 wt% copper) to Al 5182 results in precipitation of Al-Mg-Cu and Al-Mn-Fe(+Cu) particles [11]. Sato *et al*. have only reported $Al_6(Mn,Fe)$ particles in the stir zone of friction stir welds of Al 5083 [2]. Also, no evidence of Mg_2Si has been observed in friction stir welded Al 5456, and only $Al_6(Mn,Fe)$ and $Al_{13}(Cr,Mn)_2$ were detected [10]. This may be related to the dissolution of Mg_2Si particles during friction stir processing which depends on the maximum temperature reached within the process and may not be relevant in all conditions. For example fragmentation assisted dissolution of Mg_2Si has been reported in friction stir welded Al 5251 [12].

ThermoCalc measurements predict the presence of $Al_6(Mn,Fe)$, Mg_2Si, Al_3Mg_2, Al_3Fe and Al_3Zr precipitates in this alloy, Figure 2-5.

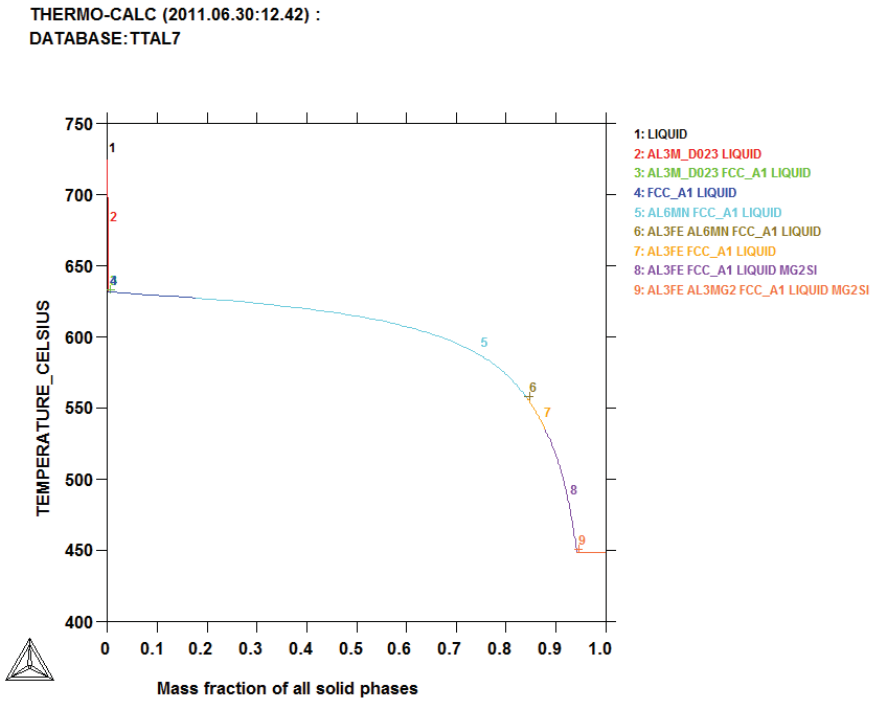

Figure 2-5: ThermoCalc analysis showing the solidification sequence in Al 5059.

TEM analysis of friction stir processed samples, showed that majority of the particles are Al_6Mn, $Al_6(Mn,Fe)$ or Mg_2Si. Using TEM microscopy, the base material was found to contain mainly $Al_6(Mn)$ types of inclusions, where Mn was substituted in various ratios with Cr, Fe, Si, and Cu, but no Al_3Zr was found, for example see Figure 2-6.

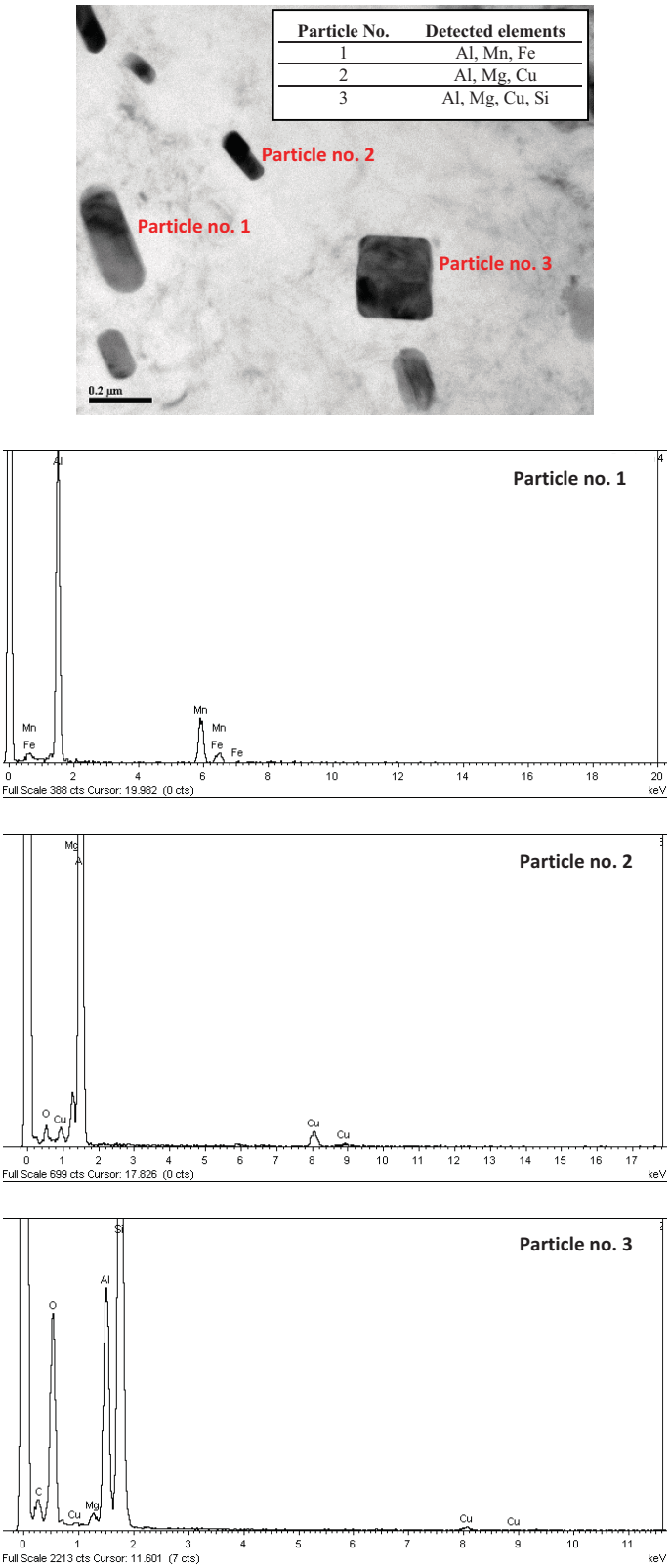

Figure 2-6: a) TEM image showing particles in the friction stir processed sample, and b, c and d) shows the corresponding EDX results.

TEM examination revealed 2 morphologies of particles in this alloy: elongated (high aspect ratio) and round or cubic (low aspect ratio), see Figure 2-7. However no relation was found between the morphologies and the chemical composition of the particles, although the observed particle compositions were similar to those reported by Rachtev *et al*. in Al 5182 alloy [13]. Similarly a 3D morphological analysis using X-ray microtomography has revealed flat, needle-like and spherical particles in Al 5182 alloy [14].

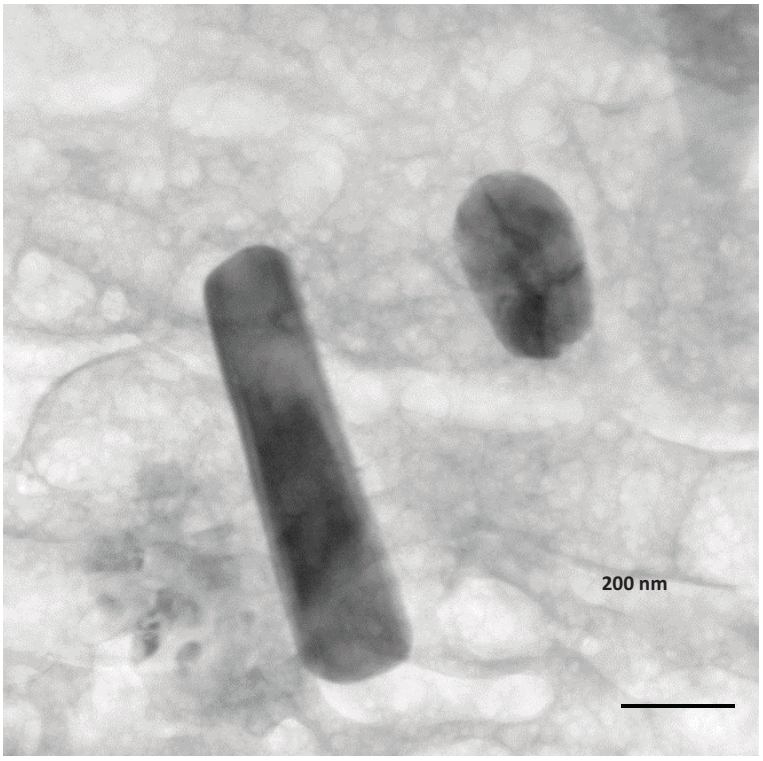

Figure 2-7: TEM micrograph of friction stir processed Al 5059 showing the morphologies of the particles.

As shown in Figure 2-5, ThermoCalc analysis also showed that the particles present are stable at elevated temperatures of over 450ºC (723 K). It was found that the temperatures reached during friction stir processing were 370ºC (643 K), as will be discussed later in Chapter 3; therefore precipitate dissolution

and reprecipitation are not expected to happen during friction stir processing of the Al 5059 base material. On the other hand particle fragmentation can easily happen as a result of thermo-mechanical cycles associated with friction stir processing. Strangwood *et al*. have indicated breakup of Al(FeMn)Si particles and fragmentation assisted dissolution of the Mg_2Si phase in friction stir welds of Al 5251 [15]. Fracture of Al_3Mg_2 particles during friction stir welding of Al 5083 is also reported [16]. Su *et al*. have described that rod-like and bar-like Al_7Cu_2Fe precipitates initially break up and then coarsen to spherical and block shape particles during friction stir welding of Al 7050 [17]. Likewise particle fragmentation is likely to happen in the Al 5059 alloy, as a large fraction of high aspect ratio particles are present in the material and prone to fracture during friction stir processing. Quantification of particle refinement was performed based on several TEM images and the results are shown in Table 2-1. To evaluate if the difference between the 2 average values are meaningful or not a T-test statistical analysis (details about T-test can be find in [18]) was performed and since the resulting P-value is small (0.027) the difference in the average values is statistically meaningful.

Table 2-1: Particles lengths in Al 5059 before and after friction stir processing.

	Equivalent diameter of elongated particles (nm)	
	Average	Standard Deviation
As-received	238	49
Friction stir processed	194	27

As indicated in Table 2-1 the average size of precipitates has decreased after FSP which is an indication of particle fragmentation during FSP. Such a change in particles size is very important in terms of the mechanical properties, which will be discussed later.

The shapes of the stir zones of the Al 5059 samples friction stir processed with the 3 tools at 894 rpm and 33 mm/min are shown in the macrographs in Figure 2-8. It is well known that the pin profile affects the flow of the plasticized material and therefore influences the shape and properties of the stir zone [19]. As shown in Figure 2-8 the tool with 3-flat surfaces on the threaded pin significantly change the shape of stir zone.

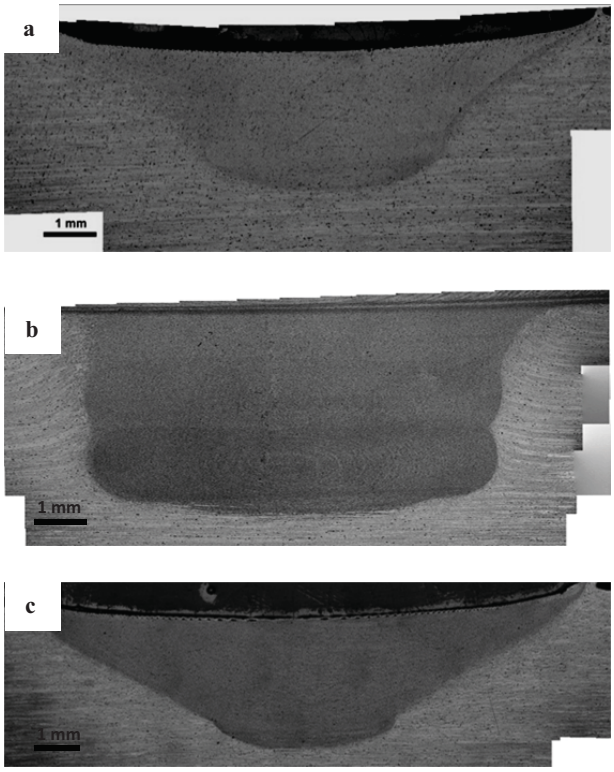

Figure 2-8: Optical macrographs showing the stir zone shape of samples friction stir processed with (a) the grooved pin, (b) the 3-flat threaded pin and (c) the conventional threaded pin.

Figure 2-9 shows the stir zone microstructure of the 3 samples indicated in Figure 2-8. At least 60 grains were selected from each of the micrographs shown in Figure 2-9 for grain size measurement and the results are shown in Table 2-2. The grain size increases from 2.54 μm for the sample produced by the 3-flat tool to 3.38 μm for the sample produced using the conventional threaded tool to 4.07 μm for the sample obtained by the grooved tool. It is well accepted that dynamic recrystallization generates fine equiaxed grains in the stir zone. Different conditions such as process parameters, tool geometry, alloy composition, temperature of work piece material, tool axial loading, and the thermal cycle on cooling affect the size of the recrystallized grains during friction stir welding and

processing [20]. Given that all the other factors were consistent, the variation in grain sizes in these samples arises from the effect of tool geometry. It has been shown that flat sides on the pin of the tool increases the amount of plastic deformation by creating a local disturbance in the material flow or pressure, [21, 22], and this would readily explain the finer grains in the stir zone.

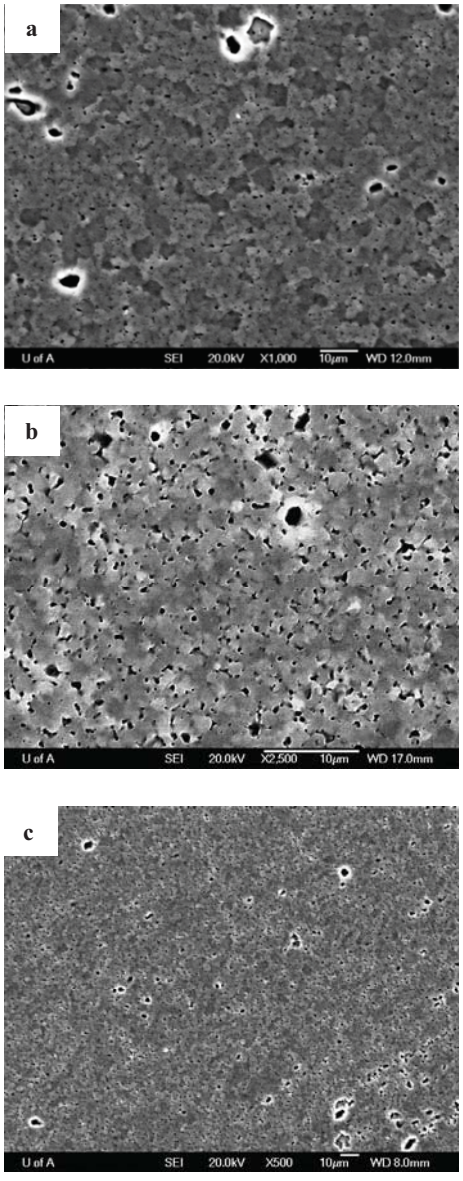

Figure 2-9: SEM micrographs showing grain structures from the middle of the stir zone obtained when using a tool with (a) a grooved pin, (b) a 3-flat threaded pin, and (c) a conventional threaded pin.

Table 2-2: Grain sizes in Al 5059 stir zone obtained with different tool geometries using a rotation speed of 638 rpm and a travel speed of 33 mm/min.

Tool Pin shape	Average grain size (μm)
3-Flat Threaded	2.54
Conventional Threaded	3.38
Grooved	4.07

The rotation speed is also known to influence the stir zone grain size by changing the amount of heat introduced to the sample. Increasing the rotation speed rises the maximum temperature of the stir zone and therefore generates larger grains [20, 23]. In order to investigate the effect of tool rotation speed on stir zone grain size in Al 5059, samples were also friction stir processed at 454 and 1595 rpm using the 3-flat threaded tool.

The sample friction stir processed at 454 rpm and a travel speed of 33 mm/min yielded a grain size of 1.96 μm while the sample friction stir processed at 1595 rpm produced a grain size of 4.73 μm, the corresponding microstructures are indicated in Figure 2-10. Considering these results, a 3-flat threaded tool in combination with a tool rotation speed of 454 rpm produced the finest grain structures in the present work. It is striking to note that such fine grain sizes were achieved without the assistance of forced cooling or repeated processing of the same location. A tool with a conventional threaded pin was also investigated, however when this was used at 454 rpm the pin sheared off. To avoid this issue a

revised version of the 3-flat tool with a tapered pin (a larger diameter near the shoulder) was utilized for the rest of experiments.

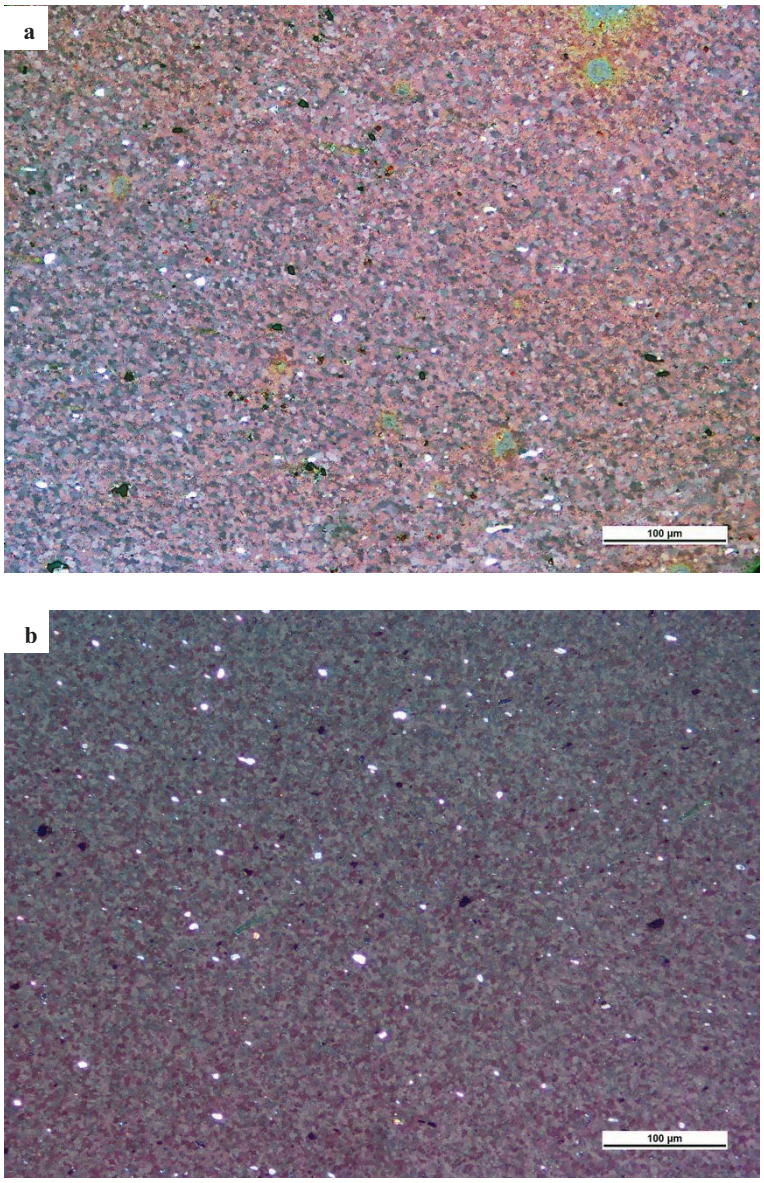

Figure 2-10: Optical micrographs showing grain structures from middle of stir zone obtained when using a 3-flat tool using a) 454 rpm resulting in a 1.96 µm grain size and b) 1595 rpm resulting in a 4.73 µm grain size.

To further study the microstructure in terms of grain structure and precipitates, TEM was performed on the samples. Figure 2-11 shows a TEM micrograph of the sample friction stir processed at 638 rpm with the 3-flat threaded tool. The size of the grains observed by TEM is also in the range measured using optical microscopy. Figure 2-11 also shows the dispersoid particles observed in the Al 5059 material. As discussed earlier, EDX indicated that these particles are $Al_6(Mn,Fe)$.

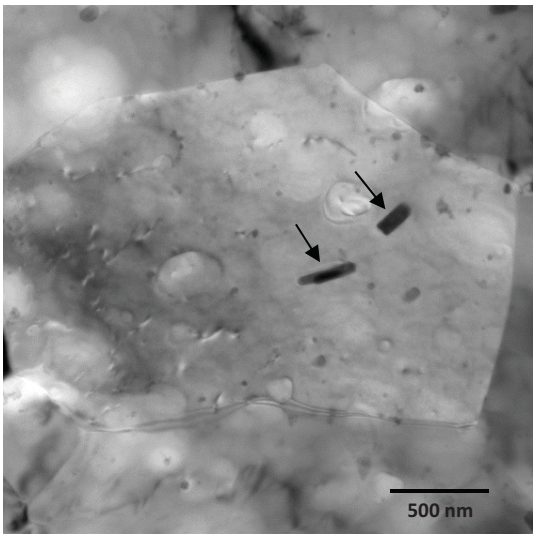

Figure 2-11: TEM micrograph of the sample friction stir processed at 638 rpm with a 3-flat threaded tool. Arrows indicate $Al_6(Mn, Fe)$ precipitates.

2.3.2 Mechanical Properties

Figure 2-12 shows the microhardness results of the sample friction stir processed using the 3-flat tool at 454 rpm and 33 mm/min. The overall hardness profile agrees well with the prior findings typically reported for wrought 5XXX series aluminum alloys [24], in which there is a marginal increase in hardness in the stir zone compared to the base material. This is the case in the present work,

and suggests that softening effects due to recovery and recrystallization in the stir zone can be compensated by strengthening due to grain refinement. Therefore to achieve higher hardness values, lower rotation speeds should promote finer grain structures and enhance this effect. It can also be observed in Figure 2-12 that the hardness is quite uniform around the center of the stir zone.

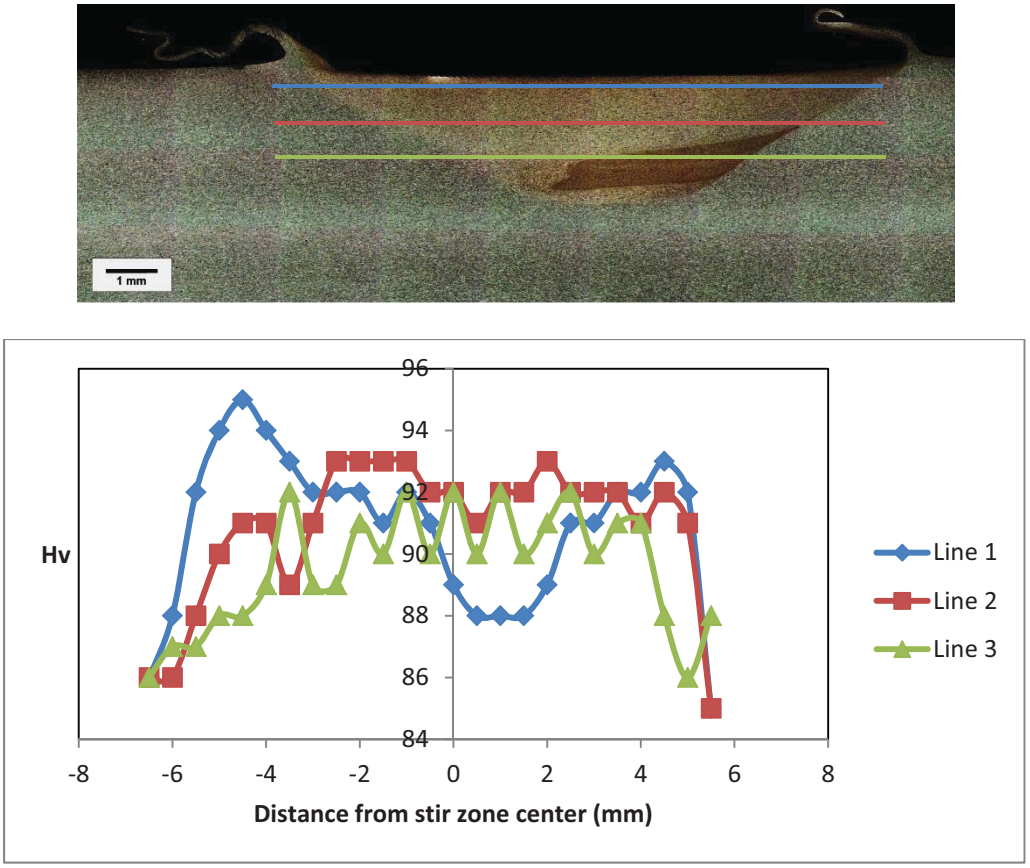

Figure 2-12: Hardness profile across the stir zone in Al 5059 after friction stir processing at 454 rpm and 33 mm/min.

Hardness values obtained from other samples are shown in Table 2-3. The presented numbers are the average of at least 5 points from the center of the stir

zone. The sample friction stir processed with the 3-flat threaded tool shows slightly higher hardness which is consistent with the grain size measurements.

Table 2-3: Hardness values of samples friction stir processed with different tools and rotation speeds. The travel speed is 33 mm/min for all samples.

Tool Profile	Rotation Speed (rpm)	Grain Size (μm)	Microhardness (Hv)
3-flat threaded pin	454	1.96	94
	638	2.54	-
	898	-	88
	1595	4.73	94
Conventional threaded pin	638	3.38	90
	898	-	85

As indicated in Table 2-3 increasing the rotation speed from 454 rpm to 898 rpm results in a reduction in microhardness which is related to coarsened grain sizes when higher rotation speeds are applied. However, further increasing the rotation speed to 1595 rpm leads to a high hardness value of 94 Hv, despite the increase in grain size. Increasing the rotation speed introduces more heat to the sample and increases the maximum temperature of the stir zone [25]. This elevated temperature may be enough to cause dissolution of some of the intermetallic particles. ThermoCalc calculations proved that Mg rich particles are likely to dissolve if enough heat is provided (see Figure 2-7). In addition as discussed earlier more particle fracture happens at higher rotation speed therefore fragmentation enhanced particle dissolution is also highly probable at increased rotation speeds. When Mg containing particles dissolve the magnesium content

will go to the aluminum matrix in the form of solid solution and can improve the hardness. This is the possible reason for hardness improvement when a rotation speed of 1595 rpm is used. Such an effect is observed in heat treated Al 5251 samples where the sample heat treated at 525 °C had a higher hardness than samples heat treated at lower temperatures (375 and 400 °C) despite the grain growth. A 4 Hv increase in hardness is attributed to dissolution of Mg_2Si particles at 525 $^{\circ}$C which adds about 0.25 wt% Mg content in solid solution [12]. In addition, Ryen *et al*. have indicated that small increase in Mg content in solid solution can result in significant rise in strength of Al-Mg alloys [26].

A minor reduction in hardness was also observed in the thermo-mechanically affected zone of samples friction stir processed at high rotation speeds. In the TMAZ the temperatures were sufficient to cause recovery of the base material but not undergo recrystallization and grain refinement since limited deformation occurred in this region [24].

Figure 2-13 shows the stress-strain curves obtained during tensile testing; comparing the mechanical properties of the as-received Al 5059 with the samples friction stir processed using a 3-flat threaded tool at different rotation speeds. The material property values obtained from the data are summarized in Table 2-4. It can be observed that there is a minor improvement in strength, while surprisingly also exhibiting a significant increase in elongation to failure. It is important to note that the increase in ductility while maintaining strength is a difficult thing to achieve, since careful optimization of rolling and recrystallization parameters have all been optimized in the "H131" condition to establish particularly

desirable properties with a compromise between strength and ductility. Here the minor strengthening may be attributed to the grain refinement occurred as a result of dynamic recrystallization in the stir zone. It is well-known that grain refinement can simultaneously improve strength and ductility, especially if the dislocation density is not very particularly high as shown in the TEM images. This is a typical microstructural feature of friction stir processed aluminum alloys. The significant improvement in ductility may be related to two mechanisms: 1) elimination of the continuous grain boundary precipitates and 2) particle refinement. As shown in Figure 2-4-b a considerable amount of network-like precipitates was available at the grain boundaries of the base material. As mentioned earlier such particles can promote fracture and reduce ductility significantly by enhancing void formation and accumulation and lead to early fracture. The deformation and stir action imposed by the tool during friction stir processing removes these phases from the grain boundaries and therefore improves the ductility. Considering this effect, it can be noted in Figure 2-13 and Table 2-4 that all the friction stir processed samples exhibited better elongation than the as-received alloy. This has been previously observed in friction stir welds of heat treatable aluminum alloys in prior work [27].

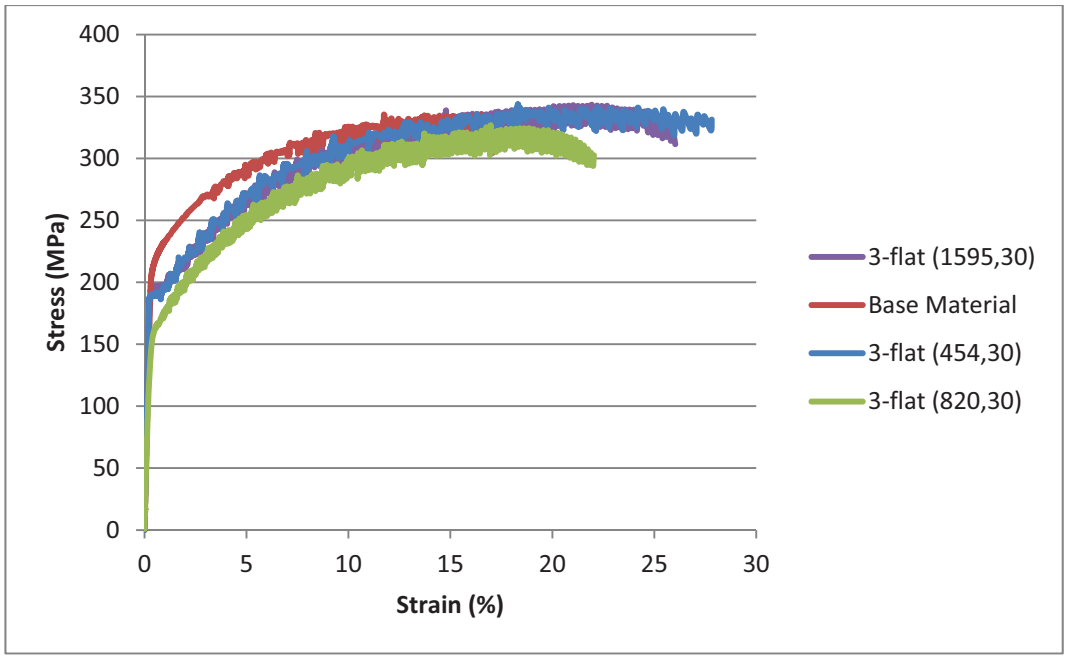

Figure 2-13: Stress-Strain curves for as-received Al 5059 plate and samples friction stir processed using a 3-flat threaded tool at different rotation speeds.

Table 2-4: Tensile properties of as-received Al 5059 plate and sample friction stir processed at 638 rpm using a 3-flat threaded tool.

Sample	Yield Stress (MPa)	UTS (MPa)	Elongation (%)
As-received	217	335	17
3-flat threaded tool, 454 rpm	193	343	26
3-flat threaded tool, 898 rpm	~150	327	22
3-flat threaded tool, 1595 rpm	~190	343	30

Any parameter that improves the capacity of the alloy to undergo work hardening increases the elongation to failure, and this is typically quantified by work hardening rate, or the normalized work hardening rate parameter [28, 29]:

$$\theta = \frac{1}{\sigma}\left(\frac{\partial\sigma}{\partial\varepsilon}\right)_{\dot{\varepsilon}} \qquad (2.1)$$

where σ and ε are true stress and strain respectively. To obtain the values of θ for each condition true stress – true strain curves were plotted using the data from tensile tests, and then a polynomial was fitted to each curve and the derivative was measured to be $\left(\frac{\partial\sigma}{\partial\varepsilon}\right)$. The results are presented in Figure 2-14.

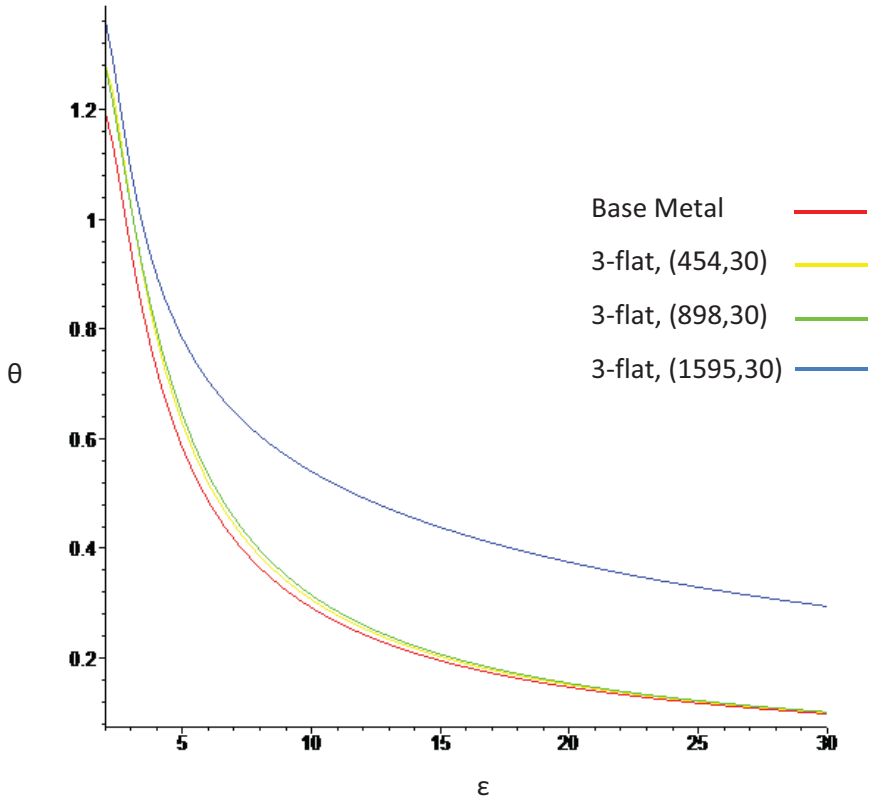

Figure 2-14: Normalized work hardening rate for as-received Al 5059 plate and samples friction stir processed using a 3-flat threaded tool at different rotation speeds.

It can be seen from Figure 2-14 that the friction stir processed samples have higher work hardening rates compared to the base material. This can be related to particle fragmentation and refinement imposed by friction stir processing. It is reported that in particle containing metals work hardening rate increases with increasing the volume fraction or decreasing the size of the particles [30, 31]. When a particle containing metal is strained as the amount of deformation is not equal for the matrix and the particles, some dislocations are generated and stored in the microstructure, which are called the "geometrically necessary dislocations". The interaction between these dislocations and the primary dislocations determines the work hardening rate at large strains in dispersion-hardened alloys where the ultimate relation between work hardening and particle diameter *d* and volume fraction *f* is [32]:

$$\frac{d\sigma}{d\varepsilon} = \acute{\alpha} G \left(\frac{fb}{d}\right)^{\frac{1}{2}} \varepsilon^{\frac{1}{2}} \qquad (2.2)$$

were $\acute{\alpha}$ is a constant, *G* is shear modulus, and *b* is the Burgers vector.

On the other hand, since the majority of the particles in this alloy are incoherent $Al_6(Mn,Fe)$ type particles, they will likely stop or cause the dislocations to loop around them. Since particles are refined during friction stir processing, cross-slip will become easier and suppress localized deformation, leading to higher ductility.

Comparing samples processed with different rotation speeds also shows a remarkable increase in work hardening rate for the sample friction stir processed at 1595 rpm. When the grains are large, as in this sample, dislocations move in

longer distances between grain boundaries, such that interaction with other dislocations and/or particles is more likely before a dislocation is annihilated at a grain boundary. Particle refinement is also more pronounced in the sample friction stir processed at 1595 rpm as a higher rotation speed is applied, therefore the work hardening rate increases due to more effective particle fragmentation. Lastly, another important parameter here is the solute content, where the high rotation speed of 1595 rpm may promote dissolution of Mg containing particles and consequently increases the amount of solid solution Mg. An increase in the amount of Mg in solid solution can in turn increase the work hardening rate [33], and this effect has also been demonstrated for Zn content in ultrafine grained aluminum [34]. It was proposed that when a higher fraction of Zn was available in solid solution, more slip bands were observed during TEM examinations and also these slip bands were more uniformly distributed in the microstructure, leading to higher ductility since the formation of localized deformation and macro shear bands were suppressed [34].

2.4 Summary and Conclusion

It was shown that the microstructure of the as-received Al 5059 contains elongated grains with network-like precipitates on the grain boundaries. After FSP the stir zone microstructure compromised fine recrystallized grains along with fine particles. By the use of TEM it was found that the majority of precipitates are $Al_6(Mn,Fe)$ type particles. Thermomechanical cycles during FSP fragmented and dispersed the particles which lead to an improvement in mechanical properties

specially ductility. Friction stir processing with a rotation speed of 454 RPM using a tool with a 3-flat threaded pin produced an average grain size of 1.96 μm in the stir zone. Larger grains were achieved when applying higher rotation speeds or by utilizing tools with a conventional threaded or grooved pin which did not contain flats. The yield and ultimate strengths of the specimen processed to maximize grain refinement were slightly better than those of the as-received material, while the elongation at fracture was significantly improved. This improvement may be related to the grain refinement occurred as a result of dynamic recrystallization during FSP. In the case of ductility, it was also discussed that particle fragmentation by FSP increases the work hardening rate which in case results in a higher elongation to failure. A minor improvement in hardness was also found for the sample processed with the relatively high rotation speed of 1595 rpm which may be attributed to the increase in the amount of solid solution Mg as a result of dissolution of Mg containing particles.

2.5 Reference

[1] Chen K, Gan W, Okamoto K, Chung K, Wagoner RH. The mechanism of grain coarsening in friction-stir-welded AA5083 after heat treatment. Metallurgical and Materials Transactions A: Physical Metallurgy and Materials Science 2011;42:488-507.

[2] Sato YS, Park SHC, Kokawa H. Microstructural factors governing hardness in friction-stir welds of solid-solution-hardened Al alloys. Metallurgical and Materials Transactions A: Physical Metallurgy and Materials Science 2001;32:3033-42.

[3] Fuller CB, Mahoney MW. The effect of friction stir processing on 5083-H321/5356 Al arc welds: Microstructural and mechanical analysis. Metallurgical

and Materials Transactions A: Physical Metallurgy and Materials Science 2006;37:3605-15.

[4] Goswami R, Spanos G, Pao PS, Holtz RL. Precipitation behavior of the β phase in Al-5083. Materials Science and Engineering A 2010;527:1089-95.

[5] Vetrano JS, Bruemmer SM, Pawlowski LM, Robertson IM. Influence of the particle size on recrystallization and grain growth in Al-Mg-X alloys. Materials Science and Engineering A 1997;238:101-7.

[6] Frankel GS, Xia Z. Localized corrosion and stress corrosion cracking resistance of friction stir welded aluminum alloy 5454. Corrosion 1999;55:139-50.

[7] Verma R, Friedman PA, Ghosh AK, Kim S, Kim C. Characterization of superplastic deformation behavior of a fine grain 5083 AI alloy sheet. Metallurgical and Materials Transactions A: Physical Metallurgy and Materials Science 1996;27:1889-98.

[8] Attallah MM, Strangwood M, Davis CL. Influence of the heating rate on the initiation of primary recrystallization in a deformed Al-Mg alloy. Scripta Materialia 2010;63:371-4.

[9] Wen W, Zhao Y, Morris JG. The effect of Mg precipitation on the mechanical properties of 5xxx aluminum alloys. Materials Science and Engineering A 2005;392:136-44.

[10] Fonda RW, Pao PS, Jones HN, Feng CR, Connolly BJ, Davenport AJ. Microstructure, mechanical properties, and corrosion of friction stir welded Al 5456. Materials Science and Engineering A 2009;519:1-8.

[11] Martinez De La Puente S, Verlinden B, Delaey L. Hot workability of an Al-Mg alloy AA5182 with 1 wt% Cu. Journal of Materials Science 1994;29:6167-74.

[12] Attallah MM, Davis CL, Strangwood M. Microstructure-microhardness relationships in friction stir welded AA5251. Journal of Materials Science 2007;42:7299-306.

[13] Ratchev P, Verlinden B, Van Houtte P. Effect of preheat temperature on the orientation relationship of (Mn,Fe)Al6 precipitates in an AA 5182 Aluminium-Magnesium alloy. Acta Metallurgica Et Materialia 1995;43:621-9.

[14] Denis EP, Barat C, Jeulin D, Ducottet C. 3D complex shape characterization by statistical analysis: Application to aluminium alloys. Materials Characterization 2008;59:338-43.

[15] Strangwood M, Davis CL, Attallah MM. Microstructural Development and Modelling in Friction Stir Welds of Strain-Hardenable Al-Alloys. In: Threadgill P, editor. 5th international symposium on friction stir welding. Metz, France: TWI; 2004.

[16] Choi DH, Ahn BW, Quesnel DJ, Jung SB. Behavior of β phase (Al3Mg2) in AA 5083 during friction stir welding. Intermetallics 2013;35:120-7.

[17] Su JQ, Nelson TW, Mishra R, Mahoney M. Microstructural investigation of friction stir welded 7050-T651 aluminium. Acta Materialia 2003;51:713-29.

[18] Montgomery DC. Design and Analysis of Experiments (8th Edition). John Wiley & Sons. p. 36-53.

[19] Rai R, De A, Bhadeshia HKDH, DebRoy T. Review: Friction stir welding tools. Science and Technology of Welding and Joining 2011;16:325-42.

[20] Mishra RS, Ma ZY. Friction stir welding and processing. Materials Science and Engineering R: Reports 2005;50.

[21] Yin YH, Sun N, North TH, Hu SS. Microstructures and mechanical properties in dissimilar AZ91/AZ31 spot welds. Materials Characterization 2010;61:1018-28.

[22] Colegrove PA, Shercliff HR. CFD modelling of friction stir welding of thick plate 7449 aluminium alloy. Science and Technology of Welding and Joining 2006;11:429-41.

[23] Gerlich A, Avramovic-Cingara G, North TH. Stir zone microstructure and strain rate during Al 7075-T6 friction stir spot welding. Metallurgical and

Materials Transactions A: Physical Metallurgy and Materials Science 2006;37:2773-86.

[24] Threadgilll PL, Leonard AJ, Shercliff HR, Withers PJ. Friction stir welding of aluminium alloys. International Materials Reviews 2009;54:49-93.

[25] Nandan R, DebRoy T, Bhadeshia HKDH. Recent advances in friction-stir welding - Process, weldment structure and properties. Progress in Materials Science 2008;53:980-1023.

[26] Ryen Ø, Holmedal B, Nijs O, Nes E, Sjölander E, Ekström H-E. Strengthening mechanisms in solid solution aluminum alloys. Metallurgical and Materials Transactions A 2006;37:1999-2006.

[27] Xu WF, Liu JH, Chen DL, Luan GH, Yao JS. Improvements of strength and ductility in aluminum alloy joints via rapid cooling during friction stir welding. Materials Science and Engineering A 2012;548:89-98.

[28] Hu CM, Lai CM, Du XH, Ho NJ, Huang JC. Enhanced tensile plasticity in ultrafine-grained metallic composite fabricated by friction stir process. Scripta Materialia 2008;59:1163-6.

[29] Considere A. Mémoire sur l'emploi du fer et de l'acier dans les constructions: Vue Ch. Dunod; 1885.

[30] Ebeling R, Ashby MF. Dispersion hardening of copper single crystals. Philosophical Magazine 1966;13:805-34.

[31] 2-Properties and Selection: Nonferrous Alloys and Special Purpose Materials. ASM International, Metals Park Ohio 1990.

[32] Smallman RE, Ngan AHW. Physical Metallurgy and Advanced Materials: Elsevier Science; 2011.

[33] Kocks UF, Mecking H. Physics and phenomenology of strain hardening: The FCC case. Progress in Materials Science 2003;48:171-273.

[34] Hu CM, Lai CM, Kao PW, Ho NJ, Huang JC. Solute-enhanced tensile ductility of ultrafine-grained Al-Zn alloy fabricated by friction stir processing. Scripta Materialia 2009;60:639-42.

3 Grain Growth Behaviour and Hall-Petch Relation in Friction Stir Processed Al 5059[1]

[1] A version of this chapter has been submitted to Metallurgical and Materials Transactions A.

3.1 Overview

Almost in all applications of friction stir processing, improvement of mechanical properties in terms of microstructural evolution is based on grain refinement which occurs as a result of dynamic recrystallization in the processed region [1, 2]. It is generally believed that fine recrystallized grains form during friction stir welding and then as the weld cools down to room temperature grain growth may occur, for example see [3]. As discussed in Chapter 1, grain sizes in the range of 1 – 10 μm are extensively reported for different aluminum alloys friction stir welded/processed with different process parameters [4]. It is shown that submicron sized grains are also attainable by forced cooling of the plates right after the process, for example see [5]. Different approaches have been applied to study the grain growth and predict the grain size during friction stir welding and processing. As in most of aluminum alloys particles available in the microstructure interact with the grain boundaries, the particle controlled grain growth model (equation 3.1) is the most used approach [6]:

$$\frac{dR}{dt} = A\left(\frac{1}{R} - \frac{1}{R_m}\right) \qquad (3.1)$$

where R is the grain radius, t is time, A is the reduced grain boundary mobility and R_m is the limiting grain size. Based on this equation, Robson *et al*. [7] have developed a model for stir zone grain evolution based on geometrical dynamic recrystallization followed by grain growth. Their model predicts the formation of submicron sized grains as a result of the initial recrystallization and subsequent rapid grain growth in the region behind the pin. Then the growth rate decreases as

the material cools down. The resulting final grain size will be smaller than R_m. They have successfully applied their model to friction stir welds of Al 2524 [7]. Similar approaches have also been used for friction stir welds of Al 6061 [8] and Al 5083 [9].

Post processing heat treatment of parts is usually needed in industrial applications for aging and annealing purposes. Therefore many researchers have studied microstructural evolution during heat treatment of friction stir welded/processed parts. In this regard a useful tool is Humphrey's model for microstructural stability [10] which predicts grain growth behavior (whether it is normal or abnormal) based on starting grain size and particles properties. This has been extensively used for aluminum friction stir welds [11-14].

Generally in Al-Mg alloys the strength is governed by grain size, volume fraction of the precipitates or dislocation density [15]. If dislocation/grain boundary interactions overcome the other two mechanisms then a good Hall-Petch relation (equation 1.7) can be established between hardness and grain size, as in case of Al-Mg alloys with lower amounts of other alloying elements [16]. However for alloys with higher amounts of alloying elements, the volume fraction of the precipitates is high and therefore strength is not anymore controlled solely by grain size. On the other hand both grain size and volume fraction of particles affect other mechanical properties such as ductility; hence while one may not significantly contribute to strength it may remarkably influence ductility.

3.2 Experimental

The 6.3 mm thick Al 5059 alloy plates studied had a composition of Al-5.26Mg-0.79Mn-0.5Zn-0.09Fe-0.07Si-0.02Ti, and were in the rolled and H131 tempered condition. These were friction stir processed at a rotation speed of 454 rpm and a travel speed of 33 mm/min. A tool with a 3-flat M4 threaded pin [17, 18] comprising a 12 mm diameter shoulder and a 5 mm diameter and 2.3 mm length pin was utilized. Care was taken during FSP to keep the axial force between 5 – 7 kN for all samples. Heat treatment was performed at 448 K for different time periods (10, 20, 30, 40, 50 and 60 min and 1 day) followed by quenching in water. For optical microscopy, samples were sectioned, polished and electroetched in Barker's reagent (5 mL HBF_4 (48%) in 200 mL water) for 50 seconds at 20 V DC and examined using polarized light. Sample preparation for TEM involved using a twin jet electropolisher, in a solution of 30 vol% of HNO_3 and 70 vol% of methanol at a temperature of -35 ºC and voltage of 12 V. A JEOL 2010 TEM operating at 200 kV was used. In order to measure the grain size at least 60 grains were selected from the middle of the stir zone and the equivalent circular diameter was obtained by the help of image analysis software, the reported numbers are the average ± standard deviation. Microhardness tests were conducted using a Tukon 2500 automatic hardness measurement system.

Temperature measurement during FSP was carried out by embedding a 0.25 mm diameter K-type thermocouple in the pin of the rotating tool, details are shown in Figure 3-1. The thermocouple was constantly in contact with the dynamically recrystallized material. The thermocouple was connected to a small

data acquisition system with internal memory which was attached to the spindle of the FSW machine. For more details about the temperature measurement system please refer to [19] where same setup and conditions have been used for friction stir spot welding.

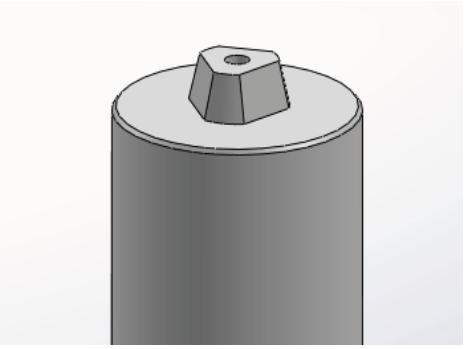

Figure 3-1: Tool geometry with thermocouple hole location at centre.

3.3 Results and Discussion

3.3.1 Grain Growth Model

As shown in Section 2.3.1 the microstructure of Al 5059 alloy before FSP contained elongated grains which are formed due to rolling. After one FSP pass, the stir zone microstructure compromises fine grains with an average radius of 0.98 μm, which are formed as a result of dynamic recrystallization, Figure 3-2. It should be considered that because of the presence of alloying elements and relatively high volume fraction of the precipitates in 5XXX series aluminum alloys formation of such small recrystallized grains is not unusual [5]. In addition, it is shown that the grain size in severely plastically deformed aluminum decreases with increasing the Mg content [20-22]. This is related to the effects of

Mg on reducing the dislocations mobility and stacking fault energy and decreasing the recovery rate [21, 22].

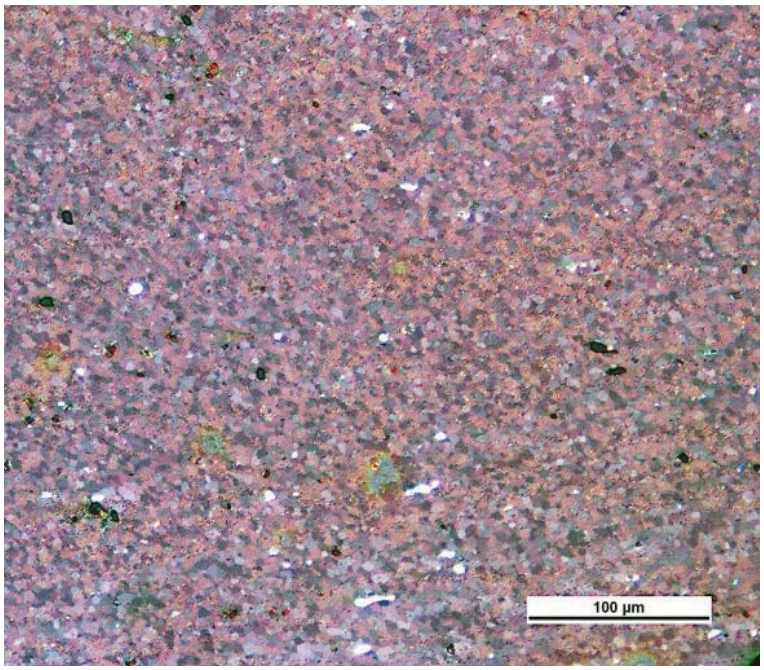

Figure 3-2: Microstructure of Al 5059 after FSP at 454 RPM and 30 mm/min.

In order to determine if grain growth happens during the cooling cycle a sample was friction stir processed while being in contact with a mixture of methanol and liquid nitrogen (approximately 193 K). The results showed that no remarkable grain growth occurs during the cooling cycles and the grain size was similar (to within ±0.5 µm) to the sample processed without forced cooling. Aside from the above considerations, increasing the amount of Mg in aluminum alloys also significantly increases the activation energy for grain boundary migration which accounts for the negligible difference in grains sizes when accelerated cooling is imposed during welding [8].

Table 3-1 indicates the measured grain sizes of the heat treated samples after one FSP pass. For instance, the stir zone grain structure for the samples heat treated for 2400 and 3000 seconds are represented in Figure 3-3.

Table 3-1: Grain radius of the samples heat treated at 448 K for different times.

Heat treatment Time (S)	Grain Radius (μm)	Standard Deviation
600	1.90	0.11
1200	1.87	0.68
1800	2.18	0.38
2400	2.33	0.43
3000	2.90	0.52
3600	3.64	0.73

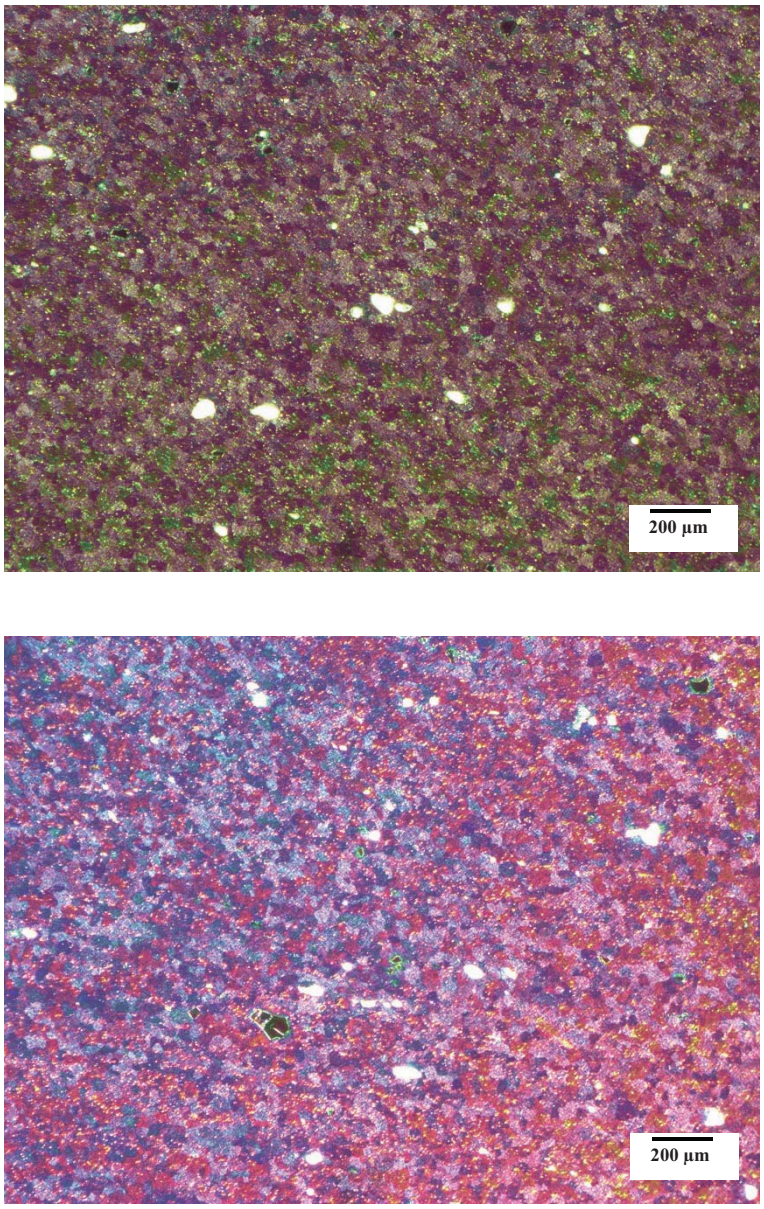

Figure 3-3: Representative images of the stir zone grain structure: a) sample heat treated for 2400 s and b) sample heat treated for 3000 s.

To study the microstructural evolution, the general particle controlled grain growth model (equation 3-1) is used in this work. This model predicts the change in grain radius with time by taking into account the effect of pinning

particles on grain boundary mobility [6]. Setting $R = R_0$ (here the starting grain radius is 0.98 μm) at $t = 0$ and solving equation (3-1) one finds that:

$$\frac{A}{R_m^2}t = \frac{R_0 - R}{R_m} + Ln\left(\frac{R_m - R_0}{R_m - R}\right) \quad (3\text{-}2)$$

In equation (3-2) R_m is the limiting grain size given by:

$$R_m = \frac{2r}{3V_f} \quad (3\text{-}3)$$

where r and V_f are the radius and volume fraction of the particles respectively.

Although 5XXX series aluminum alloys are not categorized among the precipitation hardened alloys, depending on the chemical composition of the alloy different second phase particles may be present in the microstructure. As discussed in Chapter 2, $Al_6(Mn,Fe)$, Al_3Fe, Mg_2Si, $Al_7(Fe,Cr)$, Al_8Mg_5, $Al_{13}Cr_2$, $Al_{13}(Cr,Mn)_2$, $Al_{12}(Fe,Mn)_3Si$, $Al_3(Mn,Fe,Cu)$ and Al_3Zr particles are generally found in 5XXX series aluminum alloys [14, 23-31]. A detailed investigation was performed to study the properties of the particles present in Al 5059 alloy (refer to section 2.3.1) and it was shown that the majority of the particles are $Al_6(Mn,Fe)$ types of inclusions with two morphologies: elongated and round or cubic. Based on several TEM images, it was found that only round particles are effective in pinning the grain boundaries in our samples (an example is shown in Figure 3-4) therefore for calculating R_m the radius (r = 0.102 μm) and volume fraction (V_f = 0.015) of round particles were only considered which gives $R_m \approx 4.53$ μm (the limiting grain size would be $d_m \approx 9$ μm).

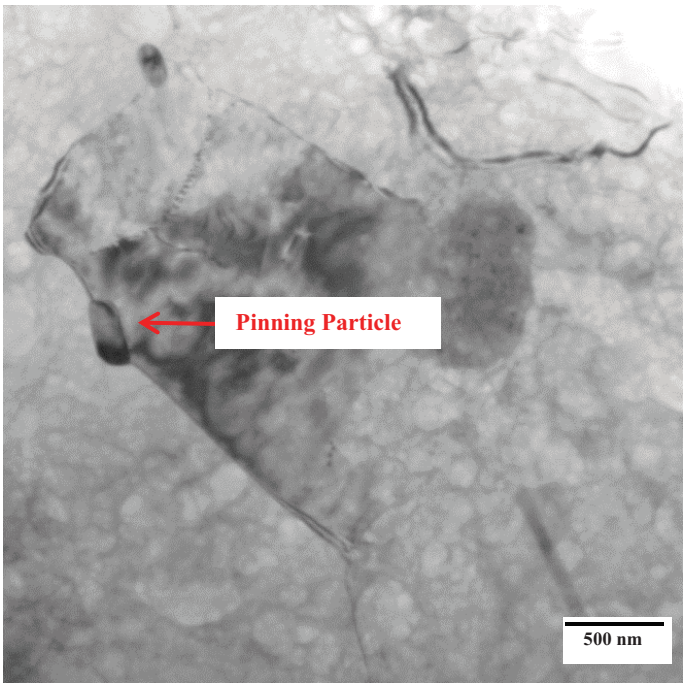

Figure 3-4: TEM micrograph of friction stir processed Al 5059 showing pinning of a grain boundary by a rhomboidal particle.

Figure 3-5 shows the temperature variations vs. time obtained from the thermocouple embedded in the pin of the tool as indicated in Figure 3-1. The thermocouple captured a maximum temperature of 432 ^{o}C (705 K). As shown in Figure 2-4, ThermoCalc analysis showed that the available particles are stable within this temperature range; therefore precipitates dissolution and reprecipitation are not expected to happen during FSP.

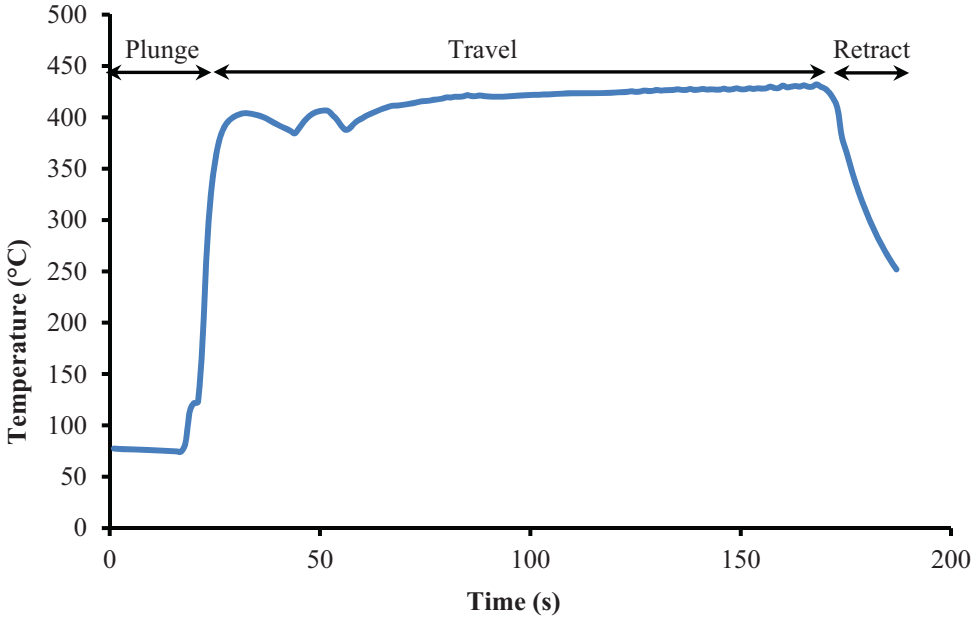

Figure 3-5: Temperature variations during friction stir processing of Al 5059 alloy at a rotation speed of 454 rpm and travel speed of 33 mm/min, location of the thermocouple is shown in Figure 3-1.

Figure 3-6 shows the grain sizes achieved after heat treatment along with a fitted graph in the form of equation 3-1. The calculated value for R_m was used here to find the best fitting curve.

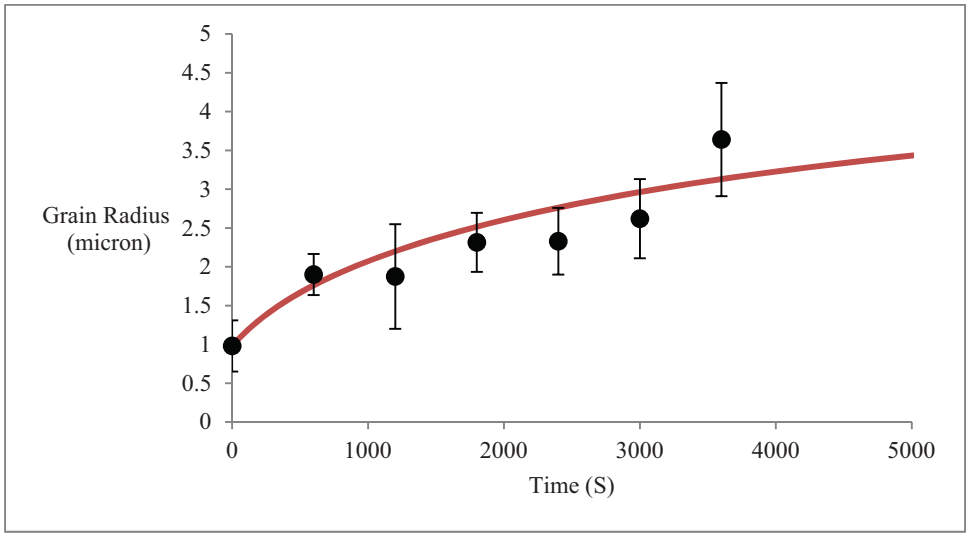

Figure 3-6: Measured stir zone grain radius of samples heat treated for different times. The line shows the fitted curve.

Based on the fitted curve on the experimental data (Figure 3-6) the average value for reduced grain boundary mobility would be $A = 2.7 \times 10^{-15}\, m^2/s$. It is also possible to calculate A using the material properties of Al 5059 alloy. A is given by:

$$A = M.\gamma \qquad (3.4)$$

where M is the high angle grain boundary mobility and γ is the high angle grain boundary energy. We know that $\gamma \approx 0.3\, J/m^2$ for aluminum and its alloys [7] and M can be calculated by the following equation [32, 33]:

$$M = \delta_G D^{GB} \frac{b}{KT} \qquad (3.5)$$

where δ_G is the thickness of the grain boundary ($\delta_G \approx 5 \times 10^{-10} m$ for aluminum [34]), D^{GB} is the coefficient for grain boundary diffusion, b is Burgers vector ($b = 2.86 \times 10^{-10} m$ for aluminum), K is the Boltzmann constant and T is absolute temperature (here $T = 448\, K$). Equation 3.5 is generally used for pure metals where the migration of high angle grain boundaries is controlled by the diffusion of atoms across the boundary, therefore for pure metals the self-diffusion coefficient should be inserted in the equation [32, 33]. It is well-known that addition of alloying elements strongly affects the grain boundary mobility by the so called solute drag [6, 35, 36]; for example Ivanov has shown that increasing the Mg content from 0.2×10^{-5} to 0.1 wt. % decreases the boundary mobility by more than one order of magnitude [37]. The main alloying element in the Al 5059

alloy is magnesium (more than 5 wt.%) therefore we have here ignored other alloying elements. In metallic alloys with high concentration of alloying elements where the solute drag effect is strong, the grain boundary migration changes from being controlled by grain boundary self-diffusion to grain boundary diffusion of the slowest diffusing alloying element [6]. Ivanov has experimentally studied this phenomena for different concentrations of magnesium in aluminum alloys [37]. It is therefore reasonable to put the coefficient for grain boundary diffusion of magnesium in aluminum as D^{GB} in equation (3.5). According to Kamp *et al*. [38] the Arrhenius relation for grain boundary diffusion of magnesium in aluminum is:

$$D_{Mg}^{GB} = 1 \times 10^{-3} \cdot exp\left(\frac{-115000}{R_g T}\right) \qquad (3.6)$$

where R_g is the universal gas constant. At T = 448 K Equation (3.6) gives $D_{Mg}^{GB} = 4 \times 10^{-17}\ m^2/s$. Now based on equations (3.4) and (3.5) A = $2.1 \times 10^{-17}\ m^2/s$; this value is comparable to the value obtained from the experimental data.

3.3.2 Microstructure – Hardness Relationship

Figure 3-7 shows the hardness values for samples with different grain sizes. It can be seen that the alloy indicates a Hall-Petch behavior (equation 1.7) with the constants being H_0 = 86 Hv and kH = 16 Hv.$\mu m^{0.5}$. The value of kh is in good agreement with the value of 14 Hv.μm0.5 reported for Al 5083 [39]. It should be noted that all the samples shown in Figure 3-7 are prepared with a

single pass FSP with similar conditions so no change in the properties of the particles is expected and the only difference between the samples arises from the difference in grain sizes.

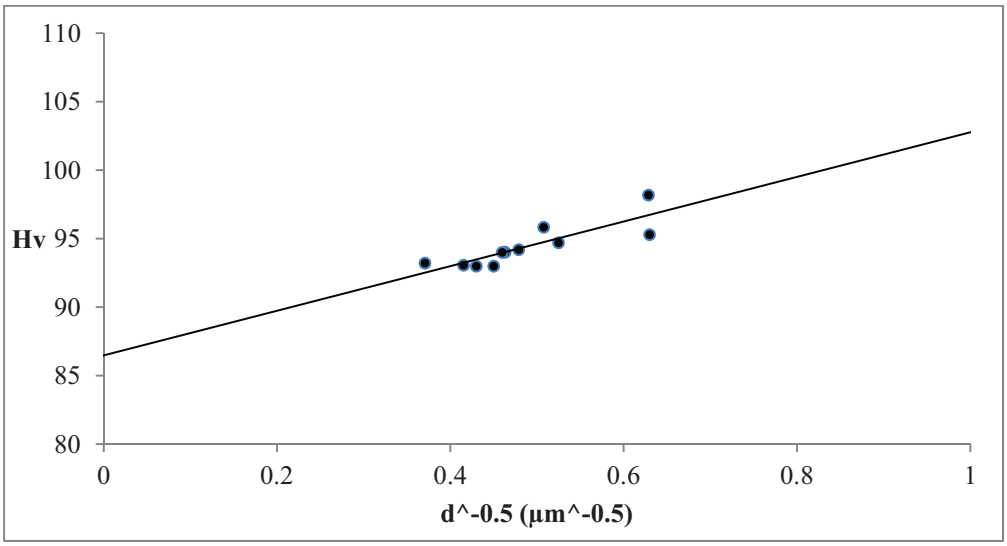

Figure 3-7: Effect of grain size on hardness friction stir processed Al 5059.

Furthermore, to investigate the effect of dislocation density on hardness two samples were rolled after FSP and one was annealed afterwards for 20 min at 423 K. This annealing is just enough to cause recovery but no grain growth is expected to happen. Figure 3-8 shows the microstructure of these two samples. Due to the extremely high dislocation content and poor contrast formed around dislocation clusters, it was difficult to measure the grain sizes using the TEM micrographs; however it is clear that the annealed sample has a significantly lower dislocation density, see Figure 3-8.

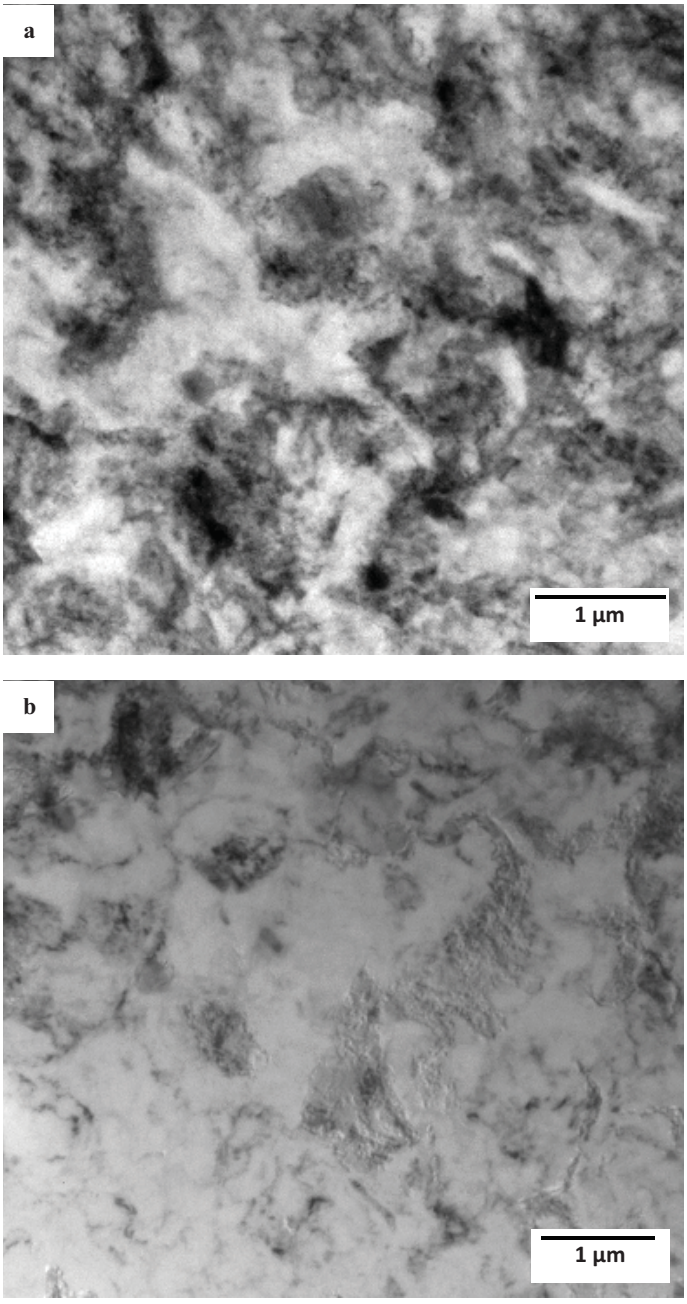

Figure 3-8: Dislocation structures in friction stir processed Al 5059 a) rolled only sample and b) rolled and annealed sample.

Despite the difference in dislocation density these two samples had similar hardness value around 97.5 ± 1.6 HV. Based on the TEM micrographs in Figure 3-8, the annealing produced a change in microstructure from a network of highly

deformed subgrains to slightly finer grains with lower dislocation density that correspond to the early stage of recrystallization. This transition from a deformed structure to finer grain structure would result in a trade-off between work hardening and grain boundary strengthening, an in this case these mechanisms appear to have a nearly equal influence on the overall hardness.

The results indicated by Figures 3-7 and 3-8 mainly indicate that the contribution of grain size and dislocation density is not very significant in terms of the strengthening of the Al 5059 alloy. Under these circumstances, one would then expect to relate most of the changes in hardness or yield strength in FSP fabricated composites using this alloy to the potential contribution of the reinforcing particles alone, since the properties of the matrix will not be significantly enhanced when its grain size is refined, or work hardening increases.

3.4 Summary and Conclusions

Microstructural evolution of Al 5059 during friction stir processing and subsequent heat treatment is studied and the following were found:

1- Microstructure of the starting material contains different particles the majority of which are $Al_6(Mn,Fe)$ type particles.

2- Two morphologies of particles were detected and it is showed that only the rhomboidal particles are effective in pinning the grain boundaries.

3- During FSP maximum temperature of the stir zone was measured to be 643 K and ThermoCalc analysis confirmed that no dissolution happens up to this 643 K in Al 5059.

4- No significant grain growth happens during friction stir processing in Al 5059 because of the effect of Mg on decreasing the grain boundary mobility.

5- As a result of high Mg content in Al 5059 grain boundary migration is controlled by diffusion of Mg atoms into Al rather than by self-diffusion of Al atoms.

6- Grain size of samples heat treated at 448 K can be related to time using the particle controlled grain growth model.

Microhardness measurements also revealed that hardness of friction stir processed Al 5059 follows Hall-Petch relationship and it was shown that particles and dislocation density play a minor role in strengthening compared to grain boundaries.

3.5 References

[1] El-Danaf EA, El-Rayes MM, Soliman MS. Friction stir processing: An effective technique to refine grain structure and enhance ductility. Materials and Design 2010;31:1231-6.

[2] Cavaliere P, De Marco PP. Friction stir processing of AM60B magnesium alloy sheets. Materials Science and Engineering A 2007;462:393-7.

[3] Sato Y, Urata M, Kokawa H. Parameters controlling microstructure and hardness during friction-stir welding of precipitation-hardenable aluminum alloy 6063. Metallurgical and Materials Transactions A 2002;33:625-35.

[4] Mishra RS, Ma ZY. Friction stir welding and processing. Materials Science and Engineering R: Reports 2005;50.

[5] Yazdipour A, Shafiei M A, Dehghani K. Modeling the microstructural evolution and effect of cooling rate on the nanograins formed during the friction stir processing of Al5083. Materials Science and Engineering A 2009;527:192-7.

[6] Humphreys FJ, Hatherly M. RECRYSTALLIZATION AND RELATED ANNEALING PHENOMENA: ELSEVIER; 2004.

[7] Robson JD, Campbell L. Model for grain evolution during friction stir welding of aluminium alloys. Science and Technology of Welding and Joining 2010;15:171-6.

[8] Gerlich A, Yamamoto M, North TH. Strain rates and grain growth in Al 5754 and Al 6061 friction stir spot welds. Metallurgical and Materials Transactions A: Physical Metallurgy and Materials Science 2007;38:1291-302.

[9] Grujicic M, Pandurangan B, Yen CF, Cheeseman BA. Modifications in the AA5083 Johnson-Cook Material Model for Use in Friction Stir Welding Computational Analyses. J of Materi Eng and Perform 2011:1-11.

[10] Humphreys FJ. A unified theory of recovery, recrystallization and grain growth, based on the stability and growth of cellular microstructures - II. The effect of second-phase particles. Acta Materialia 1997;45:5031-9.

[11] Jana S, Mishra RS, Baumann JA, Grant G. Effect of process parameters on abnormal grain growth during friction stir processing of a cast Al alloy. Materials Science and Engineering A 2010;528:189-99.

[12] Charit I, Mishra RS, Mahoney MW. Multi-sheet structures in 7475 aluminum by friction stir welding in concert with post-weld superplastic forming. Scripta Materialia 2002;47:631-6.

[13] Hassan KAA, Norman AF, Price DA, Prangnell PB. Stability of nugget zone grain structures in high strength Al-alloy friction stir welds during solution treatment. Acta Materialia 2003;51:1923-36.

[14] Chen K, Gan W, Okamoto K, Chung K, Wagoner RH. The mechanism of grain coarsening in friction-stir-welded AA5083 after heat treatment. Metallurgical and Materials Transactions A: Physical Metallurgy and Materials Science 2011;42:488-507.

[15] Huskins E, Cao B, Ramesh K. Strengthening mechanisms in an Al–Mg alloy. Materials Science and Engineering: A 2010;527:1292-8.

[16] Sun Y, Fujii H, Takaki N, Okitsu Y. Novel spot friction stir welding of 6061 and 5052 Al alloys. Science and Technology of Welding & Joining 2011;16:605-12.

[17] Yin YH, Sun N, North TH, Hu SS. Microstructures and mechanical properties in dissimilar AZ91/AZ31 spot welds. Materials Characterization 2010;61:1018-28.

[18] Colegrove PA, Shercliff HR. CFD modelling of friction stir welding of thick plate 7449 aluminium alloy. Science and Technology of Welding and Joining 2006;11:429-41.

[19] Gerlich A, Avramovic-Cingara G, North TH. Stir zone microstructure and strain rate during Al 7075-T6 friction stir spot welding. Metallurgical and Materials Transactions A: Physical Metallurgy and Materials Science 2006;37:2773-86.

[20] Chen YJ, Chai YC, Roven HJ, Gireesh SS, Yu YD, Hjelen J. Microstructure and mechanical properties of Al-xMg alloys processed by room temperature ECAP. Materials Science and Engineering A 2012;545:139-47.

[21] Iwahashi Y, Horita Z, Nemoto M, Langdon TG. Factors influencing the equilibrium grain size in equal-channel angular pressing: Role of Mg additions to aluminum. Metallurgical and Materials Transactions A: Physical Metallurgy and Materials Science 1998;29:2503-10.

[22] Morishige T, Hirata T, Uesugi T, Takigawa Y, Tsujikawa M, Higashi K. Effect of Mg content on the minimum grain size of Al-Mg alloys obtained by friction stir processing. Scripta Materialia 2011;64:355-8.

[23] Sato YS, Park SHC, Kokawa H. Microstructural factors governing hardness in friction-stir welds of solid-solution-hardened Al alloys. Metallurgical and Materials Transactions A: Physical Metallurgy and Materials Science 2001;32:3033-42.

[24] Fuller CB, Mahoney MW. The effect of friction stir processing on 5083-H321/5356 Al arc welds: Microstructural and mechanical analysis. Metallurgical and Materials Transactions A: Physical Metallurgy and Materials Science 2006;37:3605-15.

[25] Goswami R, Spanos G, Pao PS, Holtz RL. Precipitation behavior of the β phase in Al-5083. Materials Science and Engineering A 2010;527:1089-95.

[26] Vetrano JS, Bruemmer SM, Pawlowski LM, Robertson IM. Influence of the particle size on recrystallization and grain growth in Al-Mg-X alloys. Materials Science and Engineering A 1997;238:101-7.

[27] Frankel GS, Xia Z. Localized corrosion and stress corrosion cracking resistance of friction stir welded aluminum alloy 5454. Corrosion 1999;55:139-50.

[28] Verma R, Friedman PA, Ghosh AK, Kim S, Kim C. Characterization of superplastic deformation behavior of a fine grain 5083 AI alloy sheet. Metallurgical and Materials Transactions A: Physical Metallurgy and Materials Science 1996;27:1889-98.

[29] Attallah MM, Strangwood M, Davis CL. Influence of the heating rate on the initiation of primary recrystallization in a deformed Al-Mg alloy. Scripta Materialia 2010;63:371-4.

[30] Wen W, Zhao Y, Morris JG. The effect of Mg precipitation on the mechanical properties of 5xxx aluminum alloys. Materials Science and Engineering A 2005;392:136-44.

[31] Fonda RW, Pao PS, Jones HN, Feng CR, Connolly BJ, Davenport AJ. Microstructure, mechanical properties, and corrosion of friction stir welded Al 5456. Materials Science and Engineering A 2009;519:1-8.

[32] Sandsttröm R. Subgrain growth occurring by boundary migration. Acta Metallurgica 1977;25:905-11.

[33] Roberts W, Ahlblom B. A nucleation criterion for dynamic recrystallization during hot working. Acta Metallurgica 1978;26:801-13.

[34] Mazilkin AA, Straumal BB, Rabkin E, Baretzky B, Enders S, Protasova SG, et al. Softening of nanostructured Al-Zn and Al-Mg alloys after severe plastic deformation. Acta Materialia 2006;54:3933-9.

[35] Molodov DA, Czubayko U, Gottstein G, Shvindlerman LS. The motion of high angle grain boundaries in Al and Al-alloys. 1996. p. 523-8.

[36] Gottstein G, Shvindlerman LS. Grain Boundary Migration in Metals: Thermodynamics, Kinetics, Applications: CRC Press; 2010.

[37] Ivanov VA. On Kinetics and Thermodynamics of High Angle Grain Boundaries in Aluminum: Experimental Study on Grain Boundary Properties in Bi- and Tricrystals: RWTH University Aachen; 2006.

[38] Kamp N, Sullivan A, Tomasi R, Robson JD. Modelling of heterogeneous precipitate distribution evolution during friction stir welding process. Acta Materialia 2006;54:2003-14.

[39] Sato YS, Urata M, Kokawa H, Ikeda K. Hall-Petch relationship in friction stir welds of equal channel angular-pressed aluminium alloys. Materials Science and Engineering A 2003;354:298-305.

4 Dispersion of Reinforcement in Composites Fabricated Using FSP[1]

[1] A version of this chapter has been published: H. Izadi, A. Gerlich, Distribution and stability of carbon nanotubes during multi-pass friction stir processing of carbon nanotube/aluminum composites, Carbon 50 (2012) p 4744 –474 9.

4.1 Overview

Friction stir processing has been shown to be a possible method for distributing reinforcing particles into a metallic matrix and a variety of composites has been fabricated using this process [1-10]. As shown in Figure 4-1, for composite fabrication by FSP, first a groove or a number of holes are machined on the surface of the matrix metal and the reinforcement is inserted into the groove/holes; then single or multi-pass FSP is performed along the groove. Material flow induced by the pin mixes the two materials and a composite layer is achieved. In addition to the forcible mixing involved with this process, another beneficial feature of friction stir processing is that no bulk melting occurs during the process [11], therefore deterioration of mechanical properties or dissolution of the reinforcing material may be suppressed, and these are typical problems in casting and powder metallurgy based metal matrix composite fabrication techniques.

As discussed in Chapter 1, FSP parameters can significantly influence the distribution of the reinforcing phase and hence affect the properties of the composite. Therefore a strategy to fabricate MMCs with uniform distribution of particles should be based on a reasonable understanding of friction stir processing. In this regard, proper rotation and travel speeds and tool geometry must be designated to impose the desired material flow and consequently the desired particle distribution. In addition to the particle distribution, the effect of FSP parameters on the properties of the matrix metal should also considered. In the present chapter it will be discussed how the current understanding of FSP can be

utilized to design a composite fabrication technique that achieves a uniform distribution of the reinforcing phase along with enhanced mechanical properties of the matrix. The results observed in Al 5059/Al_2O_3 and Al 5059/MWCNT composites produced via the proposed method will also be discussed.

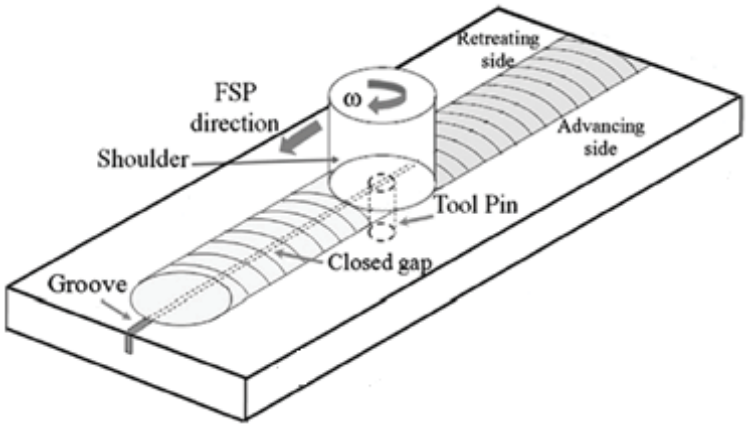

Figure 4-1: Schematic of composite fabrication process by FSP [12].

Ceramic particles such as Al_2O_3, SiC or B_4C can be added to aluminum for fabrication of composites with improved properties. Among these Al/Al_2O_3 composites have attracted more attention due to their greater availability and ease of production or processing methods and lower reactivity between aluminum and alumina [13-15]. In particular, addition of Al_2O_3 to aluminum is known to be an effective and relatively inexpensive technique to improve wear resistance of aluminum and its alloys [15-17]. Currently most of aluminum matrix composites are fabricated through casting or powder metallurgy methods, both of which involve high temperatures that can negatively affect the mechanical properties of the composite [15, 18, 19]. Recently solid-state processes such as FSP have been

also used for aluminum matrix composite fabrication [17, 20, 21]. For example, it is shown that FSP can be utilized to produce A356/Al_2O_3 composites which provide approximately a 30 Hv increase in the hardness [22]. Raaft *et al*. have produced A390/Al_2O_3 composites by FSP and have shown that increasing the tool rotation speed or decreasing the traverse speed result in a more uniform distribution of the alumina particles [23]. They have also reported a higher wear resistance for the composite samples. Sharifitabar *et al*. have used a multi-pass FSP technique to fabricate Al 5052/nano Al_2O_3 composites [24],and show that increasing the number of FSP passes to up to 4 passes improves the ultimate tensile and yield strength.

Given the exceptional mechanical properties of carbon nanotubes (CNTs), they are considered one of the most promising reinforcing materials for metal matrix composite production [25]. Although different production techniques have been successfully applied to incorporate CNTs to metals, obtaining a uniform distribution is still a challenge even though a great deal of research has aimed at addressing this issue [26-28]. Recently, friction stir processing (FSP) has been applied to disperse CNTs into alloy plates in order to fabricate metal matrix composites [4, 29-31], however achieving a uniform distribution along with a high concentration of CNT material has yet to be demonstrated. For example, Morisada *et al*. [4] used friction stir processing to fabricate AZ31/multi-walled CNT composite using different processing parameters, and concluded that the best distribution is achieved by using a relatively high rotation speed (1500 rpm) with a travel speed of 25 mm/min. An improvement in hardness by 50% was reported

for the composite compared to the unreinforced friction stir processed alloy, and this was attributed to a combination of grain refinement and strengthening due to the presence of multi-walled carbon nanotubes (MWCNTs).

Another major issue related to composite fabrication by FSP is the survivability of the CNT material during the severe deformation at high temperatures. The stability of the structure of CNTs in the presence of aluminum at elevated temperatures has been studied, and the formation of aluminum carbide (Al_4C_3) may occur particularly when the processing temperatures exceed 723 K [32, 33]. However it should be noted that the surface of the CNT structure does not react with Al even at high temperatures [34] and carbide formation preferentially occurs at defect sites and along the residual amorphous carbon layers on the surface of CNTs [35, 36]. A similar effect was observed during hot pressing of Al/CNT composite at 793 K, in which Al_4C_3 formed at the interface of the CNT and aluminum due to a reaction with the amorphous carbon on the CNT surfaces [37]. Choi *et al*. [38] have shown that carbides rarely form if fullerenes are individually dispersed in Al which is related to the low diffusivity of carbon in Al at temperatures around 773 K. It was also noted that when Al 2024/MWCNT alloy composite was fabricated from powders sintered at 873 K and 25 MPa, degradation of CNT into Al_4C_3 depended heavily on the surface condition and presence of impurities such as Al_2O_3 at the interface [39].

The stability of single-walled carbon nanotubes (SWCNTs) in Al 7075 matrix during friction stir processing has been studied by Johannes *et al*. [30], and by the use of Raman spectroscopy it was shown that SWCNTs survive processing

with a tool rotation speed of 400 rpm and a travel speed of 25.4 mm/min. In another work Lim *et al*. [29] have studied the effects of FSP rotation speed on the distribution of MWCNTs in Al 7075 and the hardness of the composite. Scanning electron microscope (SEM) and transition electron microscope (TEM) were used to confirm that the multi-walled structure of the CNTs used survive FSP when rotation speeds from 1500 to 2500 rpm are used, however some evidence of fracture was noted. It was shown that increasing rotation speed and tool shoulder penetration depth may enhance the distribution but a uniform distribution was not achieved using one FSP pass. Xu *et al*. [31] have reported that adding CNTs by friction stir processing significantly improves wear properties of Al 1060, however the distribution and survivability of the CNTs were not examined.

This section will discuss how applying the proposed multi-tool multi-pass FSP technique can be used to fabricate aluminum based composites with uniform distribution of the particles and improved mechanical properties. In addition since prior work suggests that FSP can influence the CNTs their stability is also studied in detail by different electron microscopy techniques.

4.2 Experimental Procedure

Fabrication of the composites involved 6.3 mm thick Al 5059 alloy matrix material with a composition of Al-5.26Mg-0.79Mn-0.5Zn-0.09Fe-0.07Si-0.02Ti, which was in the rolled and H131 temper condition. Alumina particles with two different sizes were used, see Figure 4-2.

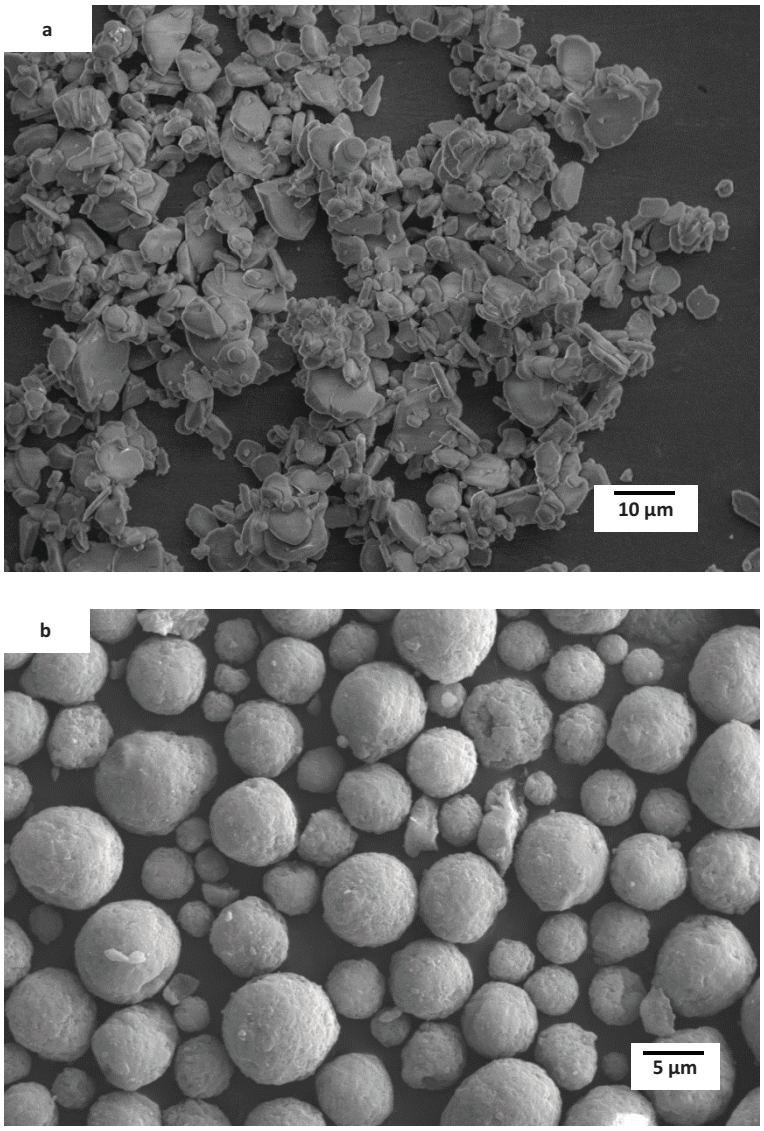

Figure 4-2: SEM micrograph showing a) 10 µm sized alumina particles and b) 5 µm agglomerates of alumina nanoparticles.

Figure 4-2-a shows the larger alumina particles with an average size of 10 µm and Figure 4-2-b shows the smaller particles which are in the form of 5 µm clusters and can be broken into 80 – 120 nm sized particles. For the initials tests the micron sized alumina particles were used to determine the correct combination of process parameters that gives a uniform particle distribution. After more than

30 to 40 tests were performed with the micron sized particles, the developed parameters were tested using the nanosized particles.

The MWCNT material had a nominal diameter of 30 to 50 nm, and axial length of 1 to 2 μm, Figure 4-3.

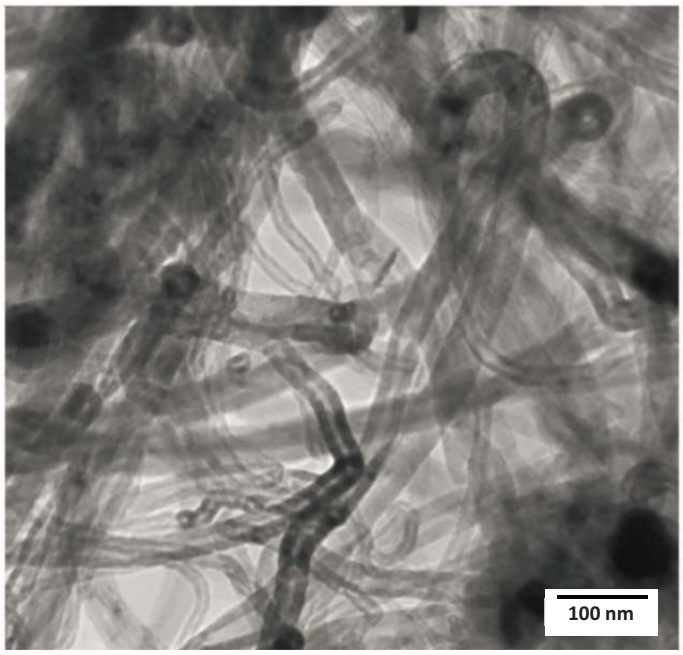

Figure 4-3: TEM micrograph showing the as-received CNTs.

The reinforcing phase was introduced into a 2.5 mm wide by 1.8 mm deep groove that was cut into the plate. This FSP fabrication procedure has been well documented elsewhere [40, 41], however one important detail to note is that before FSP was performed, the groove was effectively sealed by traversing a rotating cylindrical tool (with no pin) over the surface of the groove, to encapsulate the particles and prevent them from ejecting out of the groove during processing [3, 12, 20, 42]. FSP was then performed using 3 passes, first using a tool with a simple 4 mm diameter threaded pin and 10 mm shoulder (at 1130

rpm), followed by up to two additional passes with a tool comprising a 5 mm diameter pin and 12 mm shoulder (at 1130 rpm in a clockwise direction and 454 rpm in a counter clockwise direction respectively) using a constant travel speed of 30 mm/min. The final pass was performed with a 0.2 mm shorter pin, which provided a more homogenous stir zone as will be illustrated in the results to follow. The exact tool geometries are described in detail in Chapter 2.

Microstructures were characterized using a JEOL JAMP-9500F SEM equipped with Auger electron spectroscope (AES) and a JEOL 2010 TEM operating at 200 keV. High resolution TEM (HRTEM) was also conducted using an FEI Titan 80-300 microscope operating at 300 keV. Samples were prepared for TEM examination using a twin jet electropolisher, in a solution of 30 vol.% of HNO_3 and 70 vol.% of methanol at a temperature of -35 ºC (238 K) and voltage of 12 V. Microhardness was performed by a Vickers Microhardness machine with a load of 200 g and a dwell time of 15 s. The volume fraction of the reinforcing phase in the composites was calculated using image analysis of SEM and TEM micrographs, and is reported as an average ± one standard deviation for a minimum of 10 numbers of fields analyzed in either microscopy technique.

4.3 Results and Discussion

4.3.1 Fabrication of Al 5059/Alumina Composite

During fabrication of the MMC material, the key issues in establishing a uniform and large fraction of reinforcing particles relate to the processing

conditions. In particular the tool geometry and parameters used control the material flow and consolidation of material in the stir zone. One of the most significant challenges is in trying to achieve a uniform distribution with a single pass, however due to the material flow and intermixing mechanisms which are imposed by the tool, it was not possible to achieve a uniform distribution with a single pass. Figure 4-4-a shows the results produced when a single pass with the 3-flat tool is used during FSP, and the majority of material is displaced towards the advancing side of the stir zone. This has been previously confirmed for different composites produced by one FSP pass [21, 29, 43]. When two passes are used, this remained the case. However, when the direction of tool rotation was reversed during the second pass, the particle distribution became more uniform, see Figure 4-4-b.

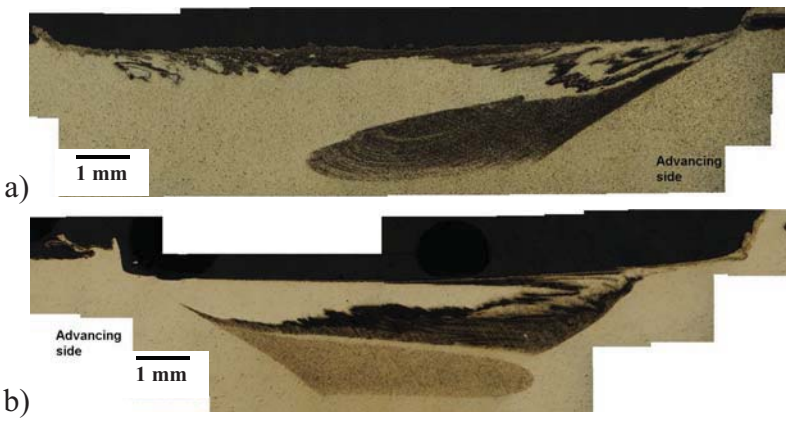

Figure 4-4: Optical micrographs of cross-sectioned FSP specimens produced using 454 RPM, a travel speed of 20 mm/min, and 10 µm alumina particles when a) one pass is used and b) two passes are used with a 3-flat tool geometry.

The accumulation of particles which was induced on the advancing side has been balanced by changing the tool rotation direction with alternating passes.

However, the distribution in the upper and low regions of the stir zone was quite different, and the hardness distribution was very non-uniform.

In order to further optimize the distribution of particles from the upper and lower portions of the stir zone, a simple threaded tool was used to disperse the particles vertically, before two additional passes were performed using the 3-flat tool which provides a finer matrix grain structure [44]. When this three-pass process was applied, the distribution of reinforcing particles was much more uniform in the upper and lower portions of the stir zone, as shown in Figure 4-5.

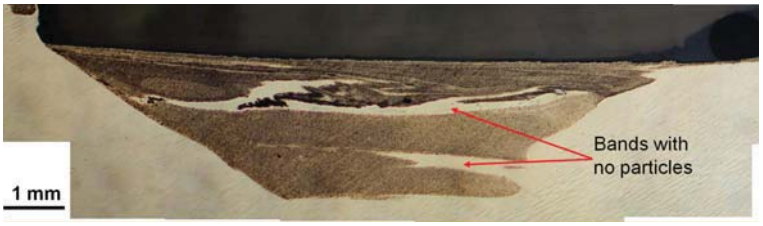

Figure 4-5: Optical micrograph of cross-sectioned FSP specimen produced using 10 μm alumina particles when a 3-pass approach was used with a constant pin length.

However, there remained two bands of material which were devoid of reinforcing particles, as noted in Figure 4-5. These were expected to result from the incorporation of the aluminum alloy material on the outer boundary of the stir zone due to the recirculating flow produced by the tool during the final pass. This recirculating flow has been studied in a number of prior studies, for example see [45], and the incorporation of the aluminum alloy material is a result of the penetration of the tool into the surface of the FSP material during the final pass. The penetration of the tool occurs as a result of the thermal softening of the material during FSP, and is inevitable since sufficient axial force must be applied

in order to prevent the formation of voids and defects within the stir zone and achieve particle distribution during FSP.

In order to avoid incorporating unreinforced aluminum alloy material into the stir zone during the final pass, a 3-flat tool with a slightly shorter tool pin (1.9 mm rather than 2.2 mm long) was used for the third pass. This ensured that when the tool penetrated into the plate, the pin did not mix new material from below the FSP region into the stir zone. This method allowed a stir zone with a uniform distribution of particles to be produced, with both micro-scale and nano-scale reinforcing particles. The optical micrograph shown in Figure 4-6 was produced when the proposed conditions were used in conjunction with alumina nanoparticles. The final pass was conducted with a slightly shorter pin to prevent the intermixing of new material into the stir zone, resulting in a uniform distribution of particles in the stir zone.

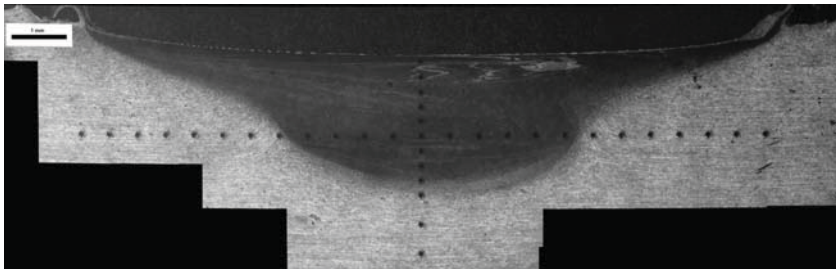

Figure 4-6: Optical micrograph of cross-sectioned FSP specimen produced using 20 nm alumina particles when a 3-pass approach was used with the parameters described in the Table.

Figure 4-7 shows the TEM micrographs obtained from the stir zone of the composite shown in Figure 4-6. Figure 4-7-a confirms that the 5μm agglomerates

were mostly fragmented during the fabrication process. However, as shown in Figure 4-7-b, they still appear to be partially agglomerated.

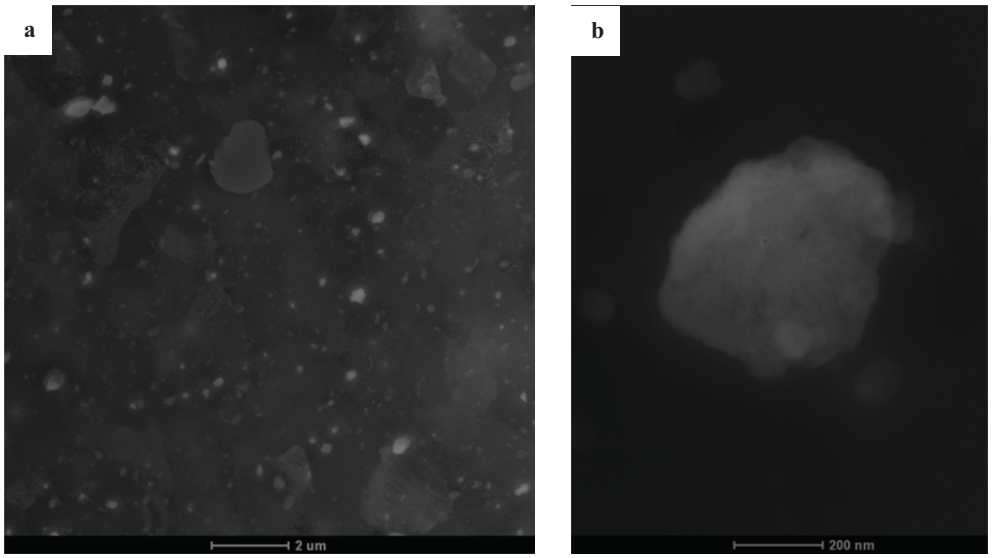

Figure 4-7: TEM micrographs showing a) microstructure of the Al 5059/nano Al_2O_3 composite produced with the proposed FSP technique, b) an Al_2O_3 particle inside the composite.

Figure 4-8 shows the microhardness of Al 5059/nano Al_2O_3 produced using different number of FSP passes, the indentations were performed along a line across the bottom of stir zone as shown in Figure 4-6 for the sample prepared with 3 passes. It is clear that a single FSP pass cannot achieve a uniform distribution, and a large scatter is observed in the hardness values. However, after 2 and 3 passes the hardness is more uniform along the stir zone. It should be noted that although the third pass does not significantly change the hardness at the bottom of stir zone (where the hardness results are from) instead it uniformly distributes the particles at top region of the stir zone, see Figure 4-4-b and Figure 4-6 for comparison. It is also obvious from Figure 4-8 that addition of nano

alumina particles has increased the hardness of the matrix from about 84 ± 3 Hv to about 97 ± 3 Hv. One might expect higher hardness values when nano particles are used. In this regard a possible reason for the relatively lower hardness improvement observed here can be the residual agglomeration in the particles, see Figure 4-7-b.

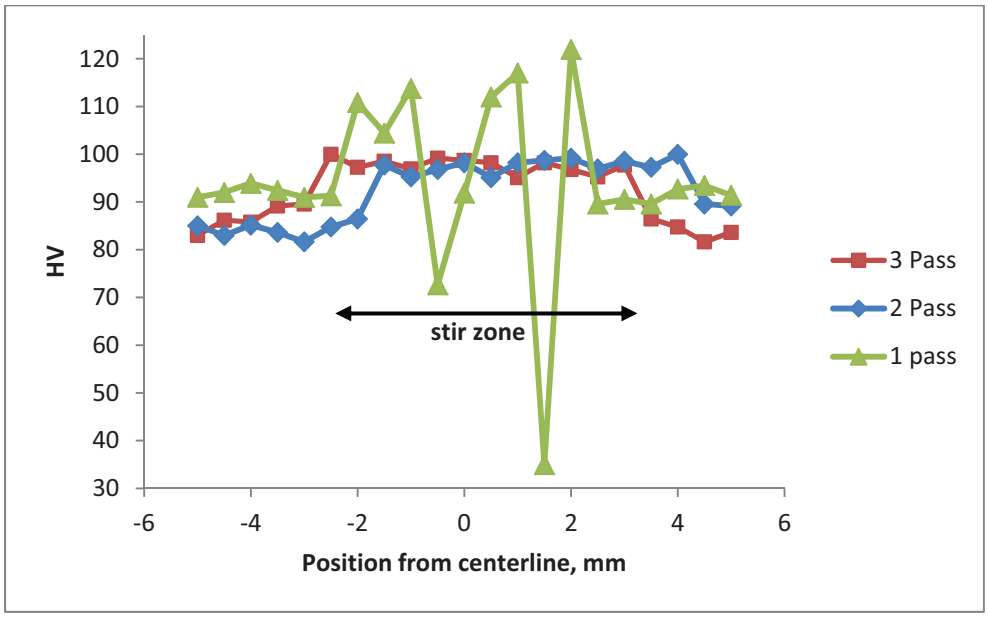

Figure 4-8: Microhardness distribution when FSP procedure is conducted in 1 to 3 passes.

4.3.2 Fabrication of Al 5059/CNT composite

4.3.2.1 Microstructure and distribution of CNT material

Figure 4.9 shows the optical micrographs of the samples after FSP using 2 and 3 passes, along with the corresponding microhardness profiles. In the sample processed using 2 passes, the distribution of the reinforcing material is uniform across the stir zone where the hardness measurements were made, however a layer

of unreinforced material (indicated by an arrow) has been transferred from the retreating to the advancing side closer to the surface of the plate. This flow from retreating to advancing side just under the tool shoulder is widely observed in friction stir welding, and is sometimes described as the 'flow arm' [41].There is also some vague evidence of 'onion ring' type flow patterns formed within the stir zone when 2 passes are applied, suggesting some segregation of the reinforcing material is present. There is a peak in hardness which occurs on the stir zone boundary at the advancing side in both micrographs shown in Figure 4-9, which indicates that some accumulation of the CNT material occurred on that side, which is consistent with the other observations of material movement from advancing to retreating side.

In order to homogenize the distribution of reinforcing material, a third FSP pass was performed with the tool rotation reversed. This appears to suppress the formation of the flow arm containing unreinforced material, and provides more uniform hardness values across the stir zone (see Figure 4-9). For example, when 3 passes are applied, there is no evidence of particle segregation, banded structure, or material flow patterns within the stir zone region. Some intermixed material is only evident near the surface of the plate, above the central stir zone region. The formation of flow patterns consisting of lamellae was noted in previous work involving FSP composite fabrication with a single pass, where the reinforcing particles were found to segregate along bands produced by the material flow around the tool [4, 29].

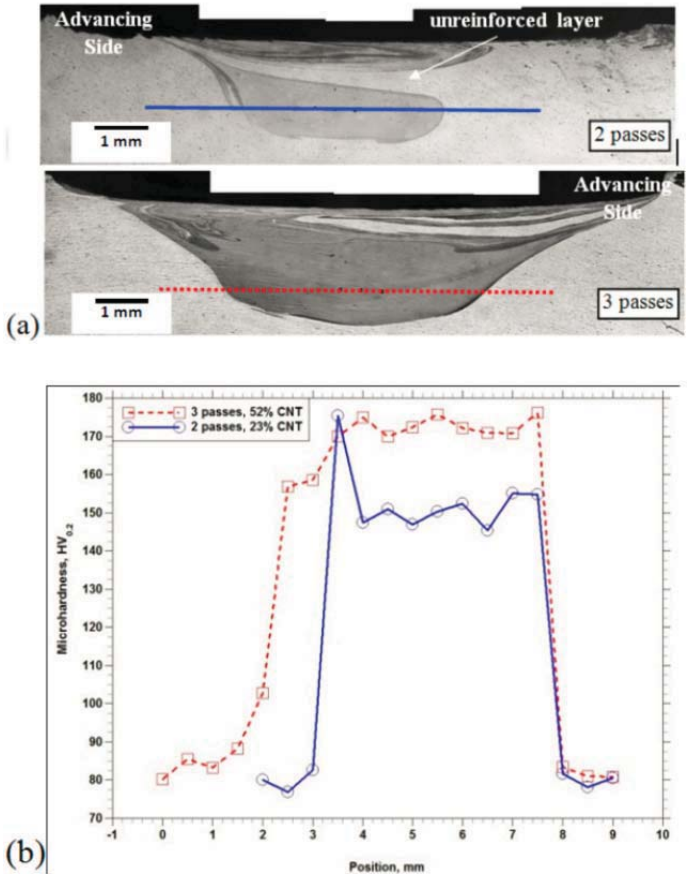

Figure 4-9: a) Optical micrographs of the composites made by FSP utilizing 2 and 3 passes, and b) microhardness profiles corresponding with the line locations indicated in the micrographs.

When examining the stir zone of friction stir processed composites, the formation of onion ring structures generally produces very scattered microhardness profiles [29, 43, 46, 47]. There is no evidence of the lamellae or onion ring formation after 3 passes, and this is supported by the uniform microhardness distribution in the stir zone which suggests that a uniform distribution of reinforcing particles has been achieved.

4.3.2.2 Microhardness measurements and CNT survivability

Figure 4-9-b shows the microhardness profiles of the two samples. The average microhardness along the stir zone of the 2 passes and 3 passes samples are 152 ± 7 Hv and 169 ± 6 Hv respectively, compared to 84 ± 3 Hv for the base metal. It should be considered that during the fabrication process, there is always some loss of the reinforcing material, making it virtually impossible to fabricate two samples with identical concentrations using 2 and 3 passes. Therefore, in addition to process parameters, the volume fraction and hardening contribution of the reinforcing material have an influence on these microhardness values; this will be discussed later in this section. The microhardness of the sample produced using 3 passes is approximately two times higher than that of the base material, and this enhancement can be attributed to the effects of high volume percentage of the reinforcement on direct strengthening and grain refinement. Dynamic recrystallization during friction stir processing leads to the formation of fine grains that gradually grow during the cooling to room temperature after the tool passes. It has been shown that different carbon nano-structures remarkably limit grain growth during friction stir processing by pinning the grain boundaries [4, 46, 48]. Morisada *et al*. [46] have reported submicron size grains for friction stir processed Al 5083 (which has similar composition to Al 5059) in the presence of fullerenes. They have also shown the MWCNTs can effectively retard grain growth due to pinning of grain boundaries in AZ31/MWCNT composite fabricated by friction stir processing [4]. The grain size measured by TEM (after quantification of several fields) indicates that the grains in the 3 passes sample

were in the range of 200 to 500 nm, while 1 to 2 micron sized grains were found in the 2 passes sample. TEM micrographs of the 2 and 3 passes friction stir processed samples are indicated in Figure 4-10 and Figure 4-11, where a sub-micron sized grain can be seen in Figure 4-11-a after 3 FSP passes.

A striking change in the morphology of the reinforcing phase is evident in the TEM micrographs shown for the 2 and 3 passes samples in Figure 4-10 and Figure 4-11.

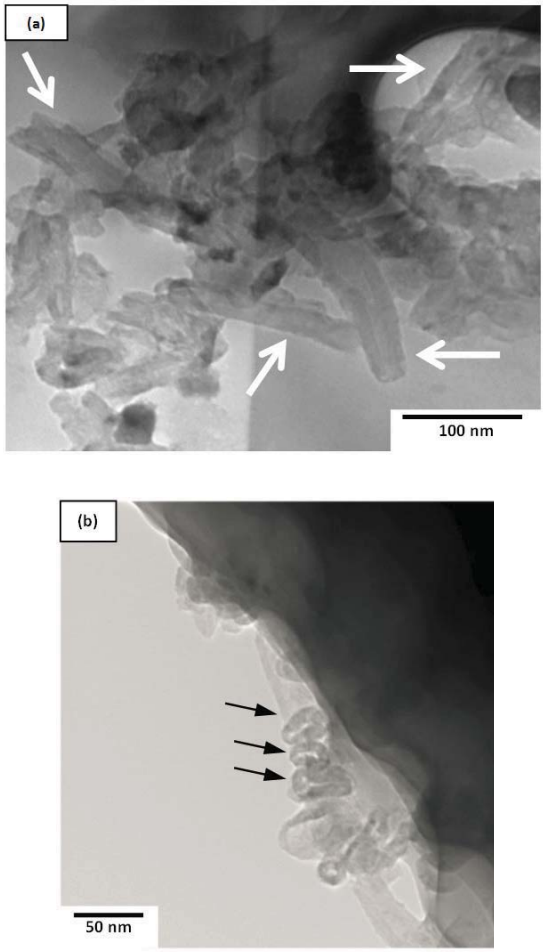

Figure 4-10: TEM micrographs of the composite material in the stir zone after 2 FSP passes, showing a) CNTs which survived 2 friction stir passes are indicated with arrows, and b) circular carbon structures.

Previous studies have shown that CNTs may survive a single friction stir processing cycle [4, 29] as well as other severe plastic deformation processes including accumulative roll-bonding [49] and equal channel angular pressing [50]. However it is clear that CNT failure occurs under the high shear stresses during high energy ball milling; for example Li *et al*. [51] and Ahn *et al*. [52] have shown that multi-walled CNTs transform to fine spheres during prolonged milling cycles.

When damage of the CNT walls occurs [53, 54], the formation of new structures such as carbon onion are possible [54], and this has been reported in CNT metal matrix composites production by spark plasma sintering which involves high temperatures and pressures. It has also been indicated that the deformation mechanism of MWCNTs at high strain rates (as in the case of FSP) is conducive to the formation of spherical structures such as carbon onion during high velocity impacts [55]. After 2 passes, extensive damage and fracture of the CNTs occur (shown in Figure 4-10-a), and spherical shelled carbon structures could be observed as well (see Figure 4-10-b). In these cases, an important factor facilitating the transformation is the progressive damage of the outer walls into broken graphitic shells, and these may then curl up into spheroidal structures in order to eliminate dangling bonds [56]. After 2 passes using FSP, a large number of tubular nano-structures are observed, however it is clear that their axial lengths (approximately 100 to 200 nm) are about 10 times shorter than the initial CNT material, and some even begin to assume circular structures (see Figure 4-10-b).

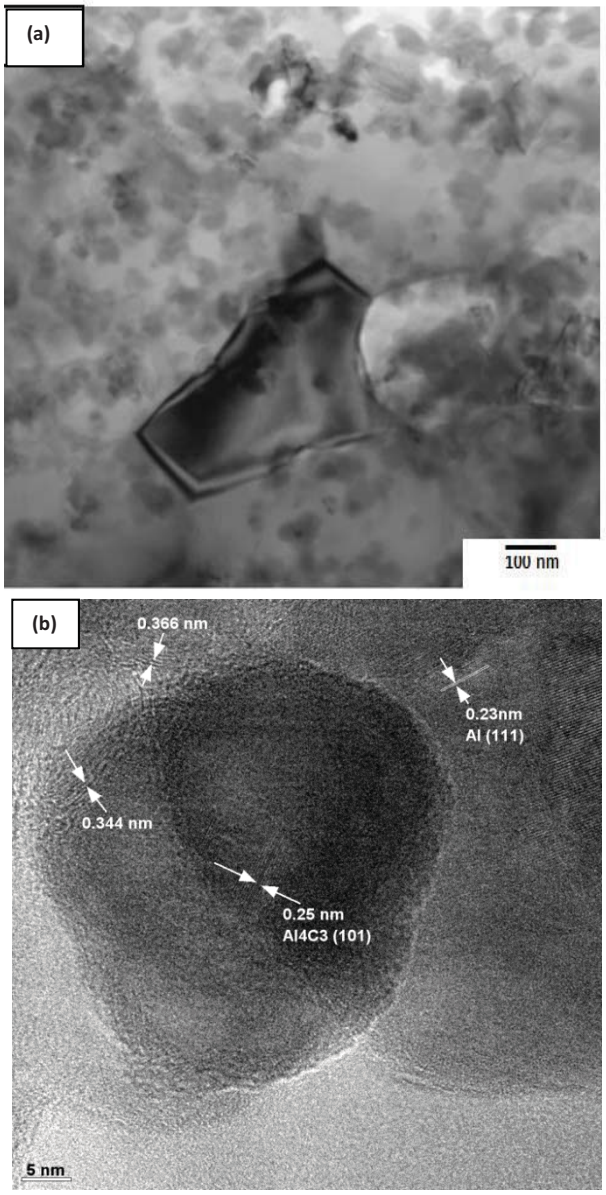

Figure 4-11: TEM micrograph of a) the stir zone of the sample processed with 3 passes in which no CNTs were found, and b) HRTEM image of the nanoparticles formed after 3 passes.

The final structure of the carbon after 3 passes appears to be mainly polyaromatic carbon structures as shown in Figure 4-11, and this has also been noted to form in SWCNTs during prolonged ball milling [57]. The present findings show that the high shear stresses along with the elevated temperatures in the stir zone have a detrimental influence on the MWCNT structure during

friction stir processing. In the case of FSP utilizing 3 passes, no MWCNT was found and the reinforcing material was in the form of spherical particles as shown in Figure 4-11. High resolution TEM was used to further analyse the newly formed particles and revealed the presence of polyaromatic carbon shells and aluminum carbide (Al_4C_3) in the microstructure, and an example of the measured inter-layer spacing values is represented in Figure 4-11-b. The lattice fringes labelled correspond with the 0.23 nm spacing for the Al (111) matrix, and the 0.25 nm spacing for the (101) plane of Al_4C_3 which was observed within the middle of the particle [38]. The outer surface and regions between particles contained carbon structures with inter-planar spacings labelled as 0.344 nm which correspond to polyaromatic carbon structures, [58, 59] and 0.366 nm for turbostratic carbon [60] which form after severe deformation. It should be noted that the majority of the interior of the particle did not have a clear crystalline structure corresponding with the 0.25 nm lattice labelled in Figure 4-11-b. Since the morphology of Al_4C_3 that forms in Al/CNT or Al/carbon fiber composites has been reported by different researchers to be needle-like or lath-like [33-35, 61, 62], it is likely that only a part of the carbon nanostructures have formed Al_4C_3, and the remainder of the particle consists of the polyaromatic and turbostratic carbon.

A SEM micrograph of the composite produced using 3 passes is shown in Figure 4-12, along with an AES map for carbon obtained from a selected region.

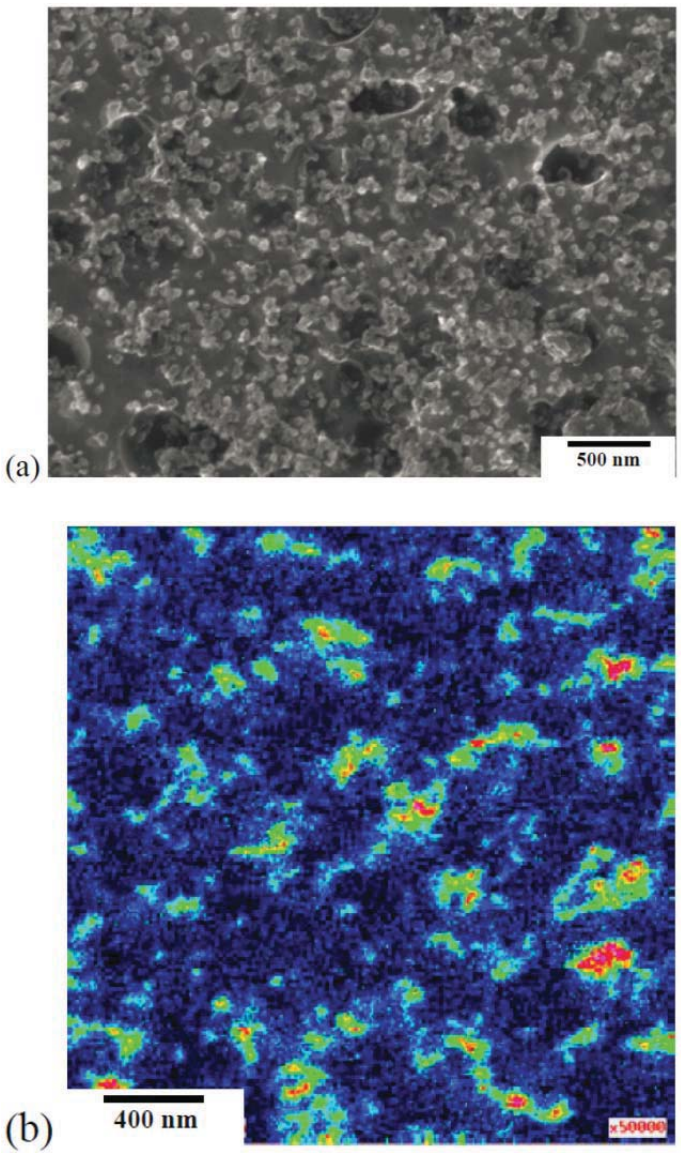

Figure 4-12: a) SEM micrograph and b) AES map for carbon, both obtained from the center of the stir zone of the 3 passes sample, red areas are almost pure Carbon.

The AES map confirms that there is a uniform distribution of carbon rich nanometer sized particles. The volume fraction of these secondary particles was measured using an image analysing software. The average volume fraction measurements from several SEM and TEM images indicate that the 2 and 3 passes samples contain 23 ± 2.5 vol.% and 52 ± 2.1 vol.% of the reinforcing

material respectively. It should be noted that although the same dimensions were used for the groove containing CNTs during FSP, the higher fraction observed after 3 passes likely resulted from possible variations in CNT powder packing and progressively increased penetration of the tool during FSP. The volume fraction of the CNTs in the composites produced previously by different techniques is up to around 20 vol.%, for example see [28, 36, 63, 64], which implies the FSP fabrication method is a potential route to produce CNT metal matrix composites with the highest reinforcing material content, although the integrity of the CNTs rapidly degrades when multiple passes are applied to improve homogeneity. Though it has been previously noted that CNT material is effective in blocking crack propagation in Al/CNT composites by bridging [65], it is of interest to note this will not be likely in this material due to their low aspect ratio.

To further investigate the contribution of the reinforcing phase on the microhardness values, the rule of mixtures ($H_{composite} = H_{matrix}V_{matrix} + H_{particle}V_{particle}$, where V is the volume fraction and H is the hardness) was applied to compare the hardness for the samples with different CNT concentrations after 2 and 3 passes. Though the authors acknowledge this is a simplistic view of the reinforcing contribution of the carbon nanostructures to the composite, it is a direct way to compare the average relative strengthening efficiency of the two structures obtained after 2 versus 3 passes, without making any assumptions regarding their properties. When the values for the composite hardness and Al 5059 matrix hardness (90 Hv ±3 when friction stir processed under the same conditions) are substituted, the effective hardness of the reinforcing phase is

calculated to be 372 Hv for sample with 2 passes and 243 Hv for sample with 3 passes, which is far lower than that expected for MWCNT material. Therefore, although the concentration of the CNT based material was lower in the 2 passes sample, the strengthening contribution was higher owing to the fact that more of the multi-walled tubular structure was still preserved. In the case of the 3 passes sample, the strengthening contribution was lower since all of the CNT material transformed into particles with an aspect ratio close to 1, and the structural changes have had a deleterious effect on the properties of these carbon nanostructures.

4.4 Summary and Conclusion

It is possible to fabricate aluminum based metal matrix composites by multi-pass FSP with different tools and processing conditions which are selected according to material flow during FSP. The results of Al 5059/Al_2O_3 and Al 5059/MWCNT composites produced using the proposed technique are presented in this chapter. It was shown that in both cases the reinforcement was uniformly distributed within the stir zone region and lead to an increase in the hardness. The improvement in the hardness is attributed to the effect of the reinforcing material on direct strengthening and grain refinement. In the case of Al 5059/MWCNT a composite with high volume percentage of nano-structured reinforcement was produced and a hardness increase of 2 times was achieved. Although observations confirmed that the MWCNTs maintained their multi-walled structure after 2

passes, a uniform distribution requires 3 passes in which case the stability of the MWCNT material could not be preserved.

4.5 References

[1] Mishra RS, Ma ZY, Charit I. Friction stir processing: A novel technique for fabrication of surface composite. Materials Science and Engineering A 2003;341:307-10.

[2] Hsu CJ, Chang CY, Kao PW, Ho NJ, Chang CP. Al-Al3Ti nanocomposites produced in situ by friction stir processing. Acta Materialia 2006;54:5241-9.

[3] Lee CJ, Huang JC, Hsieh PJ. Mg based nano-composites fabricated by friction stir processing. Scripta Materialia 2006;54:1415-20.

[4] Morisada Y, Fujii H, Nagaoka T, Fukusumi M. MWCNTs/AZ31 surface composites fabricated by friction stir processing. Materials Science and Engineering A 2006;419:344-8.

[5] Jun Q, Zhili F, Hanbing X, Frederick DA, Jolly BC, David SA. Producing a composite surface using friction stir processing. Seattle, WA2008. p. 33-6.

[6] Lee IS, Kao PW, Ho NJ. Microstructure and mechanical properties of Al-Fe in situ nanocomposite produced by friction stir processing. Intermetallics 2008;16:1104-8.

[7] Qu J, Xu H, Feng Z, An K, Battiste R, An L, *et al*. Forming AI-AI2O3 nanocomposite surfaces using friction stir processing. Greenville, SC2009. p. 349-56.

[8] Chen CF, Kao PW, Chang L, Ho NJ. Mechanical properties of nanometric Al2O3 particulate-reinforced Al-Al11Ce3 composites produced by friction stir processing. Materials Transactions 2010;51:933-8.

[9] Sun K, Shi QY, Sun YJ, Chen GQ. Microstructure and mechanical property of nano-SiCp reinforced high strength Mg bulk composites produced by friction stir processing. Materials Science and Engineering A 2012;547:32-7.

[10] Soleymani S, Abdollah-zadeh A, Alidokht SA. Microstructural and tribological properties of Al5083 based surface hybrid composite produced by friction stir processing. Wear 2012;278-279:41-7.

[11] Nandan R, DebRoy T, Bhadeshia HKDH. Recent advances in friction-stir welding - Process, weldment structure and properties. Progress in Materials Science 2008;53:980-1023.

[12] Alidokht SA, Abdollah-zadeh A, Soleymani S, Assadi H. Microstructure and tribological performance of an aluminium alloy based hybrid composite produced by friction stir processing. Mater Design 2011;32:2727-33.

[13] Zhang J, Alpas AT. Wear regimes and transitions in Al2O3 particulate-reinforced aluminum alloys. Materials Science and Engineering: A 1993;161:273-84.

[14] Shorowordi KM, Laoui T, Haseeb ASMA, Celis JP, Froyen L. Microstructure and interface characteristics of B4C, SiC and Al2O3 reinforced Al matrix composites: A comparative study. Journal of Materials Processing Technology 2003;142:738-43.

[15] Rahimian M, Parvin N, Ehsani N. Investigation of particle size and amount of alumina on microstructure and mechanical properties of Al matrix composite made by powder metallurgy. Materials Science and Engineering A 2010;527:1031-8.

[16] Surappa MK, Prasad SV, Rohatgi PK. Wear and abrasion of cast Al-Alumina particle composites. Wear 1982;77:295-302.

[17] Shafiei-Zarghani A, Kashani-Bozorg SF, Hanzaki AZ. Wear assessment of Al/Al2O3 nano-composite surface layer produced using friction stir processing. Wear 2011;270:403-12.

[18] Liu YB, Lim SC, Lu L, Lai MO. Recent development in the fabrication of metal matrix-particulate composites using powder metallurgy techniques. Journal of Materials Science 1994;29:1999-2007.

[19] Tahamtan S, Halvaee A, Emamy M, Zabihi MS. Fabrication of Al/A206-Al2O3 nano/micro composite by combining ball milling and stir casting technology. Materials and Design 2013;49:347-59.

[20] Shafiei-Zarghani A, Kashani-Bozorg SF, Zarei-Hanzaki A. Microstructures and mechanical properties of Al/Al2O3 surface nano-composite layer produced by friction stir processing. Materials Science and Engineering A 2009;500:84-91.

[21] Yang M, Xu C, Wu C, Lin KC, Chao YJ, An L. Fabrication of AA6061/Al2O3 nano ceramic particle reinforced composite coating by using friction stir processing. Journal of Materials Science 2010;45:4431-8.

[22] Mazaheri Y, Karimzadeh F, Enayati MH. A novel technique for development of A356/Al2O3 surface nanocomposite by friction stir processing. Journal of Materials Processing Technology 2011;211:1614-9.

[23] Raaft M, Mahmoud TS, Zakaria HM, Khalifa TA. Microstructural, mechanical and wear behavior of A390/graphite and A390/Al2O3 surface composites fabricated using FSP. Materials Science and Engineering A 2011;528:5741-6.

[24] Sharifitabar M, Sarani A, Khorshahian S, Shafiee Afarani M. Fabrication of 5052Al/Al2O3 nanoceramic particle reinforced composite via friction stir processing route. Materials and Design 2011;32:4164-72.

[25] Harris PJF. Carbon nanotube composites. International Materials Reviews 2004;49:31-43.

[26] O'Connell MJ. Carbon Nanotubes Properties and Applications: Taylor & Francis; 2006.

[27] R Zhong, H Cong, Hou P. F abrication of nano-Al based composites reinforced by single-walled carbon nanotubes. Carbon 2003;41:848-51.

[28] Xu CL, Wei BQ, Ma RZ, Liang J, Ma XK, Wu DH. Fabrication of aluminum-carbon nanotube composites and their electrical properties. Carbon 1999;37:855-8.

[29] Lim DK, Shibayanagi T, Gerlich AP. Synthesis of multi-walled CNT reinforced aluminium alloy composite via friction stir processing. Materials Science and Engineering A 2009;507:194-9.

[30] Johannes LB, Yowell LL, Sosa E, Arepalli S, Mishra RS. Survivability of single-walled carbon nanotubes during friction stir processing. Nanotechnology 2006;17:3081-4.

[31] Xu W, Ke L, Xing L, Zhao X. On the influence of carbon nanotubes on the wear performance and hardness of aluminium matrix composites. Materialwissenschaft und Werkstofftechnik 2011;42:375-8.

[32] Ci L, Ryu Z, Jin-Phillipp NY, Rühle M. Investigation of the interfacial reaction between multi-walled carbon nanotubes and aluminum. Acta Materialia 2006;54:5367-75.

[33] Poirier D, Gauvin R, Drew RAL. Structural characterization of a mechanically milled carbon nanotube/aluminum mixture. Composites Part A: Applied Science and Manufacturing 2009;40:1482-9.

[34] He CN, Zhao NQ, Shi CS, Song SZ. Fabrication of aluminum carbide nanowires by a nano-template reaction. Carbon 2010;48:931-8.

[35] Bakshi SR, Singh V, Seal S, Agarwal A. Aluminum composite reinforced with multiwalled carbon nanotubes from plasma spraying of spray dried powders. Surface and Coatings Technology 2009;203:1544-54.

[36] Laha T, Agarwal A, McKechnie T, Seal S. Synthesis and characterization of plasma spray formed carbon nanotube reinforced aluminum composite. Materials Science and Engineering A 2004;381:249-58.

[37] Xu CL, Wei BQ, Ma RZ, Liang J, Ma XK, Wu DH. Fabrication of aluminum-carbon nanotube composites and their electrical properties. Carbon 1999;37:855-8.

[38] Choi HJ, Shin JH, Bae DH. Self-assembled network structures in Al/C60 composites. Carbon 2010;48:3700-7.

[39] Deng CF, Zhang XX, Wang DZ, Ma YX. Calorimetric study of carbon nanotubes and aluminum. Materials Letters 2007;61:3221-3.

[40] Ma ZY. Friction stir processing technology: A review. Metallurgical and Materials Transactions A: Physical Metallurgy and Materials Science 2008;39 A:642-58.

[41] Mishra Rs, Mahoney Mw. Friction Stir Welding and Processing. First ed: ASM International; 2007.

[42] Asadi P, Faraji G, Besharati MK. Producing of AZ91/SiC composite by friction stir processing (FSP). International Journal of Advanced Manufacturing Technology 2010:1-14.

[43] Mahmoud ERI, Ikeuchi K, Takahashi M. Fabrication of SiC particle reinforced composite on aluminium surface by friction stir processing. Science and Technology of Welding and Joining 2008;13:607-18.

[44] Yin YH, Sun N, North TH, Hu SS. Influence of tool design on mechanical properties of AZ31 friction stir spot welds. Science and Technology of Welding and Joining 2010;15:81-6.

[45] Nandan R, Roy GG, Debroy T. Numerical simulation of three dimensional heat transfer and plastic flow during friction stir welding. Metallurgical and Materials Transactions A: Physical Metallurgy and Materials Science 2006;37:1247-59.

[46] Morisada Y, Fujii H, Nagaoka T, Nogi K, Fukusumi M. Fullerene/A5083 composites fabricated by material flow during friction stir processing. Composites Part A: Applied Science and Manufacturing 2007;38:2097-101.

[47] Cavaliere P. Mechanical properties of Friction Stir Processed 2618/Al2O3 metal matrix composite. Composites Part A: Applied Science and Manufacturing 2005;36:1657-65.

[48] Morisada Y, Fujii H, Nagaoka T, Fukusumi M. Nanocrystallized magnesium alloy - uniform dispersion of C60 molecules. Scripta Materialia 2006;55:1067-70.

[49] Salimi S, Izadi H, Gerlich AP. Fabrication of an aluminum-carbon nanotube metal matrix composite by accumulative roll-bonding. Journal of Materials Science 2011;46:409-15.

[50] Quang P, Jeong YG, Yoon SC, Hong SH, Kim HS. Consolidation of 1 vol.% carbon nanotube reinforced metal matrix nanocomposites via equal channel angular pressing. Journal of Materials Processing Technology 2007;187-188:318-20.

[51] Li YB, Wei BQ, Liang J, Yu Q, Wu DH. Transformation of carbon nanotubes to nanoparticles by ball milling process. Carbon 1999;37:493-7.

[52] Ahn JH, Shin HS, Kim YJ, Chung H. Structural modification of carbon nanotubes by various ball milling. Journal of Alloys and Compounds 2007;434-435:428-32.

[53] Bakshi SR, Musaramthota V, Virzi DA, Keshri AK, Lahiri D, Singh V, *et al*. Spark plasma sintered tantalum carbide-carbon nanotube composite: Effect of pressure, carbon nanotube length and dispersion technique on microstructure and mechanical properties. Materials Science and Engineering A 2011;528:2538-47.

[54] Lahiri D, Singh V, Keshri AK, Seal S, Agarwal A. Carbon nanotube toughened hydroxyapatite by spark plasma sintering: Microstructural evolution and multiscale tribological properties. Carbon 2010;48:3103-20.

[55] Bakshi SR, Singh V, Graham McCartney D, Seal S, Agarwal A. Deformation and damage mechanisms of multiwalled carbon nanotubes under high-velocity impact. Scripta Materialia 2008;59:499-502.

[56] Cao L, Gao C, Sun H, Zou G, Zhang Z, Zhang X, *et al*. Synthesis of diamond from carbon nanotubes under high pressure and high temperature. Carbon 2001;39:311-4.

[57] Pierard N, Fonseca A, Colomer JF, Bossuot C, Benoit JM, Van Tendeloo G, *et al*. Ball milling effect on the structure of single-wall carbon nanotubes. Carbon 2004;42:1691-7.

[58] Monthioux M, Smith BW, Burteaux B, Claye A, Fischer JE, Luzzi DE. Sensitivity of single-wall carbon nanotubes to chemical processing: An electron microscopy investigation. Carbon 2001;39:1251-72.

[59] Sergiienko R, Shibata E, Kim S, Kinota T, Nakamura T. Nanographite structures formed during annealing of disordered carbon containing finely-dispersed carbon nanocapsules with iron carbide cores. Carbon 2009;47:1056-65.

[60] Dobb MG, Guo H, Johnson DJ. Image analysis of lattice imperfections in carbon fibres. Carbon 1995;33:1115-20.

[61] Kwon H, Park DH, Silvain JF, Kawasaki A. Investigation of carbon nanotube reinforced aluminum matrix composite materials. Composites Science and Technology 2010;70:546-50.

[62] Steffens HD, Reznik B, Kruzhanov V, Dudzinski W. Carbide formation in aluminium-carbon fibre-reinforced composites. Journal of Materials Science 1997;32:5413-7.

[63] Daoush WM, Lim BK, Mo CB, Nam DH, Hong SH. Electrical and mechanical properties of carbon nanotube reinforced copper nanocomposites fabricated by electroless deposition process. Materials Science and Engineering A 2009;513-514:247-53.

[64] Uozumi H, Kobayashi K, Nakanishi K, Matsunaga T, Shinozaki K, Sakamoto H, *et al*. Fabrication process of carbon nanotube/light metal matrix composites by squeeze casting. Materials Science and Engineering A 2008;495:282-7.

[65] Choi HJ, Bae DH. Strengthening and toughening of aluminum by single-walled carbon nanotubes. Materials Science and Engineering A 2011;528:2412-7.

5 Conclusions and Recommendations

5.1 Conclusions

Friction stir processing has been used as a tool for microstructural modification, in which fine grains form as a result of dynamic recrystallization. In the case of Al 5059 alloy these fine grains do not grow during the cooling cycle because of the effect of magnesium on decreasing the grain boundary mobility in aluminum alloys. The amount of heat generated during FSP directly depends on the rotation speed therefore in order to achieve smaller grains the lowest rotation speed that gives a defect free stir zone should be utilized. On the other hand a tool with a 3-flat threaded pin produced the smallest grains, therefore in the range of the parameters studied during this thesis work, a 3-flat tool with a rotation speed of 454 rpm generated smallest grains. It should be mentioned that these parameters can also be used for friction stir welding of Al 5059.

Commercial Al 5XXX series or Al-Mg based alloys usually contain a significant amount of particles; and in Al 5059 the majority of particles present are $Al_6(Mn,Fe)$ type precipitates. ThermoCalc analysis showed that dissolution of these particles is not likely to happen during FSP but stresses and thermal cycles associated with FSP can break up these particles and affect mechanical properties of the alloy. Firstly, such particles are shown to preferably form on grain boundaries and promote fracture by enhancing void formation and coalescence. Secondly they influence the work hardening behaviour of the alloy. Therefore particle fragmentation during FSP improves ductility by eliminating those grain boundary particles and also by increasing the work hardening rate. While the ductility of Al 5059 alloy may be noticeably improved by FSP, the strength of the

alloy does not very significantly increase after FSP. This suggests adding secondary particles can be considered to be a more effective method for strengthening.

Particles also pin the grain boundaries and control grain boundary migration, therefore a particle controlled grain growth model can be used to study the relation between grain size and annealing time during heat treatment of friction stir processed Al 5059. With the use of this model a limiting grain size can be also obtained for a given annealing temperature. This limiting grain size is the maximum grain size that can be reached at a given temperature and depends on the volume fraction and radius of the pinning particles.

FSP can be utilized for fabrication of metal matrix composites but the distribution of the reinforcement in the matrix depends on the process parameters such as tool geometry, rotation speed and number of passes. In this regard a multi-pass FSP technique with different tools and processing conditions was developed based on iterative testing and microstructure analysis. The parameters developed for production of Al 5059/Al_2O_3 and Al 5059/MWCNT composites produced a uniform distribution of the reinforcing phase within the stir zone region. The fabricated composites show significantly improved mechanical properties due to a homogeneous dispersion of the particles in the stir zone, and refined matrix microstructure. It should be noted that the severe plastic deformation and relatively high temperatures associated with FSP may have a detrimental effect on the structure of the reinforcement, as this effect was observed in the case of Al

5059/MWCNT where CNTs completely transformed to other carbon nanostructures after 3 FSP passes .

5.2 Recommendations

1. While a comprehensive characterization was performed on the particles present in Al 5059 using TEM microscopy and ThermoCalc analysis a more detailed investigation is suggested to see if a relation can be found between the morphology and chemical composition of the particles, and if an orientation relation can be found between the particles and the matrix. These will help to recognize the pinning particles from those that do not affect grain boundaries. More studies are also recommended to find out how the aspect ratio of the particles can affect grain boundary mobility and grain growth.

2. It is suggested to heat treat friction stir processed Al 5059 at different temperatures and investigate the grain growth behaviour (normal vs. abnormal grain growth).

3. The Hall-Petch relation was shown to be valid within the range of grain sizes achieved in this work. It is suggested to produce samples with smaller grain sizes and study the grain size/hardness relation in the submicron range.

4. The proposed composite fabrication technique was tested for micron and nanosized alumina particles and MWCNTs. It is suggested to apply this technique for other reinforcements with different chemical compositions, sizes and aspect ratios. Using a combination of two or more types of particles is also an interesting topic for future work.

5. While tool wear was not a serious problem during production of CNT and alumina reinforced composites, it can be a limitation for other cases. It is suggested to perform a systematic study on tool wear during fabrication of composites with different types, volume fractions and sizes of the reinforcing particles.

6. It was shown that the CNTs did not survive the fabrication process. Use of CNTs with properties (such as length or number of walls) different from the ones used in this study is suggested to see if the stability depends on the properties of the CNTs or not. This aspect of the process may also be used in a positive way to change a cheap particle to a hard and effective reinforcement. In this regard it is suggested to use graphite particles as the starting reinforcement and see if they transform to harder carbon phases during the process.